

# **Modification of Wood Surfaces via controlled Polymerization Methods**

**Dissertation**

zur Erlangung des mathematisch-naturwissenschaftlichen  
Doktorgrades  
„Doctor rerum naturalium“  
der Georg-August-Universität Göttingen

im Promotionsprogramm Materialforschung Holz  
der Georg-August University School of Science (GAUSS)

vorgelegt von  
**Martin Königsmann**  
aus Seesen  
Göttingen, 2018

## **Betreuungsausschuss**

Prof. Dr. Philipp Vana, MBA	<i>Institut für Physikalische Chemie, Georg-August-Universität Göttingen</i>
Jun.-Prof. Dr. Kai Zhang	<i>Holztechnologie und Holzchemie, Georg-August-Universität Göttingen</i>
Prof. Dr. Holger Militz	<i>Holzbiologie und Holzprodukte, Georg-August-Universität Göttingen</i>

## **Mitglieder der Prüfungskommission**

### **Referent**

Prof. Dr. Philipp Vana, MBA	<i>Institut für Physikalische Chemie, Georg-August-Universität Göttingen</i>
-----------------------------	--

### **Korreferent**

Jun.-Prof. Dr. Kai Zhang	<i>Holztechnologie und Holzchemie, Georg-August-Universität Göttingen</i>
--------------------------	---

### **Weitere Mitglieder der Prüfungskommission**

Prof. Dr. Holger Militz	<i>Holzbiologie und Holzprodukte, Georg-August-Universität Göttingen</i>
Prof. Dr. Carsten Mai	<i>Holzbiologie und Holzprodukte, Georg-August-Universität Göttingen</i>
Dr. Florian Ehlers	<i>Institut für Physikalische Chemie, Georg-August-Universität Göttingen</i>
PD Dr. Thomas Zeuch	<i>Institut für Physikalische Chemie, Georg-August-Universität Göttingen</i>

**Tag der mündlichen Prüfung:** 27.09.2018

*Für Papa*

"Life is like a bicycle.  
To keep balance, you must keep moving."

– Albert Einstein



---

# Abstract

The present study was conducted to explore the possibilities of wood modification by reversible-deactivation radical polymerization (RDRP) techniques in order to tailor surface properties. Surface-initiated reversible addition–fragmentation chain transfer (SI-RAFT) polymerization was carried out on bulk wood to obtain a non-leaching polymer coating on the wood surface, which offers enhanced hydrophobicity and the possibility to easily cleave the polymer coating from wood. Furthermore, surface-initiated activators regenerated by electron transfer atom transfer radical polymerization (SI-ARGET ATRP) was used to graft a hydrophobic polymer on wood flour. The grafted wood was used as a filler material in a thermoplastic polymer matrix to obtain a composite material that maintains the ductility of the polymer matrix but possesses higher strength and toughness.

A xanthate was immobilized on the wood surface via the Z-group approach through esterification of the superficial hydroxyl groups in a one-pot reaction with minimal reaction steps on the surface. Afterwards, SI-RAFT polymerization of vinyl acetate and methyl acrylate was conducted to obtain a tailored polymer layer. Water contact angle (WCA) measurements showed a significant change in surface hydrophobicity indicated by a smaller contact angle compared to unmodified wood. Thermogravimetric analysis (TGA) of modified wood depicted combined properties of both polymer and wood, which demonstrated a successful surface-initiated polymerization. The grafted polymer was cleaved from the wood surface by a radical induced single addition-fragmentation chain transfer step. The cleaved polymer showed the characteristics of a controlled polymerization.

The immobilization of an ATRP initiator on wood was conducted using  $\alpha$ -bromoisobutyryl bromide. Surface-initiated ARGET ATRP of methyl acrylate was performed in the absence of a sacrificial initiator using ascorbic acid as an environmentally friendly reducing agent. Attenuated total reflectance Fourier-transform infrared (ATR-FTIR) spectroscopy and differential scanning

---

calorimetry (DSC) measurements revealed the successful grafting of poly(methyl acrylate) (PMA) on the wood surface. Through TGA experiments, it was possible to assess the amount of grafted polymer, which increased with progressing polymerization time. Furthermore, the wetting properties were examined via WCA and dynamic vapor sorption (DVS) measurements demonstrating a greatly increased hydrophobicity. To examine the properties of the grafted polymer, control experiments were performed using wood flour covered with a cleavable ATRP initiator bearing a disulfide moiety. Size-exclusion chromatography (SEC) analysis of the detached polymer confirmed the living character of the polymerization. After cleavage, the amount of resulting surface-located thiol groups was determined quantitatively via UV/vis spectroscopy using ELLMANN'S reagent to assess the grafting density of the initiator.

Wood flour-reinforced thermoplastics consisting of PMA as polymer matrix were produced by solvent casting. Within these composites, functionalized wood particles with varying amount of grafted polymer were incorporated into the polymer matrix in a constant mass fraction. In a second series of measurements, grafted wood particles with constant amount of grafted polymer were incorporated into the polymer matrix in varying mass fractions. Tensile testing showed that a longer polymerization time led to a higher reinforcing effect on the resulting composite and revealed an optimum of added grafted wood particles at 7 wt%. The YOUNG'S modulus, yield point and tensile toughness were increased up to 150 % compared to the polymer matrix. Dynamic mechanical analysis (DMA) revealed decreased viscous behavior of the composite when wood with a low amount of grafted polymer was incorporated and increased viscous behavior with longer polymerization times. The higher the amount of added grafted wood, the higher the elastic behavior of the composite. The glass transition temperature of the composites was observed to be hardly affected by the incorporation of wood particles.

The results presented here show that addition of grafted wood particles into a polymer matrix results in composites with increased strength and ductility when compared to the pure polymer while maintaining the same thermal range of application.

---

# Zusammenfassung

Im Rahmen dieser Arbeit wurde die Oberfläche von Holz mittels oberflächeninitiierten kontrollierten radikalischen Polymerisationen modifiziert. Dabei wurden Holzkörper mit Hilfe von *reversible addition-fragmentation chain transfer* (RAFT) Polymerisation mit einer hydrophoben Polymerschicht bedeckt, welche anschließend kontrolliert abgespalten und untersucht wurde. Außerdem wurde *atom transfer radical polymerization* (ATRP) verwendet, um Holzmehl mit einer hydrophoben Polymerhülle zu versehen. Diese modifizierten Holzpartikel wurden anschließend als Füllmaterial in eine Polymermatrix eingebracht. Das resultierende Komposit zeigte im Vergleich zur reinen Polymermatrix eine erhöhte Festigkeit und Duktilität.

Ein Xanthogenat wurde durch die Veresterung der Hydroxylgruppen unter Verwendung des Z-Gruppen-Ansatzes in einer Eintopfreaktion auf der Holzoberfläche verankert. Hiervon ausgehend wurden Polymerschichten aus Polyvinylacetat (PVAc) und Polymethylacrylat (PMA) synthetisiert und die Oberfläche mittels Wasserkontaktwinkelmessungen und thermogravimetrischer Analyse untersucht. Hierbei wurde eine im Vergleich zur ursprünglichen Holzschicht hydrophobere Oberfläche und ein kombiniertes thermisches Verhalten von Holz und dem entsprechenden Polymer erhalten. Die gebildeten Polymerschichten wurden anschließend radikalisch von der Oberfläche abgespalten und mittels Gelpermeationschromatographie untersucht, wodurch eine zugrundeliegende kontrollierte Polymerisation bestätigt werden konnte.

Holzpartikel wurden durch oberflächeninitiierte *activators regenerated by electron transfer* (ARGET) ATRP mit Ascorbinsäure als umweltfreundliches Reduktionsmittel mit PMA funktionalisiert. Hierbei wurde explizit auf einen Initiator in Lösung verzichtet, um kein ungebundenes Polymer zu erzeugen. Nach der Immobilisierung des ATRP-Initiators wurden Polymerhüllen mit verschiedenen Polymerisationsgraden hergestellt. Die erfolgreiche Pfropfpolymerisation wurde mittels *attenuated total reflection* (ATR)-Infrarotspektroskopie und dynamischer Differenzkalorimetrie festgestellt. Durch thermogravimetrische Analyse konnte

---

der Massenanteil des Polymers auf den Holzpartikeln berechnet werden. Zudem zeigte sich ein erhöhter Polymeranteil bei längerer Polymerisationszeit. Die hygroskopischen Eigenschaften und die Benetzbarkeit wurden durch Wasserkontaktwinkelmessungen und dynamische Wasserdampfsorption bestimmt. Dabei wurde eine deutliche Hydrophobierung der Oberfläche festgestellt. Zur Untersuchung des gepfropften Polymers wurden identische Polymerisationen mit einem reduktiv-spaltbaren ATRP-Initiator durchgeführt. Gelpermeationschromatographie des abgespaltenen Polymers bestätigte den lebenden Charakter der Polymerisation. Nach der Abspaltung wurde zusätzlich die Beladungsdichte des Initiators mit Hilfe von UV/VIS-Spektroskopie bestimmt.

Holzverstärkte Thermoplaste wurden mittels *solvent casting* durch das Einbringen von funktionalisierten Holzpartikeln in eine Polymethylacrylat-Matrix hergestellt. Ein konstanter Massenanteil von Partikeln mit variierendem Polymerisationsgrad der oberflächenverankerten Ketten und variierende Massenanteile von Partikeln mit konstantem Polymerisationsgrad wurden in die Polymermatrix eingebracht. Die mechanischen und thermischen Eigenschaften dieser Komposite wurden durch Zugversuche und dynamisch-mechanische Analyse untersucht. Die Zugversuche zeigten einen verstärkenden Effekt mit höheren Polymerisationsgraden der funktionalisierten Holzpartikel mit einem Optimum der Zugabe bei 7 wt%. Hierbei steigerten sich der Elastizitätsmodul, die Streckgrenze und Zähigkeit im Vergleich zu der Polymermatrix jeweils um bis zu 150%. Die dynamisch-mechanische Analyse zeigte, dass der viskose Anteil der Komposite mit Einbringung von wenig funktionalisierten Partikeln zunächst verringert wird, aber mit steigendem Polymerisationsgrad ansteigt. Je größer der Massenanteil der eingebrachten Partikel, desto höher der elastische Anteil des Komposits. Zusätzlich konnte beobachtet werden, dass das Einbringen der Partikel lediglich einen geringen Einfluss auf die Glasübergangstemperatur der Polymermatrix hat.

Die hier vorgestellten Ergebnisse zeigen, dass die Einbringung von polymerfunktionalisierten Holzpartikeln in eine Polymermatrix zu einem Kompositmaterial mit erhöhter Festigkeit und Duktilität führt, welches im gleichen Temperaturbereich angewendet werden kann.

---

# Contents

<b>I</b>	<b>Introduction and motivation</b>	<b>1</b>
<b>1</b>	<b>Preface and motivation</b>	<b>3</b>
1.1	Chemical composition of wood . . . . .	6
1.1.1	Components of wood . . . . .	6
1.1.2	Structure of wood . . . . .	8
1.2	Wood-plastic composites and wood reinforced thermoplastics . . .	13
1.2.1	Additives . . . . .	14
1.2.2	Wood surface modification . . . . .	15
1.3	Polymerization methods . . . . .	15
1.3.1	Reversible-deactivation radical polymerization (RDRP) . .	16
1.3.2	Surface-initiated polymerization . . . . .	17
<b>II</b>	<b>Surface-initiated RAFT polymerization – modification of bulk wood</b>	<b>19</b>
<b>2</b>	<b>Preface</b>	<b>21</b>
2.1	Reversible addition-fragmentation chain transfer polymerization .	21
2.2	Mechanism of the RAFT process . . . . .	22
2.3	Surface-initiated RAFT polymerization . . . . .	24
<b>3</b>	<b>Surface-initiated RAFT polymerization on wood</b>	<b>27</b>
3.1	Immobilization of the RAFT agent . . . . .	28
3.2	Surface-initiated RAFT polymerization . . . . .	30
<b>4</b>	<b>Cleavage of tethered polymer</b>	<b>39</b>
<b>5</b>	<b>Conclusions of Chapter II</b>	<b>43</b>

<b>III</b>	<b>Surface-initiated ARGET ATRP of wood flour</b>	<b>45</b>
<b>6</b>	<b>Preface</b>	<b>47</b>
6.1	Atom transfer radical polymerization (ATRP) . . . . .	47
6.2	Activators regenerated by electron transfer (ARGET) ATRP . . . . .	50
6.3	Surface-initiated ATRP . . . . .	51
<b>7</b>	<b>ARGET ATRP of wood</b>	<b>53</b>
7.1	Immobilization of ATRP initiator . . . . .	53
7.2	ARGET ATRP of methyl acrylate . . . . .	58
<b>8</b>	<b>Determination of initiator content and surface-bound polymer</b>	<b>67</b>
8.1	Selective cleavage of polymer grafts . . . . .	67
8.2	Surface analysis . . . . .	70
<b>9</b>	<b>Conclusions of Chapter III</b>	<b>73</b>
<b>IV</b>	<b>Wood flour-reinforced thermoplastic</b>	<b>75</b>
<b>10</b>	<b>Preface</b>	<b>77</b>
10.1	Mechanical properties of polymers and their composites . . . . .	77
10.2	Tensile testing . . . . .	78
10.3	Dynamic mechanical analysis (DMA) . . . . .	80
<b>11</b>	<b>Mechanical analysis of composites</b>	<b>83</b>
11.1	Preparation of the composites . . . . .	83
11.2	Tensile testing measurements . . . . .	87
11.3	Dynamic mechanical measurements . . . . .	92
<b>12</b>	<b>Conclusions of Chapter IV</b>	<b>99</b>
<b>V</b>	<b>Experimental part</b>	<b>101</b>
<b>13</b>	<b>Instrumentation</b>	<b>103</b>
13.1	Chromatography . . . . .	103
13.1.1	Column chromatography . . . . .	103
13.1.2	Thin-layer Chromatography (TLC) . . . . .	103
13.1.3	Size-exclusion chromatography (SEC) . . . . .	103

13.2	Spectroscopy . . . . .	104
13.2.1	UV/vis spectroscopy (UV/vis) . . . . .	104
13.2.2	Nuclear magnetic resonance (NMR) spectroscopy . . . . .	106
13.2.3	Attenuated total reflection Fourier-transform infrared spectroscopy (ATR-FTIR) . . . . .	107
13.3	Microscopy . . . . .	107
13.3.1	Scanning electron microscopy (SEM) and Energy-dispersive X-ray spectroscopy (EDX) . . . . .	107
13.3.2	Fluorescence microscopy . . . . .	107
13.3.3	Optical microscopy . . . . .	108
13.4	Mechanical analysis . . . . .	108
13.4.1	Tensile testing . . . . .	108
13.4.2	Dynamic mechanical analysis (DMA) . . . . .	108
13.5	Thermal analysis . . . . .	108
13.5.1	Thermogravimetric analysis (TGA) . . . . .	108
13.5.2	Differential scanning calorimetry (DSC) . . . . .	109
13.6	Wetting analysis . . . . .	109
13.6.1	Water contact angle (WCA) . . . . .	109
13.6.2	Dynamic vapor sorption (DVS) . . . . .	109
13.7	Other Methods . . . . .	110
13.7.1	Electrospray ionization mass spectrometry (ESI-MS) . . . . .	110
13.7.2	Elemental analysis (EA) . . . . .	110
<b>14</b>	<b>Substances and synthesis</b>	<b>111</b>
14.1	Commercially acquired substances . . . . .	111
14.1.1	Solvents . . . . .	111
14.1.2	Monomers and initiator . . . . .	111
14.1.3	Miscellaneous . . . . .	112
14.2	Synthesis of substances . . . . .	112
14.2.1	2-Ethoxythiocarbonylsulfanyl-propionic acid ethyl ester . . . . .	112
14.2.2	2-((2-Hydroxyethyl)disulfanyl)ethyl 2-bromo-2-methylpropanoate . . . . .	113
14.2.3	4-(2-((2-(2-bromo-2-methylpropanoyloxy)-ethyl)disulfanyl)ethoxy)-4-oxobutanoic acid . . . . .	114
14.2.4	2-((2-(2-bromo-2-methylpropanoyloxy)-ethyl)disulfanyl)ethyl 4-chloro-4-oxobutanoate . . . . .	114
14.3	Pretreatment of wood . . . . .	115
14.3.1	Soxhlet extraction . . . . .	115

14.3.2	Alkaline treatment . . . . .	115
14.4	Immobilization reactions . . . . .	115
14.4.1	Immobilization of xanthate on wood surface . . . . .	115
14.4.2	Immobilization of BIBB on wood . . . . .	116
14.4.3	Immobilization of the disulfide initiator on wood . . . . .	116
14.5	Polymerizations . . . . .	117
14.5.1	Synthesis of poly(methyl acrylate) as polymer matrix . . . . .	117
14.5.2	Grafting of vinyl acetate via MADIX Polymerization . . . . .	117
14.5.3	Grafting of methyl acrylate via MADIX Polymerization . . . . .	117
14.5.4	Grafting from wood dust via ARGET ATRP . . . . .	118
14.6	Detachment of surface-tethered polymer . . . . .	118
14.6.1	Cleavage of polymer grafts via radicals . . . . .	118
14.6.2	Cleavage of disulfide-initiator polymer grafts . . . . .	118
14.7	Preparation of composite materials . . . . .	119

<b>VI</b>	<b>References</b>	<b>121</b>
-----------	-------------------	------------

<b>VII</b>	<b>Appendices</b>	<b>137</b>
------------	-------------------	------------

	<b>Tables and figures</b>	<b>139</b>
--	---------------------------	------------

	<b>Abbreviations</b>	<b>159</b>
--	----------------------	------------

	<b>Acknowledgements</b>	<b>165</b>
--	-------------------------	------------

# **Chapter I**

## **Introduction and motivation**



# 1 Preface and motivation

In 2016, the worldwide polymer production exceeded 320 million tons.<sup>[1]</sup> Synthetic polymers offer many possibilities for application due to their low weight, high resistance to corrosion, cheapness in production and their good workability. Especially in automotive industry, health care, building & construction as well as packaging, high-end polymeric products have replaced traditional materials such as wood, metal, alloys and glass.<sup>[2]</sup> Thermoplastics including polypropylene (PP), polyethylene (PE) and polystyrene (PS) are the majority of industrially produced polymers, which are prepared by radical polymerization.<sup>[2,3]</sup> However, so-produced polymers exhibit no chain-end functionality and feature a wide molecular mass distribution. To overcome these drawbacks, reversible-deactivation radical polymerization (RDRP) methods were invented, giving well-defined polymers with tunable properties.<sup>[4,5]</sup> Thermoplastics are an important industrial polymer class, because they can be repeatedly reshaped by heating and processed by techniques such as injection molding, calendaring and extrusion in large quantities.<sup>[6,7]</sup> In general, disadvantages of thermoplastics include high coefficients of thermal expansion, susceptibility to creep and low stiffness, limiting the overall application scope. In order to eradicate these drawbacks, filler materials can be added to form novel composite materials.<sup>[6-8]</sup>

Wood is a particularly suitable filler for composite materials, since it is environmentally friendly and the resulting compound possesses high strength combined with low density. It has been an essential material for mankind since the primitive state and was used for the construction of shelter, tools, furniture and even as raw material for energy.<sup>[9]</sup> Wood is a composite mainly made of three biopolymers (cellulose, hemicellulose and lignin) which, in cooperation with a cellular structure, create a high-performance material.<sup>[10]</sup> Compared to most synthetic materials, wood is a cheap raw material, which is recyclable and abundant on earth. However, wood has several disadvantages, such as poor dimensional stability (*e.g.* response to moisture variation, shrinking and swelling), susceptibility to microorganisms and natural variability across species and even within one tree.<sup>[11]</sup> Some wood species naturally have a high durability making them

---

suitable for high-demanding products. These species are often less available and consequently more expensive.<sup>[12]</sup> Therefore, utilization of cheap wood should be a desired aim from an economic and ecological point of view. However, this wood usually does not meet the requirements for high-quality products. Hence, much effort is spent to eliminate these disadvantages by chemical or physical wood modification.<sup>[9]</sup>

In principle, there are two ways to create beneficial combinations of wood and thermoplastics. The first approach refers to bulk materials, whereas the second approach relates to composite materials. In case of bulk materials, wood modification can either take place within the wood or on the surface.<sup>[9,11]</sup> Polymerization within the wood uses the highly sophisticated structure of wood as template and mostly targets increased dimensional stability and strength properties (*e.g.* stiffness, toughness) which for example is important for construction materials. Wood modification by simply covering the surface with a polymer layer is an easy way to raise durability against environmental hazards, such as microorganisms or structural damages due to repetitive water absorption and desorption.<sup>[13,14]</sup> The second approach deals with the synthesis of a composite material by combining two or more components to obtain a new material with enhanced properties.<sup>[12,15]</sup> Wood-plastic composites (WPCs) are a non-recyclable combination of thermoplastics and wood (fibers or particles), in which the good processability of polymers and the strength of wood are combined.<sup>[10]</sup> A distinction must be made between WPCs, that are usually composed of 30 – 80 % wood and wood reinforced thermoplastics, that are mainly made of polymer as a matrix and wood as an additive to increase strength and durability.<sup>[16-18]</sup> Both composites are the combination of a hydrophobic and a hydrophilic material resulting in an insufficient interfacial adhesion and therefore poor mechanical properties, *e.g.* tensile strength and ductility. These shortcomings can be overcome by modification of either the wood or the polymer surface.<sup>[16]</sup>

The purpose of this study was to investigate the modification of wood surfaces via reversible-deactivation radical polymerization (RDRP) techniques to tailor desired surface properties.<sup>[19]</sup> Particularly, non-durable wood was modified to increase its range of application. Surface-initiated reversible addition-fragmentation chain transfer (SI-RAFT) polymerization was used to graft thermoplastic polymer onto wood with regard to improved bulk materials.<sup>[20]</sup> The chain transfer agent was tethered to the surface such that subsequent removal

and analysis of the polymer is possible.<sup>[21]</sup> This leads to a recyclable composite by separation of wood from the polymer. Sacrificial RAFT agent was added in solution to obtain a better control over the polymerization. However, this leads to unbound polymer in solution which can be undesired.

As a second RDRP technique, activators regenerated by electron transfer atom transfer radical polymerization (ARGET ATRP) was used to graft thermoplastic polymer onto wood particles.<sup>[22]</sup> Unlike in the case of RAFT polymerization, ATRP can be conducted directly on the surface without formation of untethered polymer, which would require time-consuming purification steps.<sup>[23]</sup> Another important advantage is that ARGET ATRP can be carried out in the presence of minor amounts of oxygen which is problematic in RAFT polymerization. So-produced grafted wood particles were used as a filler material in a thermoplastic matrix to achieve an enhanced interfacial adhesion between the hydrophilic wood and the hydrophobic polymer matrix in the resulting composite material, leading to improved mechanical properties. Based on the wood particle modification described above, another aim of this work was to systematically study the effect of polymer-grafted wood particles incorporated into a poly(methyl acrylate) matrix on mechanical properties of the composite. The influence of the degree of grafting of the surface-tethered polymer was investigated at first, followed by studies on the mechanical properties of the matrix with different ratios of incorporated particles. To determine mechanical properties, tensile testing and dynamic mechanical analysis were used to understand and validate the reinforcing character of modified wood.

## 1.1 Chemical composition of wood

On a macroscopic scale wood is a fiber-reinforced composite. It is a porous and fibrous tissue found in many plants. Mankind has used wood for centuries as fuel, construction material, for making paper, tools, weapons and furniture.<sup>[10]</sup> Besides water, wood has three main components – it is constituted of about 43 – 46 % cellulose, 27 – 37 % hemicellulose and 20 – 27 % lignin.<sup>[12]</sup> Lignin and hemicelluloses act as a soft polymer matrix, which is reinforced by rigid cellulosic microfibrils, so called lignocellulosic fibers.<sup>[24]</sup> These three main components will be discussed in more detail in the following sections. Additionally, the structure and substructure of wood along with the accessibility of surface hydroxyl groups, important for understanding the reactivity, is discussed below.

### 1.1.1 Components of wood

#### Cellulose<sup>[25]</sup>

Cellulose is the most abundant biopolymer on earth and forms the structural basis of plant cells.<sup>[26]</sup> The unbranched polymer is derived from D-glucopyranose, forming cellobiose repeating units of approximately 1 nm length which are linked by a  $\beta(1,4)$ -glycosidic bond (see Figure 1.1).<sup>[27]</sup> The degree of polymerization (DP) depends on both origin and treatment of the raw material and ranges between 300 and 10000.<sup>[28]</sup> Due to its linear form, it is capable of forming three-dimensional microfibrils through strong inter- and intra-molecular hydrogen bonds, which form crystalline regions.<sup>[29]</sup> These microfibrils are randomly oriented and mainly responsible for the high tensile strength of 120 – 140 GPa (10 to 1000 times stronger

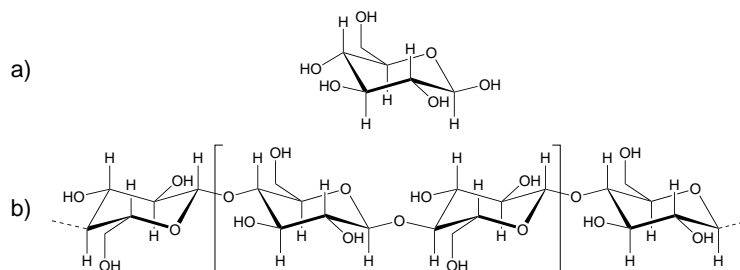


Figure 1.1: a) Chemical structure of a glucose unit, b) Chemical structure of a cellulose polymer with cellobiose as repeating unit.<sup>[27]</sup>

than most synthetic thermoplastics), making cellulose a good candidate for high performance materials.<sup>[10,30–32]</sup> Around 65 % of wood-derived cellulose is present in the crystalline state, whereas the rest forms amorphous regions. The amorphous regions are prone to moisture sorption, extractions, chemical treatments and interactions with microorganisms.<sup>[33]</sup>

### Hemicellulose<sup>[25]</sup>

Generally, hemicelluloses are constituted of heterogeneous polysaccharide polymers with lower degree of polymerization (average DP of 100 – 200) compared to cellulose. In contrast to cellulose, hemicellulose forms short-branched chains and consists of sugars such as mannose, xylose, glucuronic acid, galactose and arabinose (see Figure 1.2).<sup>[10,26]</sup> Due to this structural variety, hemicellulose barely forms hydrogen bonds, resulting in an amorphous structure, which explains its highly hygroscopic behaviour, higher reactivity towards chemical treatment and lower thermal stability in comparison to cellulose or lignin.<sup>[27]</sup> Hemicelluloses act as glue between lignin and cellulose microfibrils and hence contribute to the structural strength of wood.<sup>[33]</sup>

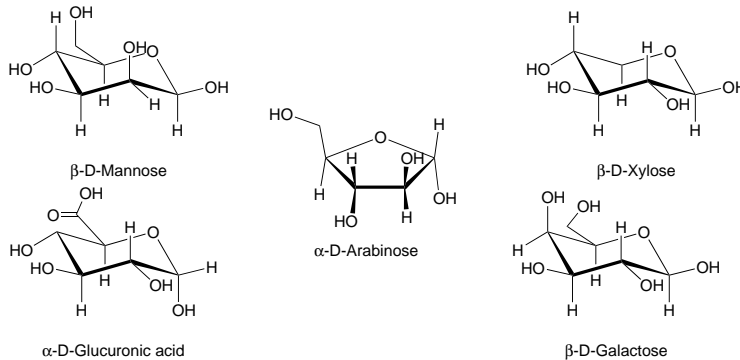


Figure 1.2: Chemical structure of representative sugars found in hemicellulose.<sup>[10,26]</sup>

### Lignin<sup>[25]</sup>

Lignin is a heterogeneous, highly complex and mainly aromatic polymer of phenylpropane units.<sup>[33]</sup> The three-dimensional phenolic polymer is based on three different monolignols, namely *p*-coumaryl alcohol, coniferyl alcohol and sinapyl alcohol (see Figure 1.3).<sup>[10]</sup> Lignin is responsible for the stiffness of wood

## 1.1 Chemical composition of wood

by forming covalent bonds with the polysaccharide backbone, stabilizing the cell wall layers and therefore increases the compression strength.<sup>[26,34]</sup>

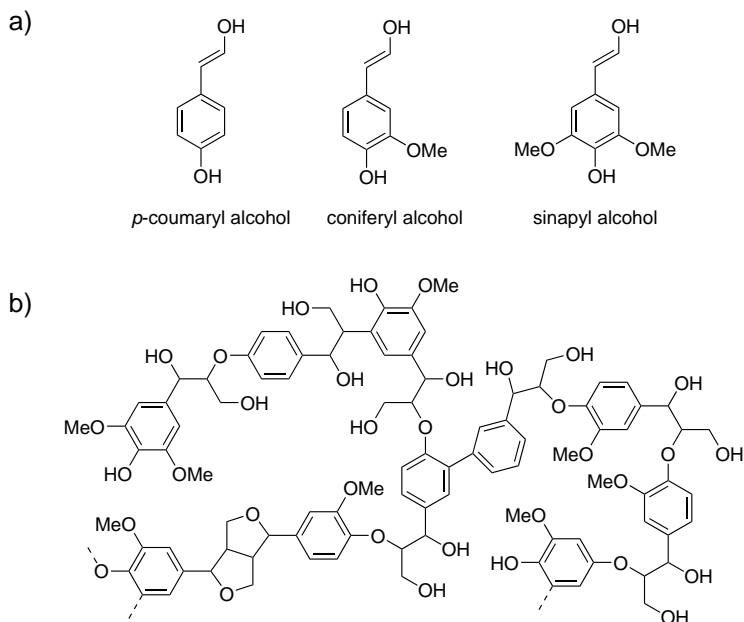


Figure 1.3: Chemical structure of monolignol units (a) and a schematic polymer network of lignin (b).<sup>[10]</sup>

### 1.1.2 Structure of wood

Wood is a heterogeneous, cellular and anisotropic material, that can be botanically classified into two groups. Softwoods, belonging to gymnosperms (mainly coniferous species) and hardwoods, which belong to angiosperms (flowering plants).<sup>[35]</sup> Hardwoods are composed of four to five different cell types and hence have a relatively complex and heterogenous structure.<sup>[9]</sup> Softwoods are evolutionary older than hardwoods and are therefore less specified and have a simpler structure.

Hereinafter, exclusively softwood will be explained in more detail, since this work is based on the modification of softwood. Due to its highly hierarchical structure, wood has three anatomical directions, that can be visualized in cross-, tangential- and radial section. A cross section of a tree trunk reveals different

parts of the stem as shown in Figure 1.4. The outermost layer is bark, protecting the tree against injury and desiccation. Bark is divided in the outer dead bark and the inner living bark. Adjacent to the inner bark is the growth zone in wood, the so called cambium layer. After that, the inner part of the stem consists of sapwood (light region) and heartwood (dark region).<sup>[33]</sup>



Figure 1.4: Cross sections of pine trunks.

New wood is initially formed as sapwood before it may be transformed into heartwood after several years. The main function of sapwood is to conduct water and nutrients from roots to leaves (and vice versa). Normally, sapwood offers almost no natural resistance versus degradation by fungi.<sup>[12]</sup> For this reason, it is necessary to use (chemical) wood preservatives to increase durability and dimensional stability which allows this wood to be used in high-demanding fields such as building and other construction sectors.

Heartwood usually possesses a higher durability than sapwood. During heartwood formation, colored polyphenolic substances are stored inside the cell walls explaining the darker color as well as higher durability and resistance to decay against microorganisms and insects.<sup>[10]</sup> In a temperate climate, growth rings can be found in both sapwood and heartwood. They are a result of different growth speeds throughout the seasons of the year.<sup>[12]</sup> The inner portion of a growth ring is called earlywood, because it is formed early in the season when

## 1.1 Chemical composition of wood

---

growth is rapid, since sufficient nutrients are present and the temperature is ideal. Earlywood consists of wood cells with large lumina and thin cell walls and therefore is less dense. Latewood, the outer dark portion, is formed at the end of the season and is composed of thick-walled cells with very small cell cavities.<sup>[25,26]</sup> Since the strength of wood originates from the sophisticated structure of wood cell walls, latewood offers a much greater strength.<sup>[36]</sup>

### Micro- and nanostructure of wood cells

On a microscopic scale, wood is composed of millions of cells, which differ in shape, size and function.<sup>[12]</sup> Figure 1.5 shows a scanning electron microscope (SEM) image taken from the cross section of pine sapwood. Cells with thick cell walls and small lumina belong to latewood, whereas cells with thin cell walls and large lumina are considered earlywood.<sup>[12,37]</sup>

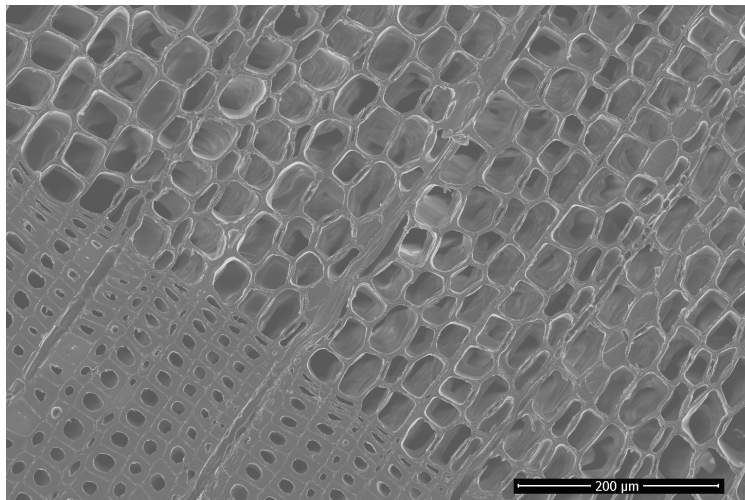


Figure 1.5: Scanning electron microscope image of a cross section of pine sapwood. Cells with thick cell walls refer to latewood, whereas cells with thin cell walls relate to earlywood.

Softwoods basically consist of two cell types, namely tracheids and parenchyma cells.<sup>[26,33]</sup> The tracheids are mostly arranged in radial files, oriented longitudinal and account for 90 – 95 % of the cells (by volume).<sup>[35]</sup> They are squarely or hexagonally shaped cells with a length of about 3 – 5 mm and a

diameter of 30 – 40  $\mu\text{m}$ .<sup>[38]</sup> Parenchyma cells are mostly horizontally oriented, smaller in comparison to tracheids (usually less than 1 mm long) and function as nutrient storage and radial conduction system. All wood cells are connected to each other through a thin layer, the so-called middle lamella (ML), which is rich in lignin, almost free of cellulose and glues adjacent cells together to form tissues (see Figure 1.6).<sup>[25,39]</sup>

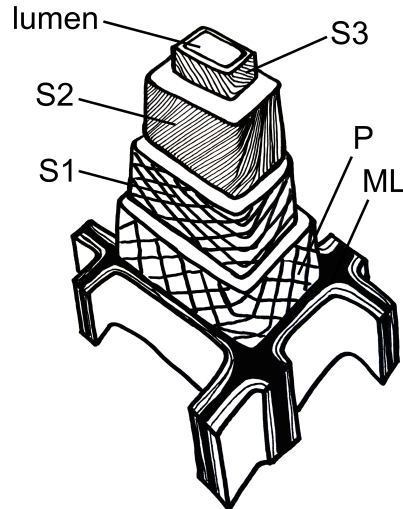


Figure 1.6: Schematic model of the cell wall structure of softwood with highlighted layers (adapted from BOOKER and SELL).<sup>[40]</sup> ML represents the middle lamella, P the primary cell wall and S1-3 the secondary wall layers.

The cell wall is made of so-called lignin-carbohydrate complexes (LCCs) and are divided in a primary and a secondary layer.<sup>[9,37]</sup> The primary layer is formed first and contains a high lignin content with a low amount of cellulose microfibrils in random orientation. The secondary layer consists of a high amount of parallelly oriented cellulose microfibrils with a low lignin content and are subdivided into three layers (S1, S2 and S3) with different arrangements of cellulose microfibrils.<sup>[12,27]</sup>

The S1 layer contains microfibrils, that are oriented more or less perpendicular to the cell axis ( $70 - 90^\circ$ ), is adjacent to the primary layer. The central S2 layer forms the majority of the cell wall and therefore contributes the most to the mechanical strength. In this layer, the cellulose microfibrils form helically winding

## 1.1 Chemical composition of wood

---

patterns in a longitudinal direction of  $0 - 30^\circ$ . The last layer (S3) is located at the luminal border and consists of a thin layer of parallelly oriented cellulose microfibrils at an angle of  $30 - 90^\circ$  to the cell axis.<sup>[25,40]</sup> Incomplete filling of the intermicrofibrillar region results in the existence of micropores in the cell wall, allowing substances to reach the inner part of the cell wall. The size of these pores is strongly dependent on the moisture content. Fully swollen cell walls have micropores with a size of about  $2 - 4$  nm, whereas in fully dried wood the micropores are smaller.<sup>[27]</sup> With regard to wood modification, it is important to know, if substances are able to penetrate the cell to either react inside the cell wall or to pass the cell connections and to react inside the lumen.<sup>[9]</sup>

The combination of all layers with different thicknesses, orientations of microfibrils and portions of cellulose, hemicellulose and lignin leads to the extraordinary toughness and durability of wood.<sup>[12]</sup> EDER *et al.* used microtensile tests of Norway spruce to determine the tensile strength of single wood cells in early wood and found a value of approximately 760 MPa.<sup>[41]</sup>

The lignin-carbohydrate complex (LCC) is made of long cellulose fibrils, which are tightly surrounded by hemicellulose, since the final formation of the amorphous hydrophilic hemicellulose polymer takes place at that location. Subsequently, the resulting carbohydrate complex serves as a template for lignification. Hemicellulose is covalently connected to lignin by ester or ether bonds, whereas the interaction between cellulose and hemicellulose is purely resulting from hydrogen bonds.<sup>[9,42]</sup>

### **Accessibility of hydroxyl groups<sup>[27]</sup>**

With regard to wood modification, it is important to understand the nature of the surface of wood and hence the accessibility of hydroxyl groups acting as a starting point for chemical wood modification. The hydroxyl groups associated with the polymeric cell wall constituents are the most abundant chemically reactive sites. However, they greatly differ in reactivity. In the case of cellulose, certain parts are inaccessible due to a crystalline structure or presence of hydrogen bonds.

The number of hydroxyl groups in wood is not precisely known and is strongly dependent on the wood species. However, rough estimations can be made by calculating the total number of hydroxyl groups associated with each cell wall constituent given calculated values for dry wood of approximately  $19.8 \times 10^{-3} \text{ mol g}^{-1}$ .<sup>[43]</sup> Naturally, the amount of accessible hydroxyl groups is lower than the total hydroxyl content and is crudely estimated by subtracting the amount of hydroxyl groups located in the crystalline region of cellulose, giving an

accessible hydroxyl content of approximately  $8.6 \times 10^{-3} \text{ mol g}^{-1}$ .<sup>[27]</sup> Additionally, the accessibility of hydroxyl groups strongly depends on the moisture content of the wood specimen. Fully dried (shranked) wood offers less hydroxyl groups, caused by its steric structure. Small polar solvents, such as water, amines, alcohols and some organic solvents (*e.g.* DMF, DMSO) act as swelling agents, that are able to increase hydroxyl accessibility since they diffuse into the wood components.<sup>[44]</sup>

## 1.2 Wood-plastic composites and wood reinforced thermoplastics

Wood-plastic composites (WPCs) are composite materials made of wood (of any form) and a thermoplastic polymer.<sup>[35]</sup> In these products, wood or polymer wastes are used, which will help to close the loop for conserving natural resources (cradle-to-cradle concept).<sup>[45,46]</sup> Usually wood is added as fibers or flour with 30 – 80 %, whereas plastics are added as granulate.<sup>[12,18]</sup> In contrast to WPCs, the major component of wood reinforced thermoplastics is the thermoplastic matrix with minor addition of wood as a reinforcing filler.<sup>[16,47]</sup>

Over the last decades, interest has rapidly grown in these composites due to their outstanding properties and advantages, such as low maintenance, light weight, high durability, improved relative strength and stiffness and the fact, that it is a natural resource. Furthermore, WPCs have a higher resistance against bioorganisms compared to the respective wood component used, making them more suitable for outdoor uses. Although they are not as stiff as solid wood, they offer a higher stiffness than pure thermoplastics.<sup>[46,48]</sup> Most of the commercially available WPCs are based on four different polymers – polyethylene (PE), polypropylene (PP), polyvinyl chloride (PVC) and polystyrene (PS).<sup>[49,50]</sup> Regarding composite production, four parameters decisively influence the properties: the properties of the wood filler and the polymer matrix (type, ratio, distribution), the modification of both components, the method with which the filler is incorporated into the matrix and the processing conditions (compounding, solvent casting, injection molding, extrusion). The morphology (aspect ratio) of the added wood has a great influence on the composites' properties.

In general, addition of wood fibers has a greater influence than wood flour. Wood flour tends to increase the stiffness of the composite but not its strength, whereas wood fibers have a great impact on the strength and stiffness of the composite.<sup>[51–53]</sup> Furthermore, certain problems have to be overcome with regard

to the production of high-end wood polymer products. First of all, wood is a natural product and therefore its properties are strongly dependent on the origin, age and previous processing. Small variations in shape and composition also have to be considered. Poor wettability and insufficient interfacial adhesion are the main obstacles resulting in low tensile strength or durability.<sup>[17]</sup> In order to produce a sophisticated product with increased mechanical properties and a long lifetime, it is necessary to improve the compatibility between hydrophilic wood and hydrophobic plastic to form a single-phase composite.<sup>[16]</sup> Generally, there are two ways to increase interfacial adhesion – utilization of additives (such as coupling agents) or surface modification of one component (wood or polymer).

### 1.2.1 Additives

Additives are used to either improve physical properties (functional additives) or to reduce production expenses (processing aids). The first group includes reinforcing additives or coupling agents and is used to improve strength, flexibility, durability, UV- or fire resistance. The second group consists of compatibilizers, plasticizers or lubricants, which are used to optimize the production process.<sup>[54]</sup>

The reinforcing effect is strongly dependent on the stress transfer from the matrix to the filler material, therefore two important requirements must be met by the reinforcing additive. Firstly, a critical fiber length or particle size and secondly a critical volume must be present, due to the fact that the reinforcing effect is strongly dependent on the stress transfer from the matrix to the filler material.<sup>[15,55,56]</sup> Talc and calcium carbonate are two of the most commonly used functional additives, because of their availability, cheap cost and ability to enhance mechanical properties and reduced absorption of water to minimize wood moisture.<sup>[18]</sup> However, they are not renewable materials, their mining has high energy consumption and causes unnecessary pollution.<sup>[10]</sup> Coupling agents are divided into two categories: surfactants and bonding agents, which are covalently bound to the wood surface.<sup>[10]</sup> Both are used to increase interfacial adhesion between fiber and matrix and have to interact with the polymer matrix on one side and with the wood filler on the other. The most commonly used agents are maleated polypropylene (MAPP) and maleated polyethylene (MAPE) depending on the corresponding thermoplastic.<sup>[57,58]</sup> In simple terms, MAPP and MAPE are bifunctional molecules, of which the anhydride groups react with the wood surface and the polymer backbone interacts with the polymer matrix.

## 1.2.2 Wood surface modification

In order to reduce surface tension and hence optimize the wood polymer interface, the surface of wood is altered physically or chemically. Physical treatments do not alter the chemical composition of wood, but lead to considerable structural changes and modified surface properties. Physical methods include stretching, calendaring, thermotreatment, electric discharge and many more.<sup>[10,50]</sup> Chemical treatment modifies wood by forming covalent bonds through chemical reactions.

The surface of wood contains high amounts of hydroxyl groups causing a poor incorporation of the wood into the hydrophobic polymer matrix. One main goal is surface hydrophobication by blocking the hydroxyl groups, that reduce surface tension, moisture absorption and dimensional movement.<sup>[12,59]</sup> Used chemicals can be divided into two classes: those which react with a single hydroxyl group (single-site addition) and those which react with one or more hydroxyl groups and are capable of polymerizing or crosslinking afterwards.<sup>[16]</sup> The most prominent examples of the first class is treatment with acetic anhydride or organic carboxylic acids (*e.g.* stearic, maleic and succinic acid). The second class includes polyisocyanates, formaldehyde and epoxides as well as graft polymerizations, improving the compatibility with nonpolar plastics (most of thermoplastics).

Graft polymerization is initiated by the formation of free radicals on the wood surface. This is achieved through treatment with an aqueous solution containing selected ions (hydrogen peroxide with ferrous iron, ceric ammonium nitrate) or by exposure to high energy radiation. In addition, alkaline treatments, so called mercerization, is one of the most used chemical treatment, because it is easy and cost effective.<sup>[59]</sup> The wood is subjected to a solution of sodium hydroxide for a short period of time, removing small proportions of hemicellulose and lignin as well as impurities, such as oils or waxes covering the external surface. Additionally, alkali treatment depolymerizes cellulose and hence increases hydroxyl accessibility.<sup>[10,60]</sup> However, this methods can considerably change mechanical properties.

## 1.3 Polymerization methods

Free-radical polymerization is the most commonly used polymerization technique for synthetic polymers in industry and academic laboratories.<sup>[61]</sup> It can be conducted with minimal experimental effort, offering an economically effi-

cient way to produce polymers in large volumes. Generally, this method is very tolerant towards most functional groups and reaction conditions. Many vinyl monomers, for instance (meth-)acrylates, (meth-)acrylamides, styrenes, vinyl acetate and butadiene are polymerized at high rates with no demand for high purity.<sup>[62]</sup> Besides these advantages, free-radical polymerization suffers from certain drawbacks, such as the high amount of radicals and side reactions (termination and chain transfer to solvent) resulting in a poor control over molecular weight (MW) and molecular weight distribution (MWD). In order to overcome these drawbacks and to produce well-defined polymers with control over molecular weight distribution, it is necessary to reduce unwanted side reactions, such as termination.<sup>[63]</sup>

### 1.3.1 Reversible-deactivation radical polymerization (RDRP)

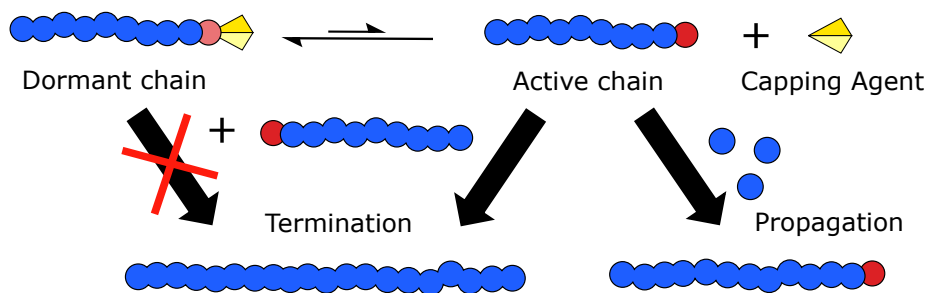
The term living polymerization was first described by *Szwarc* in 1956.<sup>[64]</sup> In an ideal living polymerization, the growth of all polymer chains starts simultaneously and neither transfer nor termination reactions take place.<sup>[65]</sup> Reversible deactivation radical polymerization (RDRP) techniques follow the concept of a living polymerization. Initially, these methods were called controlled (or living) polymerization.<sup>[19,61]</sup> Nowadays, the term reversible-deactivated radical polymerization (RDRP) is recommended by IUPAC.<sup>[4,66]</sup> The academically most used RDRP<sup>[4,5]</sup> methods are nitroxide mediated radical polymerization (NMP),<sup>[67-70]</sup> atom transfer radical polymerization (ATRP),<sup>[61,71-73]</sup> and reversible addition-fragmentation chain transfer (RAFT) polymerization.<sup>[74-77]</sup>

RDRP methods are divided into two groups, based on how they control the polymerization. The former follows the concept of reversible chain transfer. The most prominent example is reversible addition-fragmentation chain transfer (RAFT) polymerization. This system requires a reversible chain transfer agent (CTA) and a radical initiator. The chain transfer agent is used in higher concentrations with respect to the initiator and therefore determines the concentration of propagating chains. Dormant chains are reversibly activated by an addition-fragmentation step (exchange reaction) with an active (macro-)radical.

The latter is based on inducing a dynamic equilibrium between a majority of dormant species and few active species (reversible termination).<sup>[19,62]</sup> In this group, NMP and ATRP are the most used methods. Both strategies require certain initiators (alkyl-halide for ATRP, alkoxyamines for NMP), that reversibly produce active radicals by a redox dissociation mechanism (ATRP) or thermal dissociation (NMP).<sup>[61,69]</sup> The radical concentration is proportional to the initiator

concentration in both cases.

A schematic mechanism of a reversible-deactivation radical polymerization is shown in Scheme 1.1. The mechanism leads to a lower overall concentration of growing radicals, reducing termination reactions, which results in similar life-times of all radicals and a narrow molar mass distribution. Additionally, the average molar mass is controlled by the stoichiometry of the system or the polymerization time.<sup>[62]</sup>



Scheme 1.1: Schematic illustration of the dynamic equilibrium in a reversible-deactivation radical polymerization (RDRP). Blue circles represent monomer units and red circle denotes a radical.<sup>[19]</sup>

### 1.3.2 Surface-initiated polymerization

For the functionalization of surfaces with covalently bound well-defined polymers, surface-initiated RDRP techniques are applied.<sup>[78]</sup> As described above, the topology, composition and functionality of the polymers are adjusted to the desired application. Hence, surface properties including hydrophobicity, antibacterial properties, roughness, toughness, biocompatibility, electrical conductivity and stimulus-response behavior can be tailored.

Polymer chains are prepared following three strategies: the "grafting-to", "grafting-through" and the "grafting-from" approach (see Figure 1.7). In the "grafting-to" strategy, prefabricated polymers with suitable functional groups (green) are attached to the surface. The main advantage of this method is the easy analysis of the prefabricated polymer before grafting. However, this method does not offer high grafting densities, because of steric hindrance of polymer chains that have to migrate to the surface. For the "grafting-through" strategy, the surface has to be modified with unsaturated units, that are incorporated in

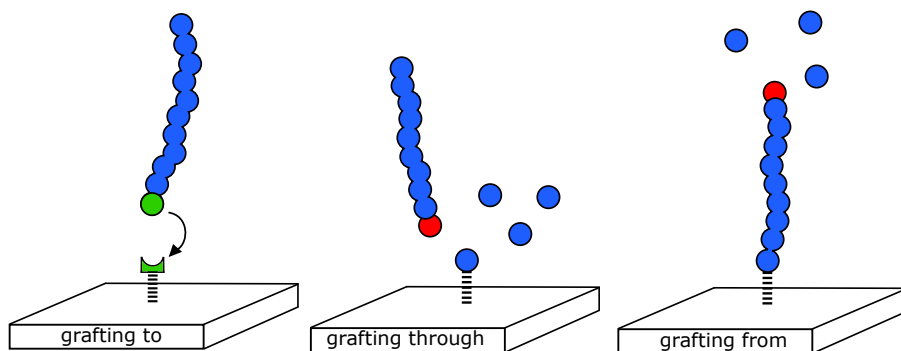


Figure 1.7: Schematic representations of possible methods for grafting polymers on surfaces (adapted from HÜBNER *et al.*).<sup>[79]</sup> Blue circles represent denote monomer units, the red circle a radical and the green forms compatible functional groups.

polymer chains propagating in solution. This is by far the least used method, since tailoring the structure of polymer films is difficult due to formation of polymer loops.<sup>[80]</sup> In the "grafting-from" approach, the surface is firstly functionalized with a radical initiator or more commonly with a RDRP control agent. This is the most used method for surface modification, since it combines high grafting density and a good control over the polymerization.<sup>[62,81]</sup>

## **Chapter II**

# **Surface-initiated RAFT polymerization – modification of bulk wood**



## 2 Preface

### 2.1 Reversible addition-fragmentation chain transfer (RAFT) polymerization

Reversible addition-fragmentation chain transfer (RAFT) polymerization proceeds via a reversible chain transfer between a chain-transfer agent (CTA or RAFT agent) and growing polymer chains. The RAFT process was developed by MOAD, RIZZARDO, and THANG in 1998.<sup>[82]</sup> Around the same time, "Macromolecular Design via the Interchange of Xanthates" (MADIX) was introduced by ZARD *et al.*, following the same reaction mechanism, but refers exclusively to xanthates (xanthic acid esters) as RAFT agents.<sup>[83,84]</sup>

A typical RAFT polymerization system consists of a conventional radical initiator, monomer, solvent (optional) and RAFT agent. RAFT agents consist of a reactive carbon–sulfur double bond, a stabilizing Z-group and an initiating R-group. The right choice of both groups is crucial to obtain a controlled polymerization and depends on the utilized monomer.<sup>[85]</sup> The R-group has to be a fast-fragmentating leaving group, that is quickly re-initiating the polymerization. Therefore, the R-group is often chosen to be structurally similar to the monomer.<sup>[86]</sup> The stabilizing Z-group determines the reactivity of the C=S double bond and hence the control over the polymerization.<sup>[87]</sup> The generic chemical structure of most commonly used RAFT agents are shown in Figure 2.1.

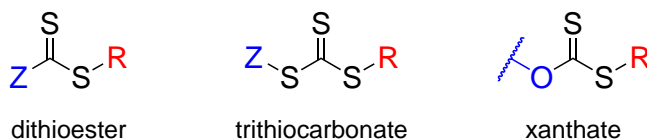


Figure 2.1: Generic chemical structure of academical important RAFT agents.<sup>[62]</sup>

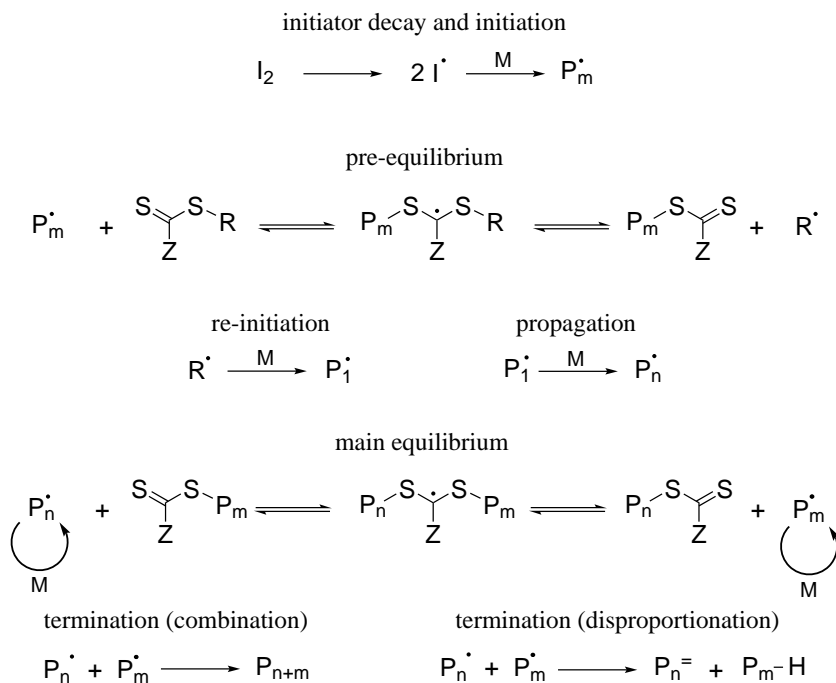
Typically used Z-groups are phenyl groups (in dithioesters) or alkylthio groups (in trithiocarbonates), guaranteeing a controlled polymerization of most monomers such as acrylates, methacrylates, acrylamides and styrenes.<sup>[88]</sup> However, less activated monomers (*e.g.* vinyl ester or vinyl amides), characterized by an electron-rich double bond or a lack of a radical-stabilizing substituent, require RAFT agents with a more unstable C=S double bond such as xanthates.<sup>[62,87]</sup> For the abovementioned reasons, RAFT polymerization is one of the most used academical used RDRP methods. It is performed with a wide range of monomers, in almost every solvent (even water), over a wide temperature and pressure range and in absence of a transition metal.<sup>[89]</sup> Furthermore, a great variety of RAFT agents are commercially available making the RAFT process easy to access.<sup>[86,90]</sup>

## 2.2 Mechanism of the RAFT process

The mechanism of the RAFT process basically follows the same elementary steps of a conventional radical polymerization: initiation, propagation and termination. However, these steps are superimposed by two RAFT equilibrium steps that create a dynamic equilibrium between dormant and active radical chains.<sup>[91]</sup> The general accepted mechanism of a RAFT polymerization is outlined in Scheme 2.1.

After the initiation step, the growing radicals quickly react with the chain transfer agent to form a tertiary radical intermediate (RAFT pre-equilibrium). The RAFT-centered radical either undergoes the reverse reaction regenerating the initial RAFT agent and the propagating radical ( $P_m^\bullet$ ) or fragmentate to a macromolecular RAFT agent and a radical R-group. The RAFT main equilibrium is reached when all R-groups have started propagating radical chains. This stage of the polymerization is characterized by a rapid exchange of growing polymer chains (active radical species) and those bound to a macromolecular RAFT agent (dormant radical species) resulting in the equal growth probability for all chains and therefore a low dispersity.<sup>[74,92]</sup> As for a conventional radical polymerization, termination reactions either take place by combination or disproportionation. However, these reaction are less likely due to a lower concentration of active radicals. All in all, the large majority of macromolecular chains carry a RAFT group, allowing for postmodification steps and a second radical polymerization to produce blockpolymers.<sup>[62,93]</sup>

## II Surface-initiated RAFT polymerization – modification of bulk wood



Scheme 2.1: Proposed general mechanism of RAFT polymerization. I represents an initiator fragment, M a monomer molecule, P a polymer chain, Z the stabilizing group and R the re-initiating leaving group.<sup>[94]</sup>

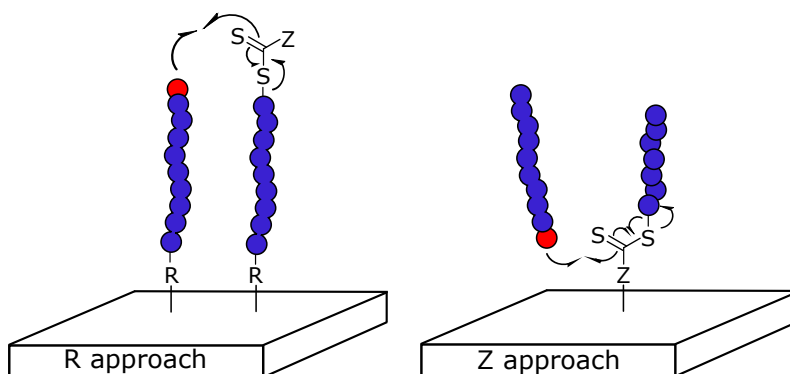
The theoretical number-weighted mean of molar mass of polymers in a RAFT polymerization is predicted using the Equation 2.1 assuming all polymer chains carry a RAFT group and all polymer chains carrying fragments of the initiator are neglected.<sup>[95]</sup>

$$\bar{M}_{n,theo} = \frac{X_M \cdot M_M \cdot c_M}{c_{RAFT}} + M_{RAFT} \quad (2.1)$$

Here,  $X_M$  represents the monomer conversion,  $M_M$  and  $M_{RAFT}$  are the molar masses of the monomer and the RAFT agent,  $c_M$  and  $c_{RAFT}$  the respective concentrations.<sup>[62]</sup>

## 2.3 Surface-initiated RAFT polymerization

Unlike other reversible-deactivated radical polymerization (RDRP) techniques, surface-initiated RAFT (SI-RAFT) polymerization offers two possibilities to attach polymer chains on surfaces. Due to the nature of a RAFT group, grafting is possible by attaching the RAFT agent to the surface via its R-group or its Z-group (see Scheme 2.2).<sup>[86]</sup>



Scheme 2.2: Schematic mechanism of surface-initiated RAFT polymerization via R and Z approach (adopted from HÜBNER *et al.*).<sup>[79]</sup>

Alternatively, it is possible to immobilize an initiator on the surface and add RAFT agent in solution. This however, leads to less controlled polymerizations, *e.g.* higher dispersities, because of a continuous initiation on the surface.<sup>[96]</sup> Tethering the RAFT agent via the R-group is referred to as the "grafting-from" approach. Addition of a radical to the tethered RAFT agent and subsequent fragmentation results in a surface-bound radical, that adds monomers. The RAFT agent is released from the surface and is either added to another radical on the surface or added to radical in solution.

Surface-attachment via Z-group is a unique feature of RAFT polymerization and it is considered as "grafting-to" approach, because the chains are growing exclusively in solution and the macromolecular radicals diffuse to the surface.<sup>[86,97]</sup> In this approach, a solution originated radical adds to the RAFT agent and the R-group is released, whereas the RAFT group always stays on the surface. The continuous exchange ideally results in a uniform molecular mass distribution

of free and surface-bound polymers. An important feature of the Z approach is the possibility of a facile cleavage of the polymer chains via addition of excess radicals or aminolysis.<sup>[92,98]</sup> In many cases, a so-called “sacrificial” RAFT agent is added to the solution, enhancing the overall control over the polymerization and indirectly providing the information about the molecular weight and dispersity of the grafted chains through the analysis of the untethered polymer. This untethered polymer, however, can be undesired since it has to be removed after the polymerization.<sup>[62,86]</sup>

In terms of wood modification via RAFT polymerization, only one example is known, in which wood fibers were immobilized with a xanthate via the R approach in a two step method.<sup>[99]</sup> Several examples are known for the modification of cellulose (as one of the main components of wood) via the R approach,<sup>[100–108]</sup> however only few examples utilize the Z approach.<sup>[109–112]</sup> Hereinafter, surface-attachment via the Z-group will be discussed in more detail, since this work is based on this method. The strategy of solid-supported RAFT polymerization via the Z-group was first introduced by PERRIER *et al.* on Merrifield resin and shortly after on silica particles by VANA *et al.* and PERRIER *et al.*<sup>[92,97,113,114]</sup> The immobilization of the CTA on both substrates were done in several reaction steps including intermediate work-up. Subsequently, the solid-supported CTAs were used to polymerize methyl acrylate, butyl acrylate, methyl methacrylate and styrene on the surface in a controlled manner. Polymerization of more reactive monomers, including vinyl acetate require xanthates as chain transfer agents to obtain a controlled polymerization. In 2008, PERRIER and VANA showed the first solid-supported MADIX polymerization allowing the controlled polymerization of vinyl acetate on Wang resin (a polymerbound benzyl alcohol).<sup>[21]</sup> The immobilization of the xanthate on the surface was done using 1,1'-thiocarbonyl diimidazole (TCDI). The decisive advantage of this method is the possibility to tether the chain transfer agent on the surface in an one-pot reaction with minimal reaction steps on the surface.<sup>[115]</sup>



## 3 Surface-initiated RAFT polymerization on wood

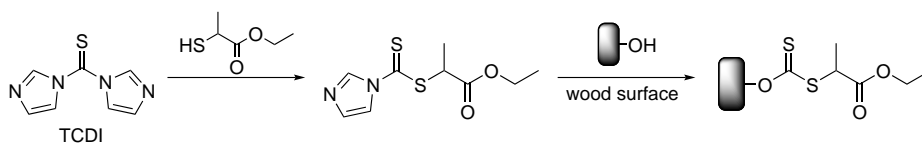
This chapter will focus on surface-initiated RAFT polymerizations via the Z approach on bulk wood using a xanthate moiety as RAFT agent. The one-pot immobilization of the RAFT agent using TCDI is based on the method introduced by PERRIER and VANA.<sup>[21,115]</sup> In this method, reactions at the surface are minimized since the intermediate is formed in solution and subsequently attaches to the surface, resulting in good yields and high purity of the surface-tethered MADIX agent.<sup>[87]</sup> The high amount of superficial hydroxyl groups originating from cellulose and hemicellulose function as reactive sites for the RAFT group attachment via esterification. This procedure allows the synthesis of a tailored polymer layer on wood surfaces in a controlled fashion forming a non-leaching coating on the surface.

Furthermore, the surface-tethered polymer can be easily separated from the wood surface and analyzed by SEC. Vinyl acetate and methyl acrylate were chosen as monomers. Poly(vinyl acetate) (PVAc) is a rubbery thermoplastic polymer that is commonly used as wood glue, glue in paper or bookbinding and as adhesive for porous structures.<sup>[116]</sup> Additionally, PVAc can function as precursor for polyvinyl alcohol and poly(vinyl acetate phthalate), which are important polymers in coating applications.<sup>[100]</sup> In addition to these outstanding adhesive properties, PVAc is considered as a good substitute for widely used formaldehyde-based wood adhesives, because of its biodegradability under certain conditions.<sup>[117]</sup> Surface-initiated polymerization of methyl acrylate yields a soft rubbery polymer on the wood surface greatly increasing the hydrophobicity. A higher hydrophobicity results in a slower water uptake and therefore less dimensional damages by swelling and shrinking of wood.

The chapter is divided in three sections. The first section addresses the immobilization of the RAFT agent on the surface, the second section focuses on the surface-initiated polymerization whereas the third section concentrates on the detachment and analysis of the surface-tethered polymer.

### 3.1 Immobilization of the RAFT agent

The surface modification of wood is a demanding task since it is not soluble in any solvent due to its hierachically complex and heterogenous structure on both the micrometer and nanometer scale (as can be seen in the Introduction 1.1.2). However, the one-pot method introduced by PERRIER and VANA offers a simple solution for the immobilization of the xanthate with minimal reaction steps on the wood surface.<sup>[21]</sup> In a typical experiment, a dried wood cube (1 cm × 1 cm × 0.5 cm) was modified based on a successive transesterification step of TCDI with first ethyl 2-mercaptopropionate and second with surface-bound hydroxyl groups of the wood. The general reaction sequence is outlined in Scheme 3.1.



Scheme 3.1: Stepwise synthesis of the CTA on bulk wood.

Several reaction conditions were studied for the immobilization of the RAFT agent, including pretreatment of wood with NaOH to increase the accessibility of hydroxyl groups, variation of the molar ratio of TCDI to wood, a higher reaction temperature and longer reaction times. Eventually, a molar fraction of TCDI of 20 mmol / g wood and toluene (tol) as solvent provided sufficient good and more importantly reproducible results. Toluene, which is known to hardly swell wood cells, was chosen as a nonpolar solvent.<sup>[44]</sup> Therefore it hinders penetration of reagents into wood cells, which in this case is important, since only surface modification is intended. However, toluene limits the hydroxyl accessibility, making immobilization of the RAFT agent more challenging.

Elemental analysis (EA) and attenuated total reflectance Fourier-transform infrared (ATR-FTIR) spectroscopy were used to evaluate the success of the immobilization reactions since the measurement of weight gains were not significant due to leaching of wood components and the low amount of formed xanthates. After modification, the wood sample was intensively washed with the respective solvent and tetrahydrofuran, dried at 105 °C under reduced pressure and kept in a desiccator. The quality of the immobilization with respect to ATR-FTIR spectroscopy was determined by comparing the intensity of vibrations originating from wood and vibrations originating from the xanthate.

2-Ethoxythiocarbonylsulfanyl-propionic acid ethyl ester, a xanthate bearing an ethoxy moiety as Z-group was used as reference (in the following section referred as free xanthate). The recorded spectra of untreated wood (A), free xanthate (B) and xanthate-modified wood (C) are shown in Figure 3.1.

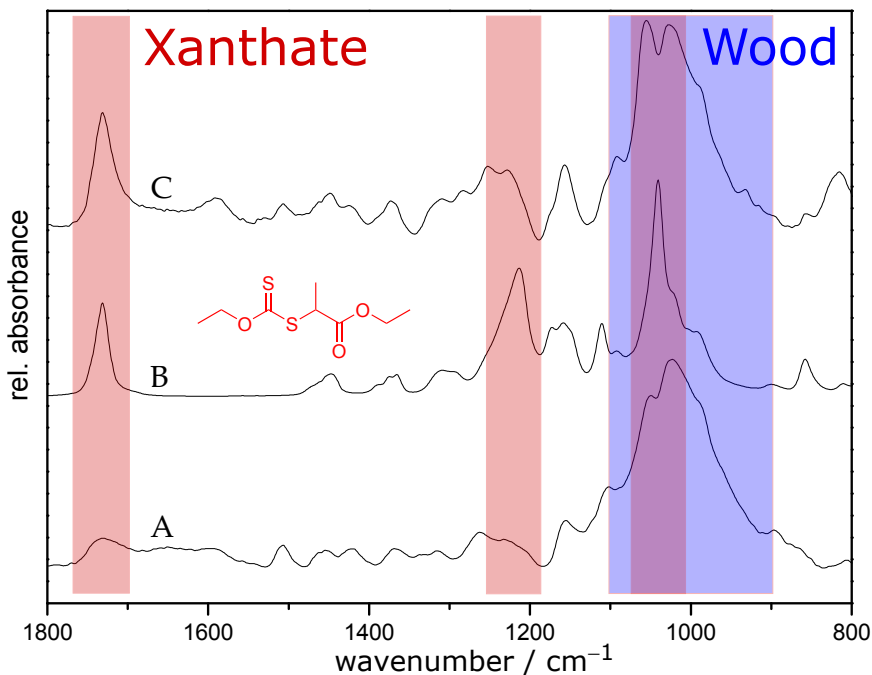


Figure 3.1: ATR-FTIR spectra of untreated wood (A), free xanthate (B) and xanthate-modified wood (C). Spectra are normalized to the highest peak ( $1030\text{ cm}^{-1}$ ).

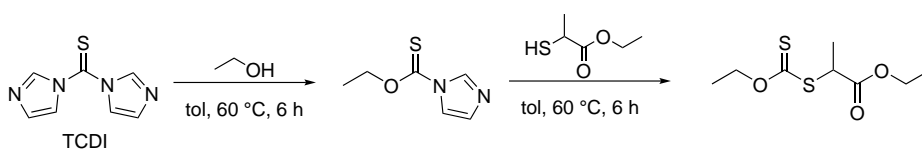
The untreated wood sample showed a small peak at  $1730\text{ cm}^{-1}$ , which corresponds to C–O stretch vibrations of hemicellulose. Minor peaks were found at  $1250\text{ cm}^{-1}$ , in the range of  $1600 - 1500\text{ cm}^{-1}$  and  $1450 - 1350\text{ cm}^{-1}$ , representing C=C stretch vibrations of lignin, C–H deformation modes and skeletal vibrations of lignin, respectively. Finally, an intense broad peak of C–O vibrations of cellulose and hemicellulose was found at  $1030\text{ cm}^{-1}$ .<sup>[118]</sup> The free xanthate exhibited distinct peaks at  $1731\text{ cm}^{-1}$ ,  $1214\text{ cm}^{-1}$ ,  $1160\text{ cm}^{-1}$ ,  $1040\text{ cm}^{-1}$  and  $859\text{ cm}^{-1}$ . The intense peak at  $1731\text{ cm}^{-1}$  was assigned to the C=O stretching mode of the ester moiety, whereas the assignment of the peaks at  $1214\text{ cm}^{-1}$  and at  $1040\text{ cm}^{-1}$  are more difficult. The peaks correspond to the C=S and C–O–C stretching

### 3.2 Surface-initiated RAFT polymerization

modes, however, the location is strongly dependent on the substituents. The peak at  $1160\text{ cm}^{-1}$  represents C–O stretching from the ester and the small peak at  $850\text{ cm}^{-1}$  corresponds to the C–S stretching mode.<sup>[119,120]</sup> A successful modification of wood with xanthate is seen by an intense carbonyl peak at  $1731\text{ cm}^{-1}$ , two broad peaks in the range of  $1250 - 1200\text{ cm}^{-1}$  and a sharp peak at  $1054\text{ cm}^{-1}$ . The quality of the immobilization was determined by the intensity of the carbonyl signal ( $1731\text{ cm}^{-1}$ ) relative to the wood peak at  $1030\text{ cm}^{-1}$ . Additionally, elemental analysis of the xanthate-modified wood was conducted of a  $100\text{ }\mu\text{m}$  thick cut from the surface, revealing a sulfur content of 3.4%. To summarize, ATR-FTIR spectroscopy and elemental analysis showed that the immobilization of a xanthate as RAFT agent on the wood surface was successful.

## 3.2 Surface-initiated RAFT polymerization

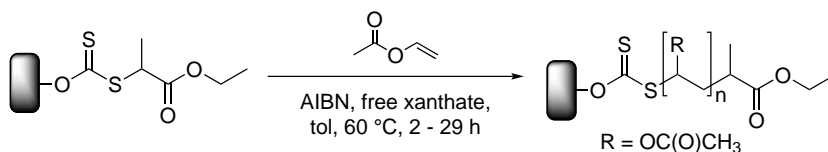
After a successful immobilization of a xanthate moiety on the wood surface as described in Section 3.1, vinyl acetate and methyl acrylate were polymerized on the surface in the presence of a free xanthate (ethyl 2-ethoxythiocarbonylsulfanyl-propionic acid ethyl ester). The synthesis was conducted according to literature and is outlined in Scheme 3.2.<sup>[115]</sup> It was shown, that in solution initial monosubstitution of TCDI with ethyl 2-mercaptopropionate and following addition of an alcohol did not result in the formation of a xanthate, but in formation of a symmetrical thiocarbonyl compound by displacement of the secondary thiol.<sup>[115]</sup> In case of a surface modification as described in Section 3.1, this displacement is highly unlikely, since the hydroxyl groups are fixed on the surface and are spatially separated.<sup>[21]</sup>



Scheme 3.2: Synthesis of the free xanthate (2-Ethoxythiocarbonylsulfanyl-propionic acid ethyl ester) according to literature.<sup>[115]</sup>

With free xanthate at hand, the surface-supported polymerization of vinyl acetate and methyl acrylate was accomplished. The focus of the polymerization was the synthesis of a functional polymer layer on the surface of wood rather

than an in depth monitoring of the kinetics. The polymerization of vinyl acetate was conducted exclusively in solution for comparison and in the presence of surface-tethered xanthate. If xanthate-modified wood was added, the amount of surface-tethered xanthate compared to sacrificial xanthate was neglected. The reaction conditions of the polymerization are outlined in Scheme 3.3.



Scheme 3.3: Solid-supported MADIX polymerization on wood.

It is important to take into account, that the addition of wood in the reaction solution can have an influence on the polymerization since lignin act as a radical trap due to its polyphenolic structure.<sup>[99,121]</sup> The conversion was determined gravimetrically and the polymer in solution was analyzed by SEC. The wood specimen was washed with toluene and extracted via a Soxhlet extraction with DCM after the polymerization to remove remaining monomer, solvent and untethered polymer.

Figure 3.2 shows the molar mass distributions and dispersities of the untethered polymer as a function of monomer conversion. The black line refers to the theoretical number-weighted molar mass estimated via Equation 2.1 in Section 2.2. The black squares represent drawn samples of the polymerization in the absence of surface-tethered xanthates. It can be seen from the data, that the molar mass increased linearly with progressing conversion. The dispersity ranged between 1.2 and 1.5 confirming a controlled radical polymerization in solution. The red dots exhibit drawn samples from the solution in the presence of surface-tethered xanthate. This surface-supported polymerization also showed its living character by linear increasing molar mass with progressing monomer conversion and dispersities between 1.2 and 1.5. Both parameters did not differ significantly from the values obtained in the absence of xanthate-modified wood, which shows that the addition of modified wood did not significantly influence the polymerization.

### 3.2 Surface-initiated RAFT polymerization

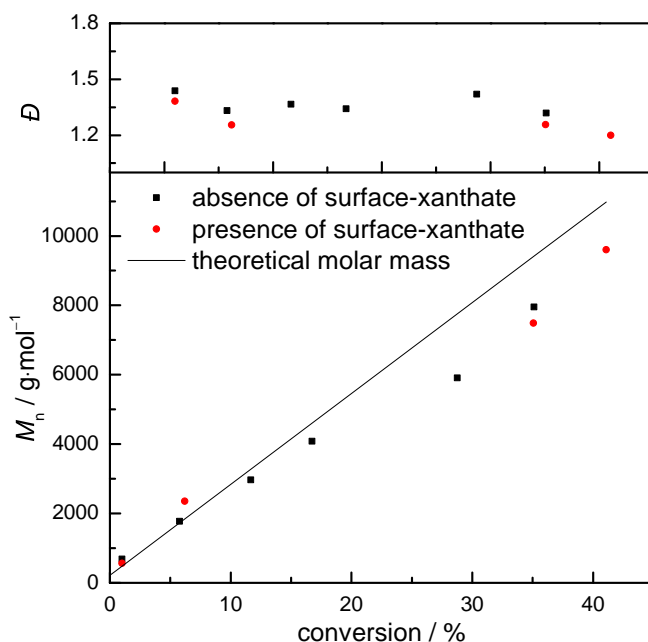


Figure 3.2: Comparison of molar mass and dispersity of the polymerization of PVAc in the presence or absence of xanthate-modified wood (RI detector).

In a different approach, methyl acrylate was polymerized on the surface with the same procedure to obtain a hydrophobic polymer layer on the wood surface. Since acrylates have a higher polymerization rate than vinyl esters, the polymerization time was reduced to 5.5 h. The monomer conversion of 73 % was determined gravimetrically and the molar mass of 26000 g mol<sup>-1</sup> and dispersity of 1.7 were obtained via SEC. The surface properties of both PVAc and PMA coated wood species were investigated via ATR-FTIR spectroscopy and the spectra are shown in Figure 3.3. Both spectra of the polymer-coated specimens showed distinct polymer-specific peaks. The PVAc-modified sample showed an increased carbonyl stretching vibration at 1735 cm<sup>-1</sup>, a CH<sub>3</sub> asymmetric deformation mode of vibration at 1373 cm<sup>-1</sup> and a C-H in-plane bending vibrational mode at 1233 cm<sup>-1</sup>.<sup>[122]</sup> The PMA-modified sample showed an increased carbonyl stretching vibration at 1725 cm<sup>-1</sup>, a symmetric bending vibration of a methyl group at 1435 cm<sup>-1</sup> and skeletal vibrations between 1250 cm<sup>-1</sup> and 1150 cm<sup>-1</sup>.<sup>[123]</sup>

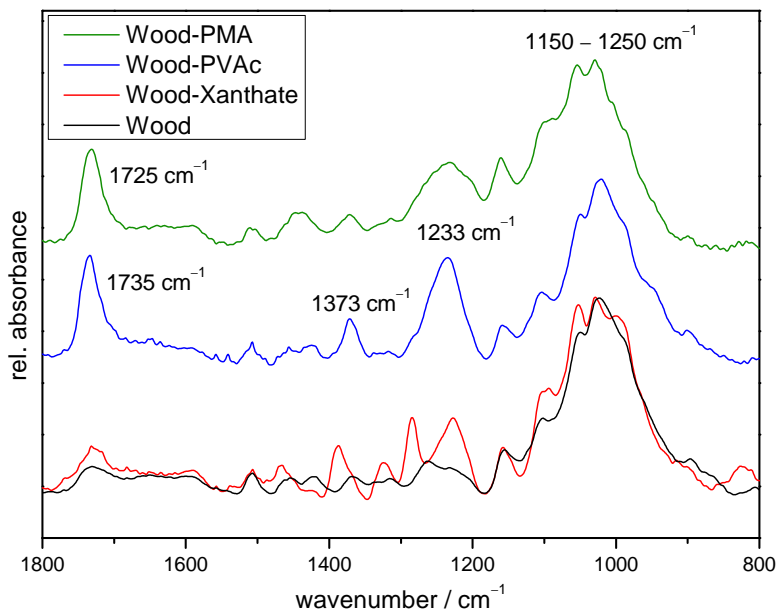


Figure 3.3: Recorded ATR-FTIR spectra of untreated wood, xanthate-modified wood, PVAc-coated wood (polymerization time 29 h) and PMA-coated wood (polymerization time 5.5 h). Spectra are normalized on highest peaks.

Additionally, water contact angle measurements were performed to obtain more information about the surface texture of the unmodified and modified wood cubes. A water droplet is casted on the surface of the substrate and the contact angle formed between the solid-liquid interface is recorded. A smaller contact angle indicates a stronger hydrophilicity of the surface. All experiments were performed with dried sample at the same temperature and humidity. Pictures were taken instantly when the water droplet hit the surface (see Figure 3.4).

In order to assess the permeability of the polymer coating, changes of the contact angle were tracked over a period of 10 s as can be seen in Figure 3.5. The unmodified wood surface started with a water contact angle of  $96^\circ$ , but rapidly decreased to  $74^\circ$  after 10 s and depicted even further until the droplet was fully soaked in. The relatively high contact angle was not expected because wood is intrinsic hydrophilic due to its surface hydroxyl groups. However, the behavior

### 3.2 Surface-initiated RAFT polymerization

---

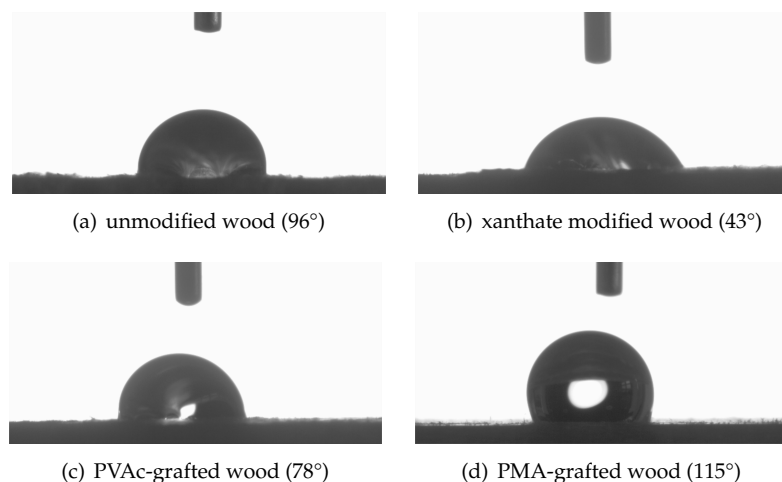


Figure 3.4: Water contact angles of unmodified wood, xanthate-modified wood, PVAc-grafted wood and PMA-grafted wood taken instantly after contact.

is explained by the dried condition, where the hydroxyl groups are collapsed and therefore less accessible. After xanthate immobilization, the wood surface became more hydrophilic, resulting in a lower contact angle of 43° compared to the start. The contact angle dropped quicker than in untreated wood to 25° in 10 s. This may be due to structural changes on the surface caused by esterification, which can have an impact on microstructure of wood, such as the crystallinity of cellulose. Surface-initiated polymerization with vinyl acetate raised the contact angle to 78°, maintaining it over the period of 10 s. This result is consistent, considering that poly(vinyl acetate) is a slightly hydrophobic polymer and a polymer layer smoothens the surface (covers cracks), reducing the angle of attack for water. Grafting of poly(methyl acrylate) lead to an intense hydrophobization of the surface, resulting in a constant water contact angle of 115° over several minutes.

Furthermore, TGA experiments were conducted to obtain more information about the polymer layer on the surface. In a typical experiment, a 100  $\mu\text{m}$  thick cut of the surface was heated from room temperature to 1000 °C under a nitrogen atmosphere and the mass loss of the sample was measured over time as the temperature increased. This method gives insights in the thermal behav-

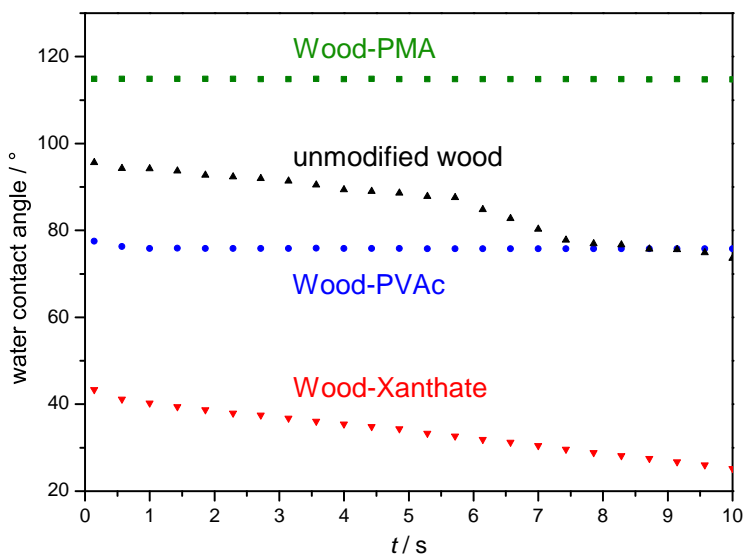


Figure 3.5: Evolution of the water contact angle over time of unmodified wood, Wood-Xanthate, Wood-PVAc and Wood-PMA.

ior of the sample, providing rough information about the composition due to the heterogenous structure of wood. Figure 3.6 shows the thermograms and derived thermograms of unmodified wood, xanthate-modified wood (Wood-Xant), polymer-grafted wood (Wood-PVAc and Wood-PMA), poly(vinyl acetate) (PVAc,  $9000 \text{ g mol}^{-1}$ ) and poly(methyl acrylate) (PMA,  $25000 \text{ g mol}^{-1}$ ). The corresponding decomposition temperatures ( $T_{\text{on}}$ : onset degradation temperature,  $T_{\text{max}}$ : temperature at the maximal degradation state) and residual masses (RM) at  $1000 \text{ }^{\circ}\text{C}$  are summarized in Table 3.1.

Untreated wood (black line) started to degrade sharply at  $180 \text{ }^{\circ}\text{C}$  with a maximum at  $360 \text{ }^{\circ}\text{C}$  and a total mass loss of 71 %. After that sharp stage, at approximately  $380 \text{ }^{\circ}\text{C}$ , wood decomposed with a slower steady rate, until a residual mass of 13 % at  $1000 \text{ }^{\circ}\text{C}$ . These results are in good agreement with decomposition measurements of the three main components of wood (cellulose, hemicellulose and lignin). The degradation of cellulose and hemicellulose, that makes up to 70 – 80 % of the mass, takes place at a high rate at  $200 - 380 \text{ }^{\circ}\text{C}$  and  $250 - 380 \text{ }^{\circ}\text{C}$ , whereas lignin slowly decomposes at  $180 - 900 \text{ }^{\circ}\text{C}$ .<sup>[12,124]</sup> Modification of the wood surface with xanthate (red line) resulted in a two-step-degradation profile. The decomposition started earlier compared to untreated wood at  $100 \text{ }^{\circ}\text{C}$  with

### 3.2 Surface-initiated RAFT polymerization

---

a higher pace. This behavior could be caused by structural changes due to the immobilization reaction and decomposition of the xanthate group, which is not stable at this temperature.<sup>[125]</sup> The mass loss reached almost the same value as untreated wood at 380 °C, but went through two maxima at 220 °C and 350 °C. The residual mass at 1000 °C barely changed to 11 % in comparison with untreated wood. Pure PVAc (black dashed line) exhibited a two-step degradation profile, that was caused by first deacetylation and second chain scission.<sup>[126]</sup> The first step shows an onset temperatures of 220 °C with a maximum at 330 °C and the second step displays a maximum at 450 °C. PMA (black dashed line) starts to decompose at 240 °C, followed by intense degradation peaks with maximum at 400 °C.

Unlike wood, both polymers decomposed nearly completely at 1000 °C to residual masses of 1.0 %, respectively. The polymer-grafted samples (blue lines) likewise exhibited two-step-degradation profiles but with increased onset temperatures, similar maximal degradation temperature, but lower residual masses compared to Wood-Xanthate (red curve). The grafted samples showed onset temperatures of 140 °C (Wood-PVAc) and 120 °C (Wood-PMA) with less degradation before 220 °C compared to Wood-Xant and therefore are thermally more stable after polymerization. The residual masses of these composites were 5 % and 2 % at 1000 °C. Overall, the residual mass decreased with each subsequent modification step, since the relative amount of lignin, as heat-resistant component, decreased. In conclusion, TGA measurements showed that immobilization of the RAFT agent and successive surface-initiated polymerization of vinyl acetate and methyl acrylate were successful. The polymer-grafted samples exhibit thermal properties, that may be interpreted as a combination of the thermal properties of both individual components wood and polymer.

## II Surface-initiated RAFT polymerization – modification of bulk wood

---

Table 3.1: Thermal degradation temperatures of untreated wood, xanthate-modified wood, PVAc-grafted wood, PMA-grafted wood, pure PVAc and pure PMA

	$T_{\text{on}} / ^\circ\text{C}$	$T_{\text{max}} / ^\circ\text{C}$	RM / %
Wood	180	- 360	13
Wood-Xant	100	220 350	11
Wood-PVAc	140	220 340	5
PVAc	220	- 330	1
Wood-PMA	120	250 340	2
PMA	240	- 400	1

---

### 3.2 Surface-initiated RAFT polymerization

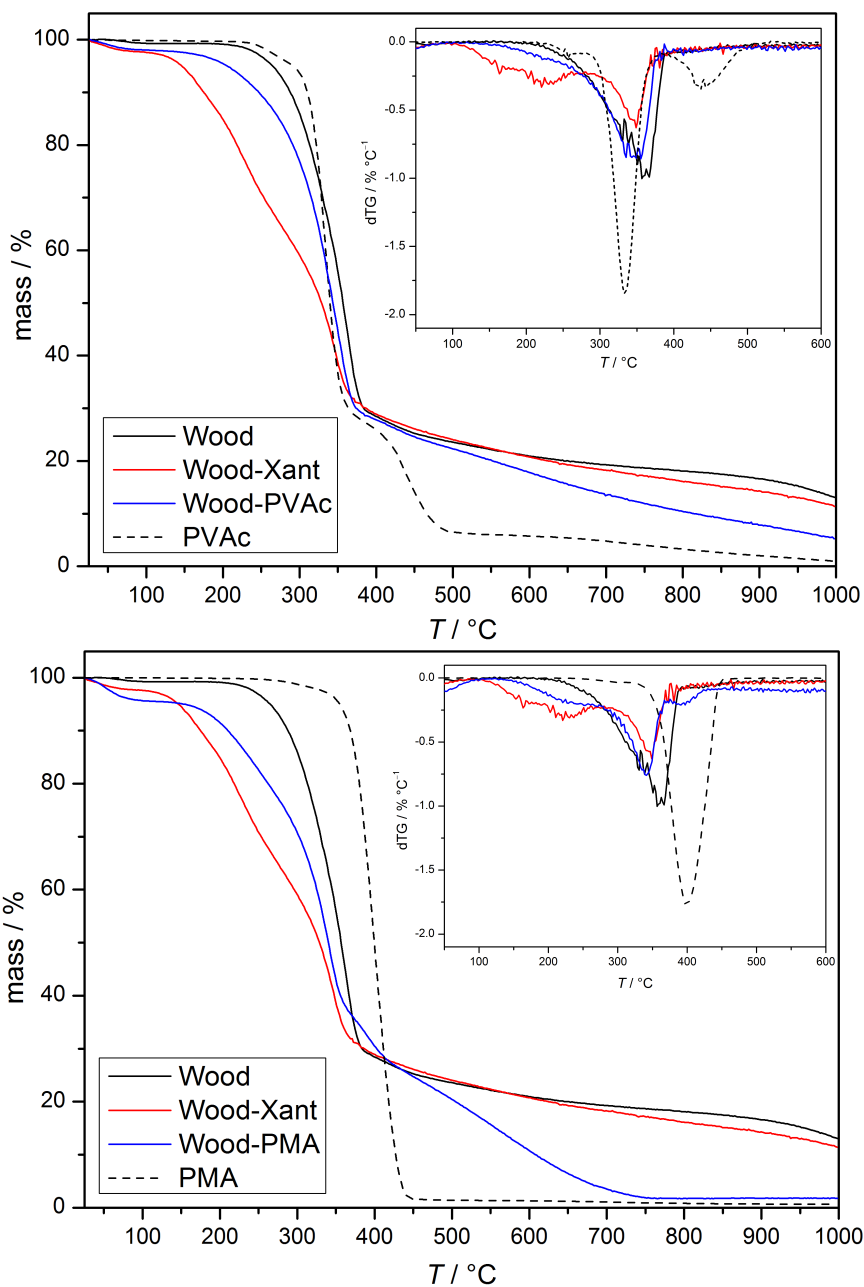
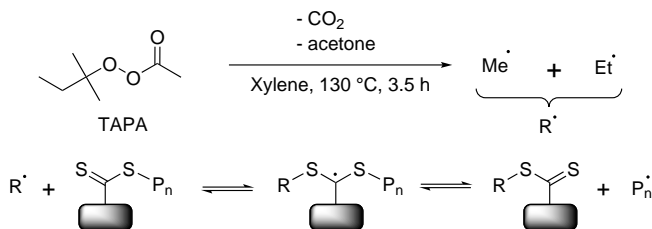


Figure 3.6: Thermograms of untreated wood, xanthate-modified Wood, PVAc-grafted wood, PMA-grafted wood, pure PVAc and pure PMA.

## 4 Cleavage of tethered polymer

To obtain a recyclable wood-polymer composite, it is necessary to remove the polymer from the wood surface. Additionally, the detached polymer can be examined via SEC and the molar masses and dispersities can be compared to the values obtained from the polymer in solution. The unique feature of the tethered RAFT agent via the Z approach offers the possibility to cleave off the polymer via either aminolysis or an addition-fragmentation chain transfer step.

The aminolysis of PVAc-grafted wood was not successful, since amines are good swelling agents for wood and react with nucleophilic moieties of wood.<sup>[44]</sup> Alternatively, treating the PVAc-grafted wood surface with an excess of a radical initiator in absence of monomer resulted in an intact wood surface bearing RAFT groups and detached polymer chains. Before treatment, the respective sample was washed extensively via Soxhlet extraction to remove any untethered polymer. The extraction was repeated until no polymer was detected in the extraction solution by SEC. It is important to use a radical initiator producing primary radicals, which are better leaving groups than the macromolecular species. 2-Cyano-isopropyl radicals generated by AIBN are more stable than polyvinyl acetate radicals and therefore not suitable. *tert*-Amyl peroxyacetate (TAPA) forms primary methyl and ethyl radicals, offering the necessary instability to release the polymer from the surface.<sup>[21,127]</sup> Consequently, grafted wood was treated with an excess of TAPA to remove the polymer from the wood surface (see Scheme 4.1).



Scheme 4.1: Radical induced removal of the surface-tethered polymer.

### 3.2 Surface-initiated RAFT polymerization

The wood specimen was filtered off and extensively washed with DCM. The detached polymer was examined via SEC and compared to the polymer in solution formed during polymerization (as described in Section 2.3). The molecular weight distributions of both tethered and untethered polymer are shown in Figure 4.1. The dispersity of both polymers are well below 1.5 indicating that both polymerizations were well-controlled.<sup>[90]</sup> It is important to note, that the untethered polymer did not feature an UV signal, which is in agreement with cleavage of the RAFT group. The untethered polymer showed a lower molecular mass compared to the polymer in solution. This result is explained by considering the underlying mechanism of a RAFT polymerization via a Z-group approach.

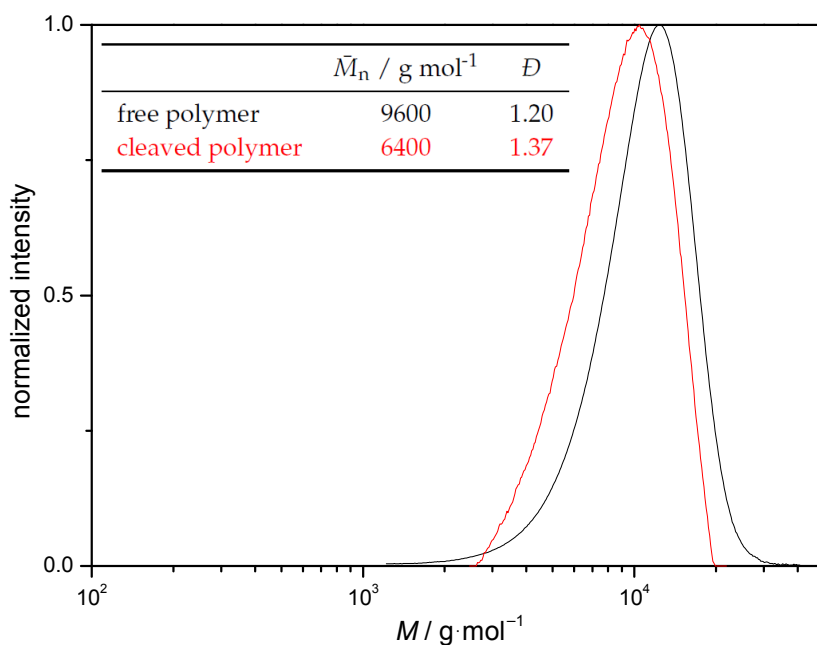


Figure 4.1: Molecular weight distribution of TAPA cleaved polymer (RI signal). The polymerization was conducted with a molar ratio of monomer : sacrificial CTA : initiator of 300 : 1 : 0.1 in 50 vol% toluene at 60 °C and a conversion of 35 %.

A growing polymer chain can undergo two competitive reactions. It either takes part in a polymerization reaction in solution (propagation, termination and chain transfer) or adds to the surface-bound RAFT agent. Polymer chains bound to the surface are captured in the dormant state, whereas radical chains in solution permanently grow.<sup>[21,114]</sup> With increasing conversion and hence longer polymer chains, the accessibility of surface-tethered xanthate gets more limited due to steric shielding of the bound polymer chains. Additionally, the rate of addition-fragmentation reactions on the surface is significantly lowered compared to the rate in solution.<sup>[128,129]</sup> Both effects lead to higher molecular weight values of the polymer in solution compared to the grafted polymers.<sup>[97,114]</sup>

The surface was analyzed via ATR-FTIR spectroscopy before and after removal of tethered polymer. The spectra of PVAc-grafted wood, pure PVAc, TAPA-treated wood and untreated wood are displayed in Figure 4.2. The red curve represents the surface of the TAPA-treated wood sample. Important changes are found at  $1233\text{ cm}^{-1}$ ,  $1370\text{ cm}^{-1}$  and at  $1735\text{ cm}^{-1}$  (red regions).<sup>[122]</sup>

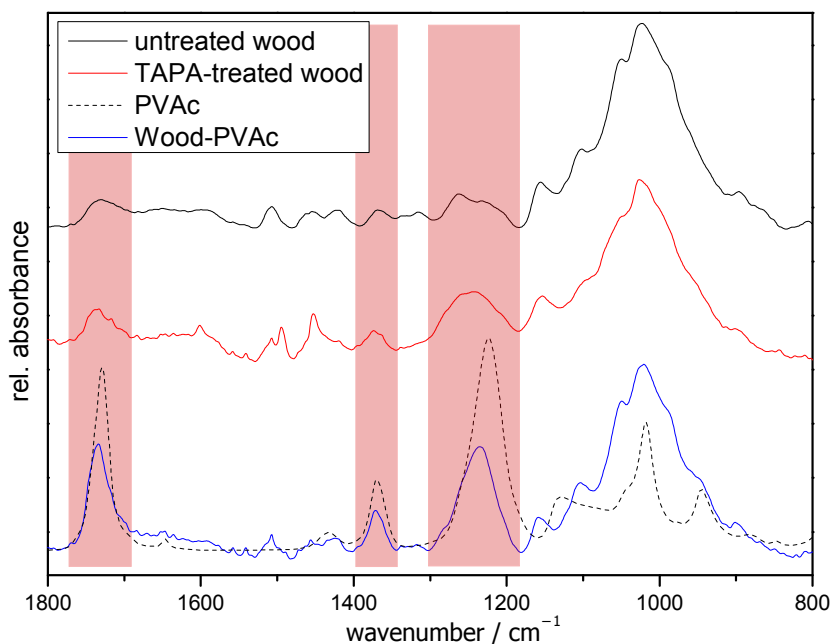


Figure 4.2: Recorded FTIR spectra of Wood-PVAc, pure PVAc, TAPA-treated wood and untreated wood.

### 3.2 Surface-initiated RAFT polymerization

---

All peaks are significantly lowered after the TAPA treatment relative to Wood-PVAc, indicating the successful removal of the polymer. Due to the underlying addition-fragmentation chain transfer mechanism, the wood surface is still covered with xanthate moieties bearing ethyl or methyl as R group. The presence of these xanthate moieties explain a remaining broad peak at  $1233\text{ cm}^{-1}$  corresponding to C=S double bonds.<sup>[119,120]</sup>

## 5 Conclusions of Chapter II

The surface modification presented in this chapter showed a simple way to introduce a non-leaching polymer coating on wood surfaces, enhancing hydrophobicity of the surface. When desired, the polymer coating and wood is easily separated afterwards resulting in a possible re-use or recycling of wood.

In summary, the surface of bulk wood was successfully modified with a xanthate moiety via the Z approach using TCDI in a one-pot reaction. The method offers an easy way to introduce a xanthate moiety on wood with minimal reactions steps on the surface.<sup>[21]</sup> The successful immobilization was confirmed by ATR-FTIR spectroscopy and elemental analysis. Afterwards, surface-initiated polymerizations of vinyl acetate and methyl acrylate were conducted in the presence of a free CTA to improve the control over the molecular weight and dispersity. Analysis of the polymer formed in solution revealed a well-controlled living radical polymerization. The molecular weight of the polymer increased linearly with progressing monomer conversion, being in good agreement with theoretical obtained values and the dispersities scattered around 1.4. The successful surface-supported polymerization was demonstrated by ATR-FTIR spectroscopy, WCA measurements and TGA. ATR-FTIR spectroscopy showed the appearance of polymer-specific signals, predominantly the carbonyl vibration at  $1730\text{ cm}^{-1}$ . WCA measurements showed a significant change of the surface texture.

Grafting of poly(vinyl acetate) and poly(methyl acrylate) presented a contact angle of  $78^\circ$  and  $115^\circ$ , respectively which were maintained for several minutes, whereas unmodified wood exhibited a quick absorption of the water droplet. TGA revealed a significant change of thermal behavior of the modified wood surface indicated by lower onset temperature compared to untreated wood. The grafted polymer was cleaved from the wood surface by a radical induced single addition-fragmentation chain transfer step. The cleaved polymer showed a narrow molecular weight distribution and a molar mass, that was similar to the results obtained from the polymer formed in solution.



## **Chapter III**

# **Surface-initiated ARGET ATRP of wood flour**



## 6 Preface

### 6.1 Atom transfer radical polymerization (ATRP)

Atom transfer radical polymerization (ATRP) is one of the most applied reversible-deactivation radical polymerization techniques. Particularly, the broad range of commercially available monomers, simple experimental setup, readily available initiators and catalysts contributed to its popularity in both industry and academia.<sup>[130,131]</sup> A conventional ATRP system consists of four components: monomer, initiator, catalyst and solvent. Generally, ATRP is very tolerant to various functional groups including hydroxy, amino, ester, epoxy, and others.<sup>[131]</sup> Therefore, plenty of monomers such as styrenes,<sup>[132]</sup> (meth)acrylates<sup>[133–135]</sup> and many more<sup>[131]</sup> have been successfully polymerized.

ATRP initiators are compounds with weak halogen-carbon or halogen-heteroatom bonds ( $R-X$ ), most commonly alkyl halides.<sup>[19]</sup> Ligand-stabilized transition metals act as catalysts. The transition metal must have two adjacent oxidation states and the ligand should complex the metal relatively strongly. Copper is the most investigated metal in ATRP, because of its low cost and suitability to a wide range of monomers.<sup>[136–139]</sup> However, other metals including iron, palladium, rhenium, ruthenium and nickel have been deployed.<sup>[131]</sup> Typically, ligands are multidentate nitrogen or phosphorus based molecules that strongly influence the catalytic activity of the complex as well as its solubility especially in organic solvents.<sup>[19]</sup> The application of highly active catalysts is preferable, because it allows for less catalyst loading, which is highly desirable with regard to toxicology and economics.

#### Mechanism of ATRP<sup>[130]</sup>

The mechanism of a conventional ATRP is shown in Scheme 6.1. The polymerization occurs through a reversible redox process involving the transition metal and an alkyl halide. The dormant species (an alkyl halide  $R-X$ ) is activated by an activator via halogen transfer. Activators are ligand-stabilized transition



## Kinetics of ATRP<sup>[130]</sup>

The polymerization rate  $R_p$  of ATRP under equilibrium conditions is given by Equation 6.1, assuming that termination and side reactions are negligible and initiation is rapid (steady-state kinetics).<sup>[130]</sup>

$$R_p = k_p \cdot [M] \cdot [P_n^\bullet] = k_p \cdot K_{\text{ATRP}} \cdot [M] \cdot [R-X] \cdot \frac{\text{Mt}^m}{\text{Mt}^{m+1}} \quad (6.1)$$

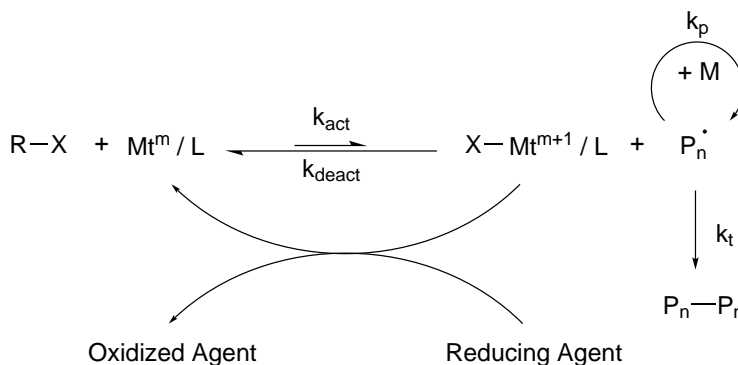
The polymerization rate depends on the propagation rate constant  $k_p$ , the concentration of monomer  $[M]$  and propagating chains  $[P_n^\bullet]$ . The concentration of propagating chains depends on the ATRP equilibrium constant  $K_{\text{ATRP}}$ , as well as the concentration of the activator  $\text{Mt}^m/L$ , deactivator  $X-\text{Mt}^{m+1}/L$  and dormant species  $R-X$ . Equation 6.1 shows that the rate of polymerization is not dependent on the absolute catalyst concentration, but rather on the ratio of concentrations of activator and deactivator. However, a sufficient concentration of deactivator ( $[X-\text{Mt}^{m+1}/L]$ ) is important to obtain a well-controlled polymerization yielding a low dispersity  $D$  as can be seen in Equation 6.2.<sup>[143]</sup>

$$D = 1 + \frac{k_p [RX]_0}{k_{\text{deact}} [X-\text{Mt}^{m+1}/L]} \left( \frac{2}{\text{conv.}} - 1 \right) \quad (6.2)$$

Additionally, the dispersity decreases with conversion, with smaller initial concentration of the alkyl halide  $[RX]_0$  and with decreasing ratio of  $k_p$  to  $k_{\text{deact}}$ .<sup>[130,142]</sup> Following Equation 6.1 and Equation 6.2 it is clear, that there is a trade-off between polymerization rate and control over the polymerization. Nevertheless, a low catalyst loading is not only highly desirable with regard to toxicological and economic concerns, but it also avoids high radical concentrations leading to a lower rate of polymerization due to undesired radical termination. Over the last years, several novel ATRP techniques were invented to decrease the amount of transition metal, among them activators regenerated by electron transfer (ARGET) ATRP,<sup>[22,144]</sup> initiators for continuous agent (ICAR) ATRP,<sup>[145]</sup> supplemental activator and reducing agent (SARA) ATRP,<sup>[146]</sup> photochemically mediated ATRP,<sup>[147]</sup> and eATRP, where  $K_{\text{ATRP}}$  is controlled electrochemically.<sup>[148]</sup>

## 6.2 Activators regenerated by electron transfer (ARGET) ATRP

Activators regenerated by electron transfer (ARGET) ATRP is a novel technique, relying on a slow and steady *in situ* regeneration of the activator species by an auxiliary reducing agent. In an ARGET ATRP system with copper as transition metal, the catalyst is introduced in its oxidatively stable and inactive Cu(II) form and will be reduced to the active Cu(I) form throughout the polymerization as can be seen in Scheme 6.2.<sup>[22]</sup> Due to the permanent activator (re-)generation, ARGET ATRP is performed with a significantly reduced amount of copper (down to 10 ppm) and in the presence of minor amounts of oxygen.<sup>[22]</sup>



Scheme 6.2: Mechanism of ARGET ATRP.<sup>[144]</sup>

Careful selection of a reducing agent with a suitable oxidation potential is important, because the use of a strong reducing agent will result in a high activator concentration and therefore poor control over the polymerization due to a higher likelihood of termination reactions. Ascorbic acid (AsAc) is one of the most commonly utilized environmentally-friendly reducing agents. However, AsAc is a very strong reducing agent, that will rapidly reduce the deactivator and consequently promote the polymerization rate as well as lower the control over the molecular weight distribution. The strength of ascorbic acid is reduced by using a reaction medium offering limited solubility such as anisole. Alternatively, weaker reducing agents *e.g.* tin(II) 2-ethylhexanoate (Sn(EH)<sub>2</sub>) are used.<sup>[144,149]</sup> Additionally, the molar ratio of ligand versus copper is important in an ARGET ATRP system. Since the catalyst loading is very low compared to

the concentration of solvent, monomer and reducing agent, an excess of ligand ensures the formation of the intended metal ligand complex (Mt / L).<sup>[150,151]</sup>

Another advantage of ARGET ATRP is the significant reduction of copper induced side reactions such as organometallic-mediated radical polymerization (OMRP) or outer-sphere electron-transfer (OSET) reactions. The former relies on a fast reversible homolytic cleavage of a transition metal-carbon bond, where the ATRP catalyst is in the low oxidation state and acts as a radical trap.<sup>[152-154]</sup> The latter describes the reduction of an active growing radical to a carbanion by an ATRP catalyst in the low oxidation state. Accordingly, ARGET ATRP is a powerful tool, making it possible to drive ATRP reactions to higher conversions with low amounts of transition metal.<sup>[155,156]</sup>

### 6.3 Surface-initiated ATRP

Surface-initiated ATRP (SI-ATRP) is a well-suited technique for the modification of surfaces with a wide variety of geometries such as flat, convex and concave surfaces as well as macro- and nanosized scaffolds. The only requirement is the covalent attachment of the initiator on the surface.<sup>[130]</sup> Most of surface-tethered functional groups are converted into ATRP initiators by a straight-forward conversion with commercially available substances.

Especially natural materials are easily modified with an ATRP initiator owing to the large amount of surface hydroxyl groups.<sup>[131,157]</sup> For this reason, SI-ATRP was already successfully conducted on natural substances including silk,<sup>[158]</sup> chitosan,<sup>[159]</sup> rice husk,<sup>[160]</sup> lignin,<sup>[161,162]</sup> cellulose<sup>[163-172]</sup> and lignocellulosic material, such as jute fibers,<sup>[173]</sup> wood pulp<sup>[174,175]</sup> and wood in form of flour<sup>[176]</sup> or on bulk wood.<sup>[13,14,177]</sup> SI-ATRP basically follows the same mechanisms as a conventional ATRP, such as dependency on the initiator concentration and the ratio of activator to deactivator.<sup>[130]</sup> Frequently, sacrificial initiator is employed to form polymer in solution and to control the length of the polymer grafts by shifting the ATRP equilibrium towards the dormant side (see Scheme 6.1).

The free polymer is easily analyzed by SEC, which allows to following the reaction progress and provides information about polymer grafts under the accepted assumption that the free polymer chains have the same properties.<sup>[178,179]</sup> Nevertheless, SI-ATRP can be conducted exclusively on the surface in the absence of free initiator, which on the one hand prevents the formation of untethered polymer and therefore avoids otherwise necessary purification steps. On the other hand the observation of the reaction process and analysis of the surface-bound

polymer becomes more challenging.<sup>[23]</sup> A possible solution is the application of specially designed ATRP initiators, that are cleavable by external stimuli. Subsequently, the released polymer and the cleaved surface are directly analyzed.

The grafting density of SI-ATRP is not only dependent on the initiator density on the surface, the concentrations of monomer, solvent and catalyst, but also on the surface-to-volume ratio of the substrate. High grafting densities on particles often lead to macroscopic gelation by interparticle termination and consequently to diffusion control and loss of polymerization control.<sup>[180–182]</sup> This is prevented by performing the polymerization in diluted concentrations or at low conversions.<sup>[183]</sup> Additionally, a sufficient accumulation of deactivator must be guaranteed to ensure a controlled polymerization, which requires a sufficient amount of surface-bound initiator. Alternatively, deactivator is added directly or more advanced techniques such as ARGET ATRP are used, when the amount of surface-bound initiator is insufficient.<sup>[184]</sup>

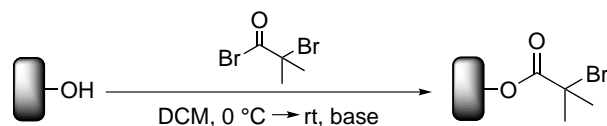
## 7 ARGET ATRP of wood

Unlike previously published studies on the surface-initiated ATRP on wood, this study was focused on the modification of wood with respect to obtaining a composite material consisting of polymer-grafted wood as a filler material in a thermoplastic matrix. Wood flour was grafted with methyl acrylate via surface-initiated ARGET ATRP. The polymerization was conducted in the absence of sacrificial initiator in order to prevent undesired formation of untethered polymer, that has to be removed after the polymerization.<sup>[23]</sup>

The chapter is divided into finding appropriate conditions for the initiator immobilization and the investigation of the graft polymerization. In this context, the main goal was the surface modification of wood while maintaining an acceptable control over the molecular weight and molecular weight distribution.

### 7.1 Immobilization of ATRP initiator

ATRP initiator-functionalized wood particles with a size of 70 – 150  $\mu\text{m}$  were synthesized in a straightforward fashion by esterification of the surface-located hydroxyl groups with  $\alpha$ -bromoisobutyryl bromide (BIBB) in the presence of an auxiliary base. Before immobilization, soluble low molecular weight components of wood were removed via a Soxhlet extraction and the washed particles were dried until a constant weight was obtained. In order to determine the appropriate reaction conditions, the immobilization was achieved by treating the wood particles with a solution of dichloromethane containing 2 wt% or 5 wt% of each an auxiliary base and BIBB. The reaction is outlined in Scheme 7.1.<sup>[14,164]</sup>



Scheme 7.1: Immobilization of the ATRP initiator on wood particles.<sup>[185]</sup>

## 7.1 Immobilization of ATRP initiator

---

Two ratios of BIBB were used to obtain different initiator loadings on the wood surface. Since wood does not have an accurate molecular weight due to its heterogenous structure, equivalents of BIBB were calculated based on glucose (Glc) as smallest unit of cellulose. Triethylamine (TEA) and pyridine (Py) were chosen as auxiliary bases. The choice of the solvent and the base has a great influence on the resulting initiator density, since properties such as basicity, molar volume, steric hindrance and hydrogen bond capability determine the accessibility of the surface hydroxyl groups.<sup>[186]</sup> TEA is a stronger base than Py. However, TEA has a higher steric hindrance and therefore it is less capable of breaking hydrogen bonds. In contrast, Py is able to break hydrogen bonds more effectively and hence is a strong swelling agent for wood by expanding the cell wall micropore network, which improves the accessibility of hydroxyl groups (see Section 1.1.2).<sup>[187]</sup>

The success of the immobilization was determined gravimetrically and by energy-dispersive X-ray spectroscopy (EDX). The reaction conditions, resulting weight percent gains (WPG) and determined bromine contents via EDX are summarized in Table 7.1 (the calculation of the WPG is describes in the experimental section 14.4.2)

Table 7.1: Reaction conditions of the ATRP Initiator immobilization.

base	eq. BIBB	WPG / %	wt% Br (EDX)
TEA (2 wt%)	2.1	3	0.4
TEA (5 wt%)	5.8	8	1.7
Py (2 wt%)	2.1	12	3.1
Py (5 wt%)	5.8	56	15

The immobilization procedure has been performed successfully with both auxiliary bases and BIBB equivalents, indicated by the weight percent gains and obtained bromine contents. More equivalents of BIBB required a longer reaction time and resulted in a higher bromine content. Immobilization with TEA resulted in lower WPGs and lower bromine contents under identical conditions compared to Py, which is in good agreement with the stronger swelling properties of Py. Additionally, the resulting immobilized particles were analyzed by ATR-FTIR spectroscopy. The spectra of untreated wood and initiator-immobilized wood treated with both bases are shown in Figure 7.1. The spectrum of untreated wood was already discussed in Chapter 3.1. Initiator immobilization using

TEA as base unexpectedly resulted in no significant change in the FTIR spectrum, although gravimetric analysis and EDX measurements clearly showed a successful immobilization. This result may be attributed to the low amount of immobilized initiator and the anisotropic nature of wood.<sup>[99]</sup> In contrast, using Py as base greatly enhanced the initiator immobilization resulting in intense peaks at  $1110\text{ cm}^{-1}$ ,  $1150\text{ cm}^{-1}$ ,  $1264\text{ cm}^{-1}$  and at  $1737\text{ cm}^{-1}$  (red regions). All peaks are in good accordance with a spectrum obtained from ethyl 2-bromoisobutyrate (EBIB, not shown here). Considering these results, treatment with 2 wt% TEA/BIBB did not lead to a sufficient amount of immobilized initiator, whereas treatment with 5 wt% Py/BIBB led to an excessive immobilization, that is undesired regarding the following ATRP.

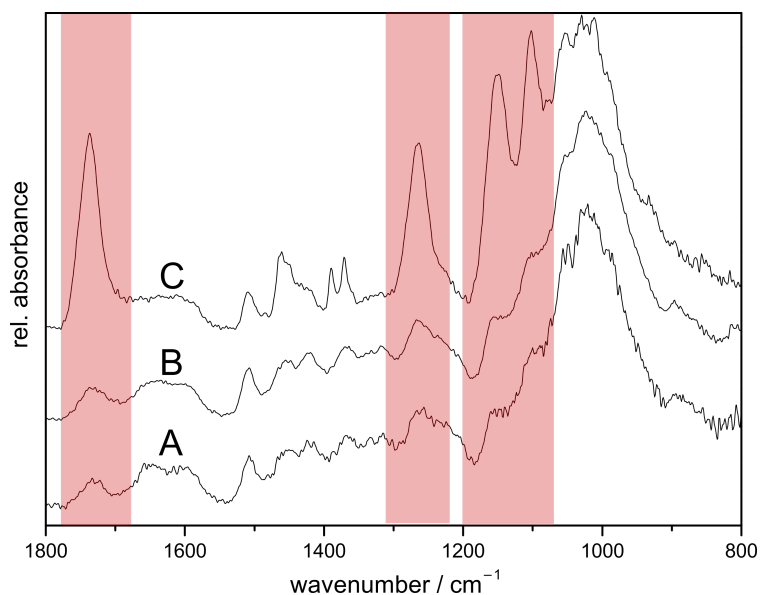


Figure 7.1: ATR-FTIR spectra of untreated wood (A) and initiator-functionalized wood with 5 wt% of TEA (B) or Py (C) as auxiliary base.

Thermogravimetric analysis (TGA) was employed to study the thermal behavior of the treated particles and to determine if either 2 wt% Py/BIBB or 5 wt% TEA/BIBB were the suitable immobilization conditions. The recorded TG and dTG curves of untreated wood and initiator-functionalized wood with both auxiliary bases and different amounts of BIBB are presented in Figure 7.2 and the respective determined degradation temperatures are summarized in Table 7.2.

## 7.1 Immobilization of ATRP initiator

Untreated wood (dashed black curve) started to degrade sharply at 200 °C with a maximum degradation at 360 °C. Afterwards, at 450 °C, wood decomposed further at a slower and steady rate. This result is in good agreement with decomposition measurements of the three main wood components – cellulose, hemicellulose and lignin. The degradation of cellulose and hemicellulose takes place at a high rate at 200 – 380 °C and 250 – 380 °C, whereas lignin slowly decomposes at 180 – 900 °C.<sup>[124]</sup> Treatment with a solution of 2 wt% TEA/BIBB (light blue curve) decreased the onset temperature to 180 °C with the same maximal degradation temperature with respect to untreated wood. Treatment with 5 wt% TEA/BIBB (dark blue curve) showed almost the same behavior as treatment with 2 % TEA/BIBB. However, the onset temperature is decreased even further to 150 °C and an additional small degradation maximum appeared at 280 °C.

Using pyridine as a base resulted in an even greater alteration of the thermal properties. The onset temperatures are shifted to 120 °C for 2 % Py/BIBB and 100 °C for 5 % Py/BIBB, respectively. Treatment with 2 % Py/BIBB (light red curve) showed a small degradation at 210 °C and a large degradation at 340 °C. Initiator immobilization using 5 % Py/BIBB (dark red curve) exhibited the greatest change in thermal decomposition behavior. The largest portion of degradation happened at a lower temperature of 265 °C and a new broad degradation appeared at 600 °C. According to literature, this behavior is explained by two reasons: firstly, esterification of cellulose damages its crystallinity and pyridine accelerates this reaction by swelling the wood components resulting in even lower onset temperatures. Secondly, hydrogen bromide may form during heating catalyzing the decomposition of wood.<sup>[13,14]</sup> Since treatment with Py greatly decreased the thermal and possibly structural stability of wood, hereinafter a solution of 5 wt% TEA/BIBB has been used for the ATRP initiator immobilization.

Table 7.2: Thermal degradation temperatures ( $T_{\text{on}}$ : onset degradation temperature,  $T_{\text{m}}$ : temperature at maximal degradation state) of the respective wood species.

	$T_{\text{on}} / \text{°C}$	$T_{\text{m1}} / \text{°C}$	$T_{\text{m2}} / \text{°C}$	$T_{\text{m3}} / \text{°C}$
untreated wood	200	-	360	-
Wood <sub>Br</sub> (2 wt% TEA)	180	-	360	-
Wood <sub>Br</sub> (5 wt% TEA)	150	280	360	-
Wood <sub>Br</sub> (2 wt% Py)	120	210	340	-
Wood <sub>Br</sub> (5 wt% Py)	100	-	265	600

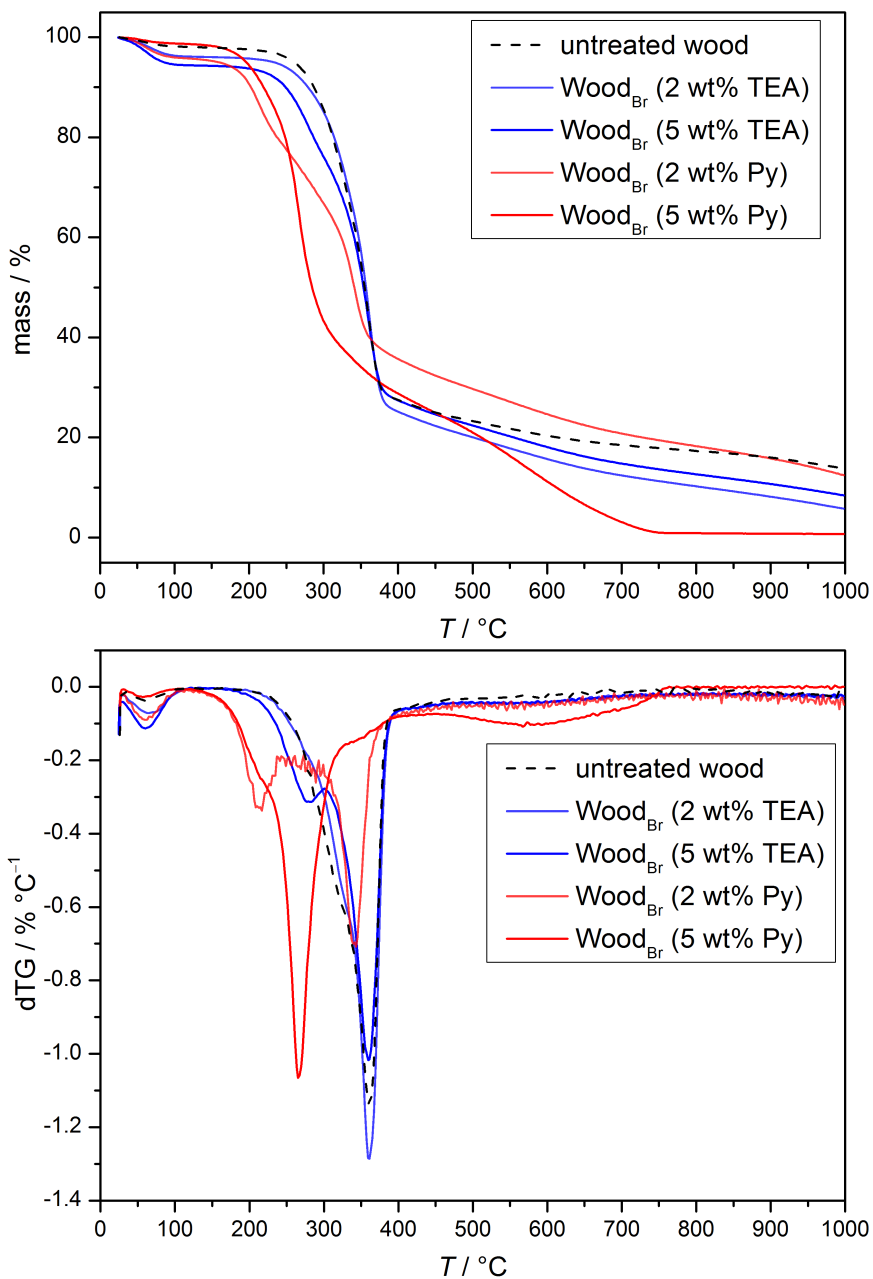
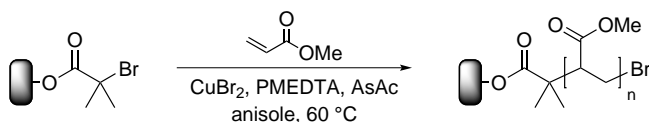


Figure 7.2: TG and dTG curves of untreated wood and initiator-functionalized wood. Mass loss below 100 °C was attributed to residual solvent and neglected.

## 7.2 ARGET ATRP of methyl acrylate

The initiator-functionalized wood particles prepared using 5 wt% TEA/BIBB (see Section 7.1) were grafted with poly(methyl acrylate) via ARGET ATRP in the absence of sacrificial initiator. The polymerization was conducted at 60 °C for 45 min to 9.5 h as can be seen Scheme 7.2.



Scheme 7.2: ARGET ATRP of methyl acrylate from wood surfaces.

Anisole was chosen as solvent, because two important requirements have to be fulfilled. On the one hand, it has to be a good solvent for the catalyst and on the other hand a poor solvent for ascorbic acid (AsAc), reducing its reduction potential and therefore preventing high radical concentrations. In order to ensure the formation of intended metal ligand complex, *N,N,N',N'',N''*-pentamethyldiethylenetriamine (PMDETA) was used as ligand in a ten-fold excess.<sup>[150,151]</sup>

The grafting procedure was performed by immersing the initiator-modified wood particles into the reaction mixture, followed by addition of AsAc and purging with inert gas for 5 min. Purging with inert gas is not *per se* necessary, but it guaranteed a better reproducibility and comparability of the samples. Parallel grafting experiments were conducted and the particles were filtered off at given times, washed extensively with tetrahydrofuran and acetone and subsequently dried. The success of the graft polymerization was already seen due to a visual change of the particles. The appearance of the wood flour significantly changes with progressing polymerization time as can be seen in Figure 7.3. Higher polymerization times led to an increasing agglomeration of the previously fine ground flour and to an intensified whitening effect.

Additionally, ATR-FTIR spectroscopy analysis of the PMA-grafted wood particles revealed the successful grafting of PMA. Figure 7.4 shows the recorded FTIR spectra of initiator-functionalized wood (A) and PMA-grafted wood with polymerization times of 45 min to 9.5 h (B – E). Graft polymerization resulted in an emersion of four distinct peaks at 1725 cm<sup>-1</sup>, 1435 cm<sup>-1</sup>, 1153 cm<sup>-1</sup> and 826 cm<sup>-1</sup> attributed to PMA.<sup>[123]</sup> The intensity of those peaks (red areas) increase with progressing polymerization time, whereas the intensity of peaks attributed to wood (blue area) at 1100 – 900 cm<sup>-1</sup> decreased significantly.



Figure 7.3: Images of untreated wood (A) and PMA-grafted wood with a polymerization times of 2 h (B) and 5 h (C).

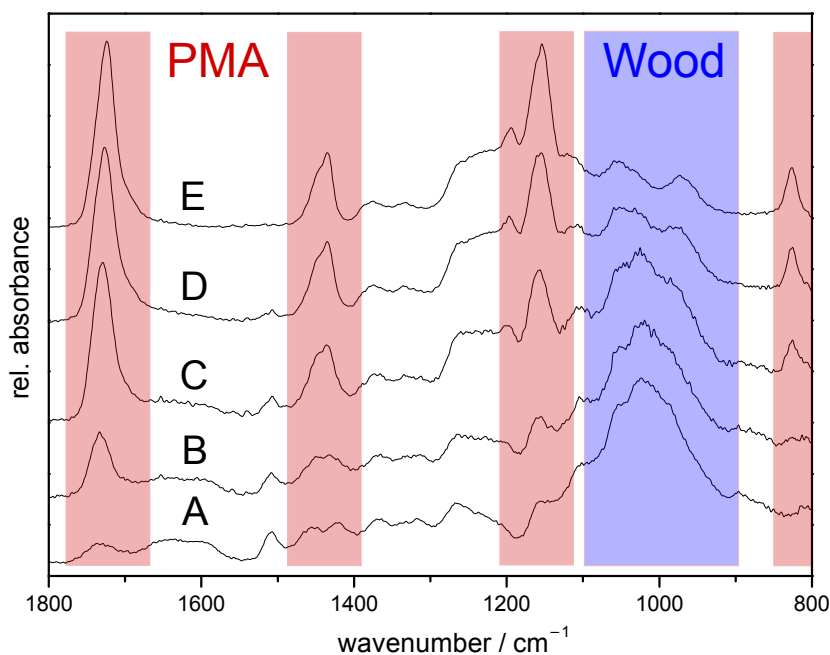


Figure 7.4: ATR-FTIR spectra of initiator-immobilized wood (A) and PMA-grafted wood with polymerization times of 45 min (B), 2 h (C), 5 h (D) and 9.5 h (E).

Scanning electron microscopy (SEM) was employed to study the surface topography of untreated wood particles, initiator-functionalized wood particles and PMA-grafted wood particles after a polymerization time of 5 h as can be seen in Figure 7.5. Untreated wood showed a fibrous structure with a smooth surface, that did not change after immobilization of the ATRP initiator. However,

subsequent to the graft polymerization the surface became rougher and more irregular due to a clearly visible polymer layer.<sup>[176]</sup>

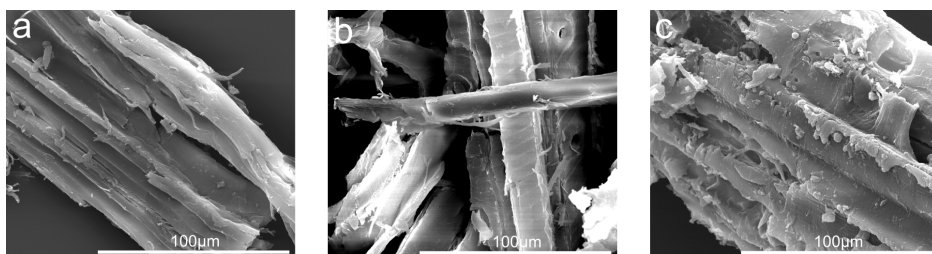


Figure 7.5: SEM images of untreated wood flour (a), initiator-functionalized wood flour (b) and PMA-grafted wood flour with a polymerization time of 5 h (c).

### Thermal properties

In order to study the thermal behavior of the different PMA-grafted samples, thermogravimetric analysis was conducted. The thermogram (TG) and derived thermogram (dTG) of unmodified and modified wood as well as pure PMA are shown in Figure 7.6 and the corresponding decomposition temperatures ( $T_{on}$ : onset degradation temperature,  $T_m$ : temperature at the maximal degradation state) and weight losses (WL) are summarized in Table 7.3. For clarity reasons, not all grafted samples are shown graphically. The interpretation of untreated wood (brown curve) is found in Section 7.1.

Pure PMA (dashed black curve,  $20 \text{ kg mol}^{-1}$ ) started to decompose at  $220^\circ\text{C}$  with a maximum of the decomposition rate at  $400^\circ\text{C}$  and a total weight loss of 98 % at  $1000^\circ\text{C}$ . All grafted samples (Wood-PMA<sub>xh</sub>) showed a two-step-degradation profile, that is interpreted as a wood decomposition stage ( $T_m$  approx.  $360^\circ\text{C}$ ) and a PMA decomposition stage ( $T_m$  approx.  $400^\circ\text{C}$ ). Generally, surface-initiated graft polymerization of PMA resulted in an improved thermal stability expressed by a smaller mass loss below  $200^\circ\text{C}$ . A longer polymerization time led to an increased temperature at the maximal degradation state ( $T_m$ ) in the wood stage and consequently a shift to the graph of pure PMA. A closer look into the weight losses at both stages showed that the WL decreased in the wood stage with progressed polymerization time, whereas the WL increased in the PMA stage. These results are in good agreement with observations from ATR-FTIR spectroscopy and water contact angle measurements.

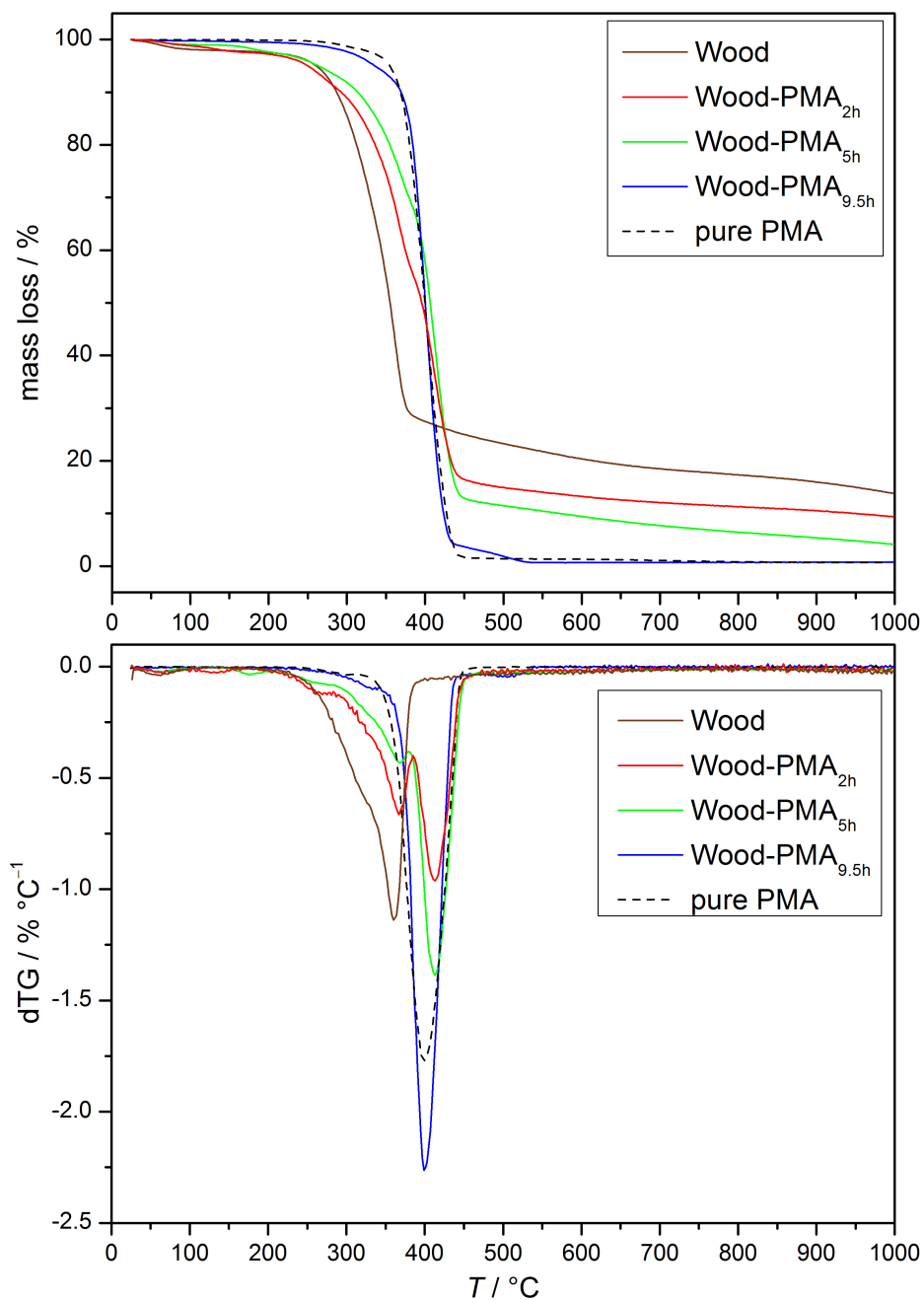


Figure 7.6: Thermograms and its derivative of untreated wood, initiator-immobilized wood, PMA-grafted wood samples and pure PMA.

## 7.2 ARGET ATRP of methyl acrylate

Table 7.3: Thermal degradation temperatures of untreated wood, initiator-immobilized wood, PMA-grafted samples and pure PMA.

	wood stage			PMA stage	
	$T_{on} / ^\circ\text{C}$	$T_m / ^\circ\text{C}$	WL / %	$T_m / ^\circ\text{C}$	WL / %
Wood	200	360	69	-	-
Wood <sub>Br</sub>	160	360	71	-	-
Wood-PMA <sub>45min</sub>	160	360	40	410	20
Wood-PMA <sub>2h</sub>	170	365	37	410	39
Wood-PMA <sub>5h</sub>	190	370	28	410	58
Wood-PMA <sub>9.5h</sub>	190	-	-	400	95
pure PMA	220	-	-	400	98

To get additional insight into the thermal behavior of the composites, TGA was used to estimate the ratio of grafted polymer to wood. Exploring the decomposition of pure polymer in more detail revealed a complete decomposition at 450 °C. Under the assumption that wood and the polymer in the composites show the same thermal behavior as the unmodified wood and pure polymer, the left over mass of the composite after this temperature belongs exclusively to the undecomposed part of wood. Therefore, comparison of the residual masses at 450 °C gives rise to information about the ratio of grafted polymer to wood. The shape of the TG curves of grafted samples support this assumption as they show a sudden flattening in the TG and no slope in the dTG. The polymer content is calculated by using the following equations, where a given  $w$  represents the mass fractions of respective species.

$$w_{\text{polymer}} = 1 - w_{\text{wood}} \quad (7.1)$$

$$w_{450^\circ\text{C}} = 0.24 \cdot w_{\text{wood}} \quad (7.2)$$

$$w_{\text{polymer}} = 1 - \frac{w_{450^\circ\text{C}}}{0.24} \quad (7.3)$$

Essentially, the mass fraction of grafted polymer ( $w_{\text{polymer}}$ ) in a composite equals 1 minus the mass of wood ( $w_{\text{wood}}$ ) as presented in Equation 7.1. Untreated wood degraded to a remaining mass of 24 % at 450 °C, allowing the expression of the measured composites' mass fraction with Equation 7.2. Combination of Equation 7.1 and Equation 7.2 leads to the final relation of  $w_{\text{polymer}}$  and  $w_{450^\circ\text{C}}$ .

The determined residual masses  $w_{450^{\circ}\text{C}}$  at  $450^{\circ}\text{C}$  and calculated polymer content  $w_{\text{polymer}}$  are summarized in Table 7.4. The residual mass of the grafted particles at  $450^{\circ}\text{C}$  decreases with progressing polymerization time, leading to higher amounts of grafted polymer according to Equation 7.3.

Table 7.4: Estimation of the amount of grafted PMA for different polymerization times.

	$w_{450^{\circ}\text{C}} / \%$	$w_{\text{polymer}} / \%$
PMA <sub>45min</sub>	24	0
PMA <sub>2h</sub>	16	33
PMA <sub>5h</sub>	13	46
PMA <sub>9.5h</sub>	4	83

DSC measurements were conducted to complete the thermal characterization of the PMA-grafted wood. The DSC curves (second heating curves) of wood, initiator-functionalized wood, PMA-grafted wood of polymerization times between 45 min and 9.5 h are presented in Figure 7.7. These data indicate that the untreated wood and initiator-functionalized wood already showed a transition in the investigated temperature range. However, these transitions did not appear in the first heating curve (not shown) that was obtained during drying of the sample. The removal of water and trapping of the inert gas inside the sample caused possible structural changes leading to the appearance of those peaks. The pure matrix polymer (PMA) showed a glass transition temperature ( $T_g$ ) of  $19^{\circ}\text{C}$ , which is close to room temperature.<sup>[188]</sup>

DSC measurements of all grafted samples yielded glass transition temperatures of approx.  $19^{\circ}\text{C}$ , that are assigned to the tethered PMA. The glass transitions became more pronounced with increasing polymerization time due to higher amount of grafted polymer. Since the glass transition temperatures of the pure matrix polymer and the grafted polymer did not differ greatly, utilization of these grafted particles as filler in thermoplastic should not change the  $T_g$  of the resulting composite and therefore its scope of application.

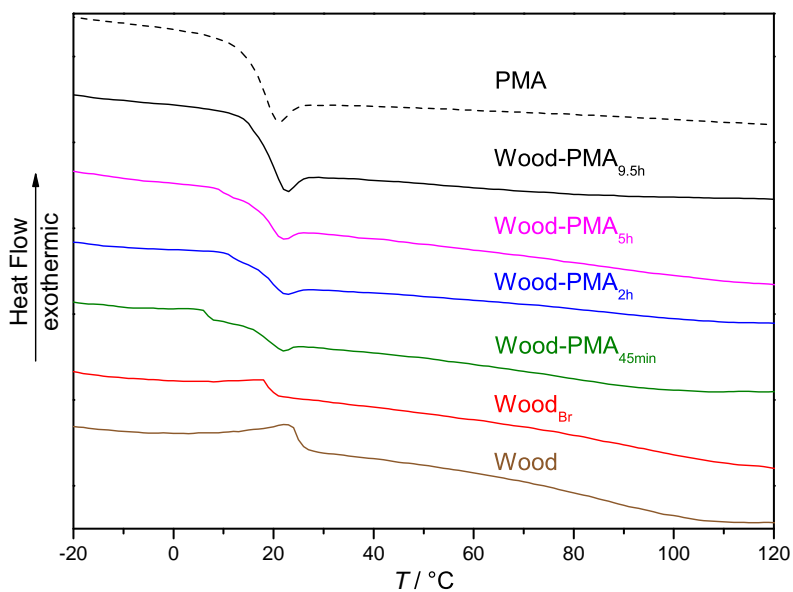


Figure 7.7: DSC curves of untreated wood, initiator-functionalized wood and PMA-grafted wood with a polymerization time between 45 min and 9.5 h.

### Wetting properties

Water contact angle (WCA) measurements were performed to evaluate the hydrophobicity of the grafted particles. Prior to measurements, the wood particles were compressed to obtain a flat surface. Figure 7.8 shows the contact angles for untreated wood and PMA-grafted wood with polymerization times of 2 h and 5 h. The unmodified wood surface is very hydrophilic due to numerous hydroxyl groups on the surface, resulting in a spontaneous absorption of the water droplet and swelling of the pressed sample. In contrast, grafting of PMA on the surface led to a contact angle of 112° and 123° respectively, that was maintained for several minutes and further demonstrated the successful grafting of PMA.

To complement the investigation of the wetting properties, dynamic vapor sorption (DVS) measurements were conducted to evaluate the sorption behavior of the grafted particles. DVS is a gravimetric technique, that is used to determine the pace and the amount of solvent absorbed by a substrate.<sup>[189,190]</sup> In a typical experiment, dried samples (moisture content 0 %) are exposed to a stepwise change in relative humidity and the mass change in the gravimetric equilibrium

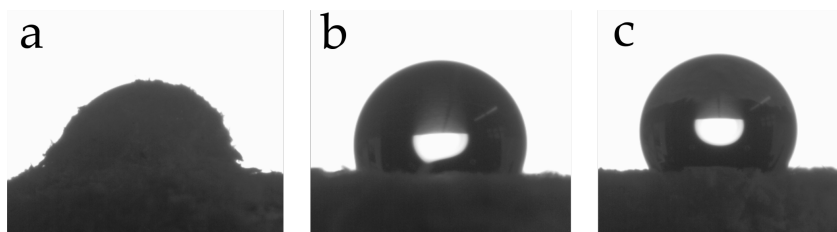


Figure 7.8: Water contact angle measurements of untreated wood (a) and PMA-grafted wood with a polymerization time of 2 h (b) and 5 h (c).

is recorded as a function of time. The adsorption and desorption properties of modified wood are either given as equilibrium moisture content (EMC) or as reduced equilibrium moisture content ( $EMC_R$ ). The EMC is based on the mass of the oven-dry modified sample (weight of wood substance plus weight of modification chemical) and therefore describes the behavior of the actual material. The  $EMC_R$  is based on the mass of the oven-dry untreated sample before modification (weight of sample minus weight of modification chemical) and hence describes the effect of the modification upon the adsorption and desorption behavior of modified wood.<sup>[27,33]</sup> The sorption behavior showed a hysteresis effect (difference between the adsorption isotherm from dry state and desorption isotherm from water-saturated state at a given RH)<sup>[190]</sup> and is divided into two parts: adsorption describes the uptake of water whereas desorption describes the release of water.<sup>[12]</sup> In general, a reduction in  $EMC/EMC_R$  at a constant relative humidity implies a higher hydrophobicity of the respective sample.<sup>[42]</sup>

Figure 7.9 shows the water sorption isotherm ( $EMC_R$ ) of untreated wood, initiator-functionalized wood and PMA-grafted wood with a polymerization time of 5 h. (The results of the measurement of the EMC are depicted in the appendix.) The isotherm of untreated wood shows a typical sigmoidal shaped found for cellulose-based materials.<sup>[191,192]</sup> Immobilization of the ATRP initiator (blue lines) resulted in a slight decrease in adsorption and desorption until a relative humidity of approximately 70% compared to untreated wood. At this point, the sorption isotherm exhibited a strong increase, that is attributed to a better accessibility of water-absorbing hemicellulose and cellulose due to the modification.<sup>[27]</sup> This finding is in good agreement with previously conducted TGA measurements, showing that immobilization of the ATRP initiator likely caused a partial destruction of the crystalline structure of cellulose, leading to the accessibility of more free sorption sites (hydroxyl groups).<sup>[193,194]</sup>

PMA grafting on the surface (red lines) resulted in a substantial reduction of  $EMC_R$  compared to untreated wood and initiator-immobilized wood as well as a reduced hysteresis behavior. Additionally, grafting reduced the adsorption and desorption of water at each given step from 0% to 95% relative humidity. The time needed to reach the EMC at a given relative humidity was greatly reduced. These results clearly show that the polymer on the surface makes the whole material more hydrophobic and decreases the wettability due to shielding of the wood surface with polymer.

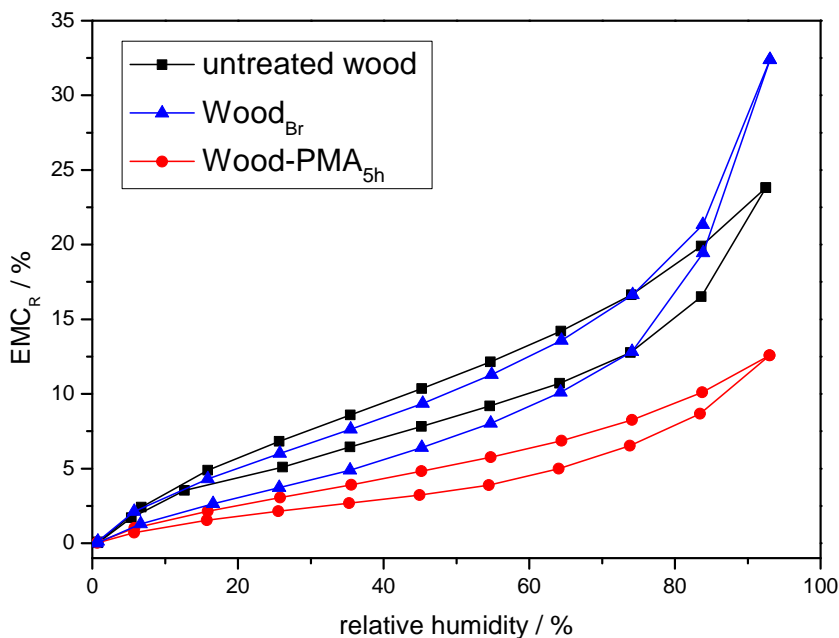


Figure 7.9: Water sorption isotherm of untreated wood, initiator-functionalized wood (WPG of 8%) and PMA-grafted wood (WPG of 46%) with a polymerization time of 5 h depending on the relative humidity.

## 8 Determination of initiator content and surface-bound polymer

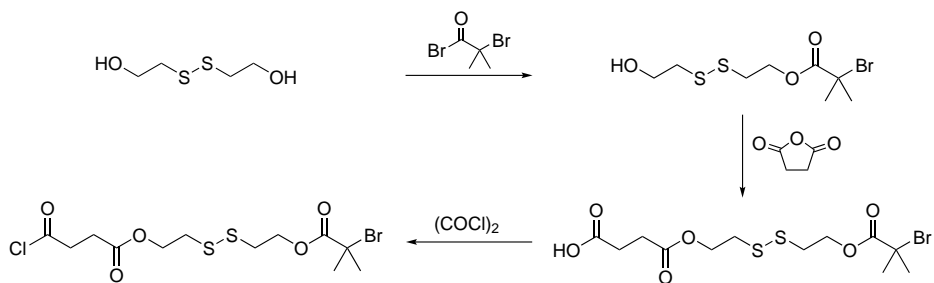
Typically, a sacrificial initiator is deployed in a solid-supported polymerization to spectroscopically follow the progress of the polymerization and to obtain information about the control over the polymerization.<sup>[130]</sup> The free polymer formed in solution is analyzed by SEC, providing estimations of the molecular weight and dispersity of the polymer grafts.<sup>[195,196]</sup>

A better approach is to directly determine the properties of the surface-bound polymer by detachment of the polymer chains from the surface. Depending on the substrate, harsh conditions (such as aggressive acids or bases) are used to degrade the substrate and release the polymer in solution. However, by doing so, the surface cannot be analyzed further and the polymer could be damaged.<sup>[197,198]</sup> Alternatively, a special designed ATRP initiator is used, that is cleavable under mild conditions preserving the surface integrity. In this study, an ATRP initiator bearing a disulfide linker was synthesized in order to allow a selective cleavage of grafted polymer chains.<sup>[199,200]</sup> The detachment is performed by reducing the disulfide linker resulting in thiol groups on the surface and untethered polymer. Additionally, the initiator content on the surface is analyzed spectroscopically by determination of the thiol content using ELLMANN'S reagent. The untethered polymer is directly analyzed by SEC.

### 8.1 Selective cleavage of polymer grafts

The synthesis of the disulfide containing ATRP initiator was performed in three steps starting from a commercially available diol and is outlined in Scheme 8.1.<sup>[201]</sup> The first step consists of the conversion of one hydroxyl moiety into the corresponding alkyl bromide using BIBB. The second step includes the transformation of the remaining alcohol to a carboxylic acid with succinyl anhydride. In the last step, the acid is activated by oxalyl chloride resulting in a carboxylic acid chloride.

## 8.1 Selective cleavage of polymer grafts



Scheme 8.1: Synthesis of disulfide containing ATRP initiator.<sup>[201]</sup>

The acid chloride of the disulfide initiator was prepared *in situ* prior to the immobilization reaction in order to prevent undesired hydrolysis during storage. The immobilization of this initiator was performed comparable to the immobilization of BIBB (see Section 7.1). The successful immobilization was confirmed via elemental analysis (EA) and energy-dispersive X-ray spectroscopy (EDX). The obtained results are shown in Table 8.1.

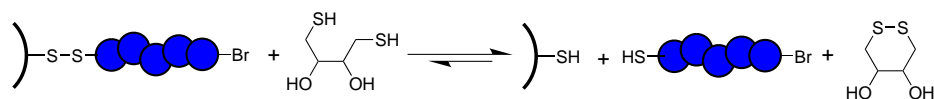
Immobilization of the disulfide-initiator using TEA resulted in a significantly lower bromine content on the surface (0.4 wt%) possibly due to a less active acid chloride compared to an acid bromide. For this reason, pyridine was used as auxiliary base and the amount of deployed initiator was adjusted. EDX data provided a bromine content of 2.0 wt%, which is very similar to the bromine content of 1.7 wt% obtained with BIBB as initiator. Due to the fact that the extent of a SI-ATRP (length of polymer chains and dispersity) is not considerably influenced by the total number of initiator sites, the grafting density of BIBB modified and disulfide-initiator modified wood should be comparable.<sup>[197]</sup>

Table 8.1: Comparison of both immobilized ATRP initiators.

Initiator	base	Br / wt% (EDX)	S / wt% (EA)
BIBB	TEA (5 wt%)	1.7	-
Disulfide	TEA (5 wt%)	0.4	0.9
Disulfide	Py (2 wt%)	2.0	1.5

After successful immobilization, the disulfide-modified particles (featuring a bromine content of 2.0 wt%) were grafted with methyl acrylate under similar polymerization conditions as described in Section 7.2. The polymerization was conducted three times with polymerization times of 1 h, 2 h and 5 h. The resulting grafted samples were extensively washed with tetrahydrofuran and dried. Afterwards, the disulfide-modified particles were treated with a solution of 1,4-Dithiothreitol (DTT) and triethylamine (TEA) in tetrahydrofuran at room temperature for several days to cleave off the polymer grafts (see Scheme 8.2).

DTT is a small reducing agent bearing two thiol groups, reacting selectively with the disulfide bond of the tethered initiator under basic conditions. During the reaction, the disulfide groups of the substrate were cleaved by reduction, leading to surface-tethered thiol moieties on the surface and the released polymer in solution bearing a thiol end group. The reaction was monitored via ATR-FTIR spectroscopy to confirm the removal of the polymer.



Scheme 8.2: Selective cleavage of polymer grafts by DTT.

However, the amount of released polymer was insufficient for precipitation and purification, therefore crude samples were analyzed by SEC. The molar masses and molar mass distributions of the investigated polymerization times are displayed in Table 8.2. The data clearly show an increasing molar mass with progressing polymerization time and almost constant dispersities, which are strong evidence for a controlled polymerization on the surface. The herein presented results should be transferable to polymerization on BIBB-functionalized wood.

Table 8.2: Properties of the cleaved polymer grafts using different polymerization times.

t / h	$M_{n, \max} / 10^3 \text{ g mol}^{-1}$	$\mathcal{D}$
1	74	1.88
2	290	1.84
5	410	1.82

## 8.2 Surface analysis

ATR-FTIR spectroscopy was utilized to confirm the detachment of the surface-tethered polymer with DTT treatment. Figure 8.1 displays the spectra of disulfide-initiator immobilized wood (A), PMA-grafted wood containing disulfide linker (B) and DTT-cleaved wood substrate (C). The spectrum of disulfide-initiator immobilized wood looks very similar to the spectrum of untreated wood (see Chapter 7.1) except for a small increase of the carbonyl signal at  $1734\text{ cm}^{-1}$ , which further shows the accomplished immobilization. Grafting of PMA resulted in a substantial increase of peak intensity attributed to PMA (red region).<sup>[123]</sup> Cleavage of the disulfide bond using DTT led to the detachment of the polymer and therefore decreased intensity of polymer signals. The resulting spectrum of DTT-cleaved wood looks very similar to the spectrum of untreated wood (shown in Figure 7.1A).

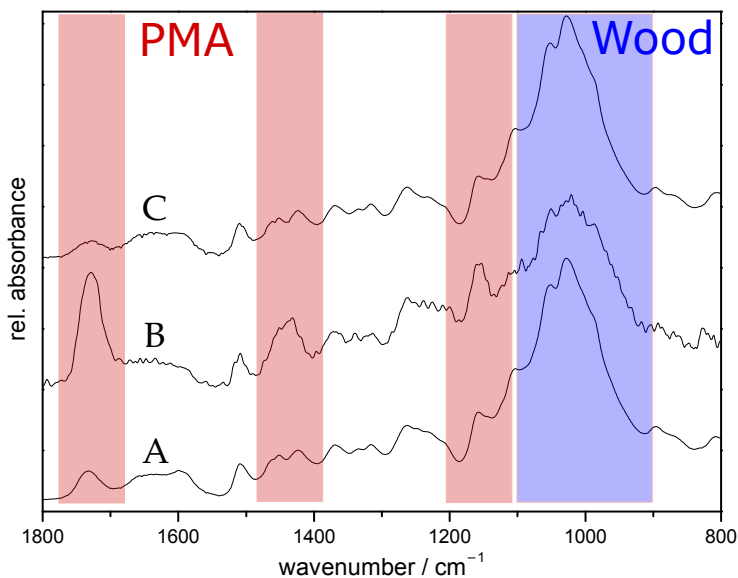


Figure 8.1: ATR-FTIR spectra of disulfide initiator-immobilized wood (A), PMA-grafted wood containing disulfide linker with a polymerization time of 5 h (B) and DTT-cleaved wood (C).

The thiol functionalities on the surface, that resulted from the cleavage of the disulfide bonds, were made visible by staining with a fluorescence dye and

subsequent observing with confocal microscopy. The dye contains a maleimide moiety as anchor group, which readily reacts with thiol groups via a thiol-ene reaction. After attachment of the dye the sample was excited at 488 nm and detected at 500 – 570 nm. A green color showed the presence of former thiol groups. The intensity of the color is correlated to the initiator density. Figure 8.2 shows two images of a wood sample (see third entry Table 8.1) after cleavage of the polymer and staining. The image revealed a satisfying surface coverage of the wood particle with a few regions with significantly higher thiol concentration. Untreated wood, that was used in a control experiment showed no fluorescence after treatment with the dye (image not shown).

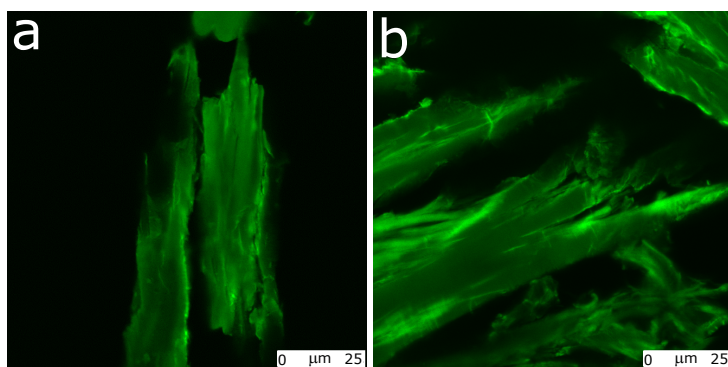
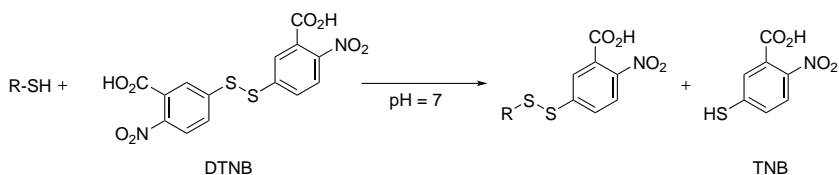


Figure 8.2: Confocal microscopy images of stained wood particles.

In addition, the thiol functionalities on the surface were quantified spectroscopically by a reaction with ELLMANN'S reagent (5,5'-dithiobis-2-nitrobenzoic acid, DTNB).<sup>[202–204]</sup> ELLMANN'S reagent undergoes a rapid and stoichiometric reaction with thiols, releasing quantitative amounts of the chromophore 5-thio-2-nitrobenzoic acid (TNB), which strongly absorbs at 412 nm in dilute buffer solutions (see Scheme 8.3).



Scheme 8.3: Determination of initiator content by reaction with ELLMANN'S reagent.

The amount of released TNB was determined via UV/vis spectroscopy. Performing a calibration experiment with known thiol concentrations is necessary to connect the absorbance of TNB to a thiol concentration. For this reason, a calibration curve was recorded using buffer solutions containing definite concentrations of glutathione as the thiol compound. The UV/vis spectra of the definite thiol concentrations and the resulting calibration curve are depicted in the experimental section. The slope of the calibration curve was  $0.01237 \cdot 10^{-3} \text{ M}^{-1} \text{ cm}^{-1}$  and is in good agreement with a calibration curve found in literature.<sup>[201]</sup> The DTT-treated wood particles were immersed in a DTNB phosphate buffer solution and the solution was analyzed by UV/vis spectroscopy. Table 8.3 shows the measured absorbance of the different samples, which were first converted into the amount of thiols using the previous obtained calibration curve and afterwards into an initiator content based on the mass. The first sample represents DTT-treated disulfide-modified particles using 5 wt% TEA as base, whereas the second sample exemplifies DTT-treated disulfide-modified particles using 2 wt% Py as base (previously mentioned in Table 8.1). Additionally, the disulfide-modified particles using 2 wt% Py as base were grafted with PMA (with a polymerization time of 5 h) and cleaved with DTT (third sample). The respective UV/vis spectra of the DTT-treated particles are depicted in the experimental section. The determined thiol contents are in good agreement with sulfur contents obtained from elemental analysis (depicted in Table 8.1). However, the cleavage of the grafted polymer does not succeed completely since the thiol quantification did not provide the same value of 1.40 at 412 nm.

Table 8.3: Determined initiators contents on the surface via UV/vis spectroscopy.

sample	Abs (412 nm)	thiol / $\mu\text{mol}$	initiator / $\mu\text{mol g}^{-1}$
Disulfide (TEA 5 wt%)	0.75	66	260
Disulfide (Py 2 wt%)	1.40	117	470
Wood-PMA <sub>5h</sub>	1.05	88	360

## 9 Conclusions of Chapter III

In summary, immobilization of an ATRP initiator on wood was conducted via esterification of the surface-located hydroxyl groups with  $\alpha$ -bromoisobutyryl bromide. Two different amounts of BIBB were used in the presence of either triethylamine or pyridine as auxiliary base. ATR-FTIR, TGA and EDX measurements were performed to determine the optimal immobilization conditions and showed that utilization of 5 wt% TEA and 5.8 eq. BIBB relative to glucose (representing wood as the smallest repeating unit of cellulose) resulted in a WPG of 8 % and an bromine content of 1.7 wt%.

The surface-initiated ARGET ATRP of methyl acrylate was performed in the absence of sacrificial initiator using ascorbic acid as an environmentally-friendly reducing agent. ATR-FTIR spectroscopy measurements and SEM images revealed the successful grafting of PMA on the wood surface. Additionally, the thermal properties of the resulting grafted particles were investigated via DSC and TGA measurements, which both confirmed the successful grafting. Through TGA experiments, it was possible to estimate the amount of grafted polymer and hence the WPG. Furthermore, the wetting properties of the PMA-grafted wood were examined via WCA and DVS measurements. Both methods showed a greatly increased hydrophobicity.

In a different approach, a cleavable ATRP initiator bearing a disulfide moiety was immobilized on the wood surface, allowing the detachment of the grafted polymer chains under mild conditions by reducing the disulfide groups. SEC analysis of the detached polymer yielded an increasing molar mass with progressing polymerization time. The dispersities scattered around 1.8 indicating strong evidence for a controlled polymerization. The remaining thiol-covered wood surface was stained with a fluorescence dye and examined microscopically, displaying a sufficient coverage of the surface. Beyond the visualization, the surface-located thiol groups were determined quantitatively via UV/vis spectroscopy using ELLMANN's reagent. Depending on the immobilization condition, initiator contents of 260 – 470  $\mu\text{mol g}^{-1}$  could be obtained. These findings are in good agreement with sulfur contents obtained from elemental analysis.



## **Chapter IV**

# **Wood flour-reinforced thermoplastic**



# 10 Preface

## 10.1 Mechanical properties of polymers and their composites

Polymers can be divided into four groups (including intermediate states) based on their molecular structure and their mechanical behavior – thermoplastics, elastomers, thermoplastic elastomers and thermosets.<sup>[205,206]</sup> Thermoplastics are unbranched polymers, with chains that are purely associated through intermolecular forces. As a result, they are moldable above the glass transition temperature and solidify upon cooling.<sup>[207,208]</sup> Since there are no intermolecular covalent bonds, thermoplastics can be reshaped by heating. However, they show a relative low strength and stiffness.<sup>[6,7]</sup> Elastomers, often referred to as rubbers, are amorphous weakly crosslinked plastics and generally have a low stiffness. Due to this formed network, they display a rubber-like elasticity, but cannot be melted. Thermoplastic elastomers are plastics, which combine the advantages of both elastomers and thermoplastics. At low temperatures, thermoplastic elastomers have certain physically cross-linked areas (such as crystallites) that are responsible for rubber-like elasticity. These areas are destroyed upon heating, resulting in a thermoplastic behavior.<sup>[8,209]</sup> Thermosets are highly crosslinked plastics, offering a high mechanical strength and hardness, but often combined with brittleness. Once hardened, they cannot be reheated and melted due to the irreversible formed chemical bonds during the curing process.<sup>[8,206]</sup>

Poly(methyl acrylate) is a hydrophobic, rubbery and ductile polymer, that offers high heat/UV resistance and belongs to the class of thermoplastics. Polyacrylates are used in coatings, paints and automotive products including seals, gaskets and actuating diaphragms.<sup>[210,211]</sup> In order to improve the mechanical properties while maintaining the easy processability and ductility, filler materials are added.<sup>[6,7]</sup> Most commonly, inorganic fillers (such as talc particles and fiberglass) or organic fillers (such as lignocellulosic particles and fibers) are added facilitating an isotropic or an anisotropic strengthening.<sup>[8,212]</sup> The desired improvement of the mechanical properties is often found even at relatively low filler

contents.<sup>[213]</sup> Wood particles are a particularly suitable filler for composite materials since wood is environmentally friendly and a cheap raw material. However, a good interfacial adhesion of the filler and the polymer matrix is necessary to ensure a sufficient stress transfer between both phases.<sup>[16]</sup> Generally, composites with wood-based fillers are known to have increased stiffness (as a result of the intrinsic properties of the wood particles) but lower ductility compared to the neat polymer due to the poor compatibility of the hydrophilic wood particles and the hydrophobic polymer matrix.<sup>[212,214]</sup> Chemical treatment (such as hydrophobization or graft polymerization) of the wood filler is used to limit aggregation and increase the interaction between filler and matrix, which greatly influence the mechanical properties.<sup>[215,216]</sup>

In this chapter, the preparation of the composite material including the PMA-grafted wood particles (see Chapter III) is discussed and the mechanical properties are investigated using tensile testing and dynamic mechanical analysis. In this context, the influence of the amount of grafted polymer was investigated at first, followed by studies on the mechanical properties of the matrix with different ratios of incorporated particles.

## 10.2 Tensile testing

Tensile testing is a fundamental test for the characterization of mechanical properties of solid materials such as wood, metals, polymers and polymer composites.<sup>[217]</sup> Tensile specimen are standardized and typically dogbone shaped with two shoulders and a gage between them and a well-known cross-section. In a typical test, the shoulders are fixed with clamps and the specimen is elongated with a constant rate while the applied force is recorded.<sup>[32]</sup> The elongation  $\varepsilon$  is defined by the deformation ( $l - l_0$ ) divided by the initial length ( $l_0$ ) of the specimen as depicted in Equation 10.1. The recorded force ( $F$ ) is used to measure the engineering stress  $\sigma$ , which is the force  $F$  divided by the initial cross-section  $A_0$  of the specimen (as can be seen in Equation 10.2).<sup>[218]</sup>

$$\varepsilon = \frac{(l - l_0)}{l_0} \quad (10.1)$$

$$\sigma = \frac{F}{A_0} \quad (10.2)$$

However, the actual cross-section of a soft material is reduced during elongation, meaning that the true stress affecting the sample is higher than the recorded engineering stress. The obtained data are plotted in so-called stress-strain curves (see Figure 10.1), that are highly dependent on the nature of the material and therefore give important insights in physical properties. In the case of polymers and polymer composites, the curve is dependent on both the nature of the polymer and as well as the amount of used additive, the processing conditions and testing conditions (*e.g.* temperature and rate of elongation).<sup>[219,220]</sup>

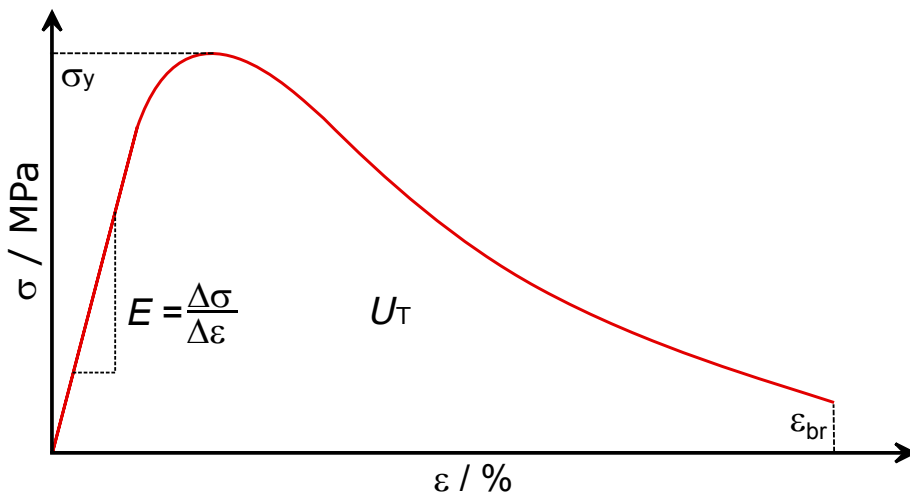


Figure 10.1: Exemplary stress-strain curve of a thermoplastic polymer.

At first, every polymer shows an elastic region, which is characterized by a reversible deformation and a linear relationship between stress  $\sigma$  and strain  $\epsilon$  following HOOKE'S law (see Equation 10.3). The proportionality constant  $E$  describes the stiffness of the polymer and is called elastic modulus or YOUNG'S modulus.<sup>[221]</sup> A material with a high YOUNG'S modulus is termed as stiff or strong. At the yield point  $\sigma_y$ , the polymer exhibits irreversible plastic deformation indicated by a slight decrease of the curve and loss of the linear relationship of stress and strain. Therefore, a high yield point represents a high resistance to plastic deformation. After the yield point, the elongation continues until the specimen breaks. The corresponding elongation to this point is called strain

at break ( $\epsilon_{br}$ ). The area under the curve is a measure for the tensile toughness  $U_T$  and illustrates the maximum energy that is absorbed by the sample (see Equation 10.4).<sup>[221]</sup> Toughness is a combination of strength and ductility. In order to be tough, a material must be able to withstand high stresses (strength) and high strains (ductility).<sup>[32,222]</sup>

$$\sigma = E \cdot \epsilon \quad (10.3)$$

$$U_T = \int_0^{\epsilon_{br}} \sigma d\epsilon \quad (10.4)$$

### 10.3 Dynamic mechanical analysis (DMA)

Dynamic mechanical analysis (DMA) is a non-destructive technique for mechanical analysis of materials. In polymeric systems, DMA is used to investigate the viscoelastic behavior and determine the glass transition temperature ( $T_g$ ).<sup>[223]</sup> In a typical experiment, a small strain is applied to a sample in a sinusoidal manner and the response (deformation) is recorded. The response is divided in an in-phase (storage modulus  $E'$ ) and an out of phase deformation (loss modulus  $E''$ ).<sup>[218]</sup> The storage modulus describes the immediate deformation of the sample and the energy, that is stored and released completely thus its elastic mechanical behavior.<sup>[224]</sup> The loss modulus represents its inelastic or viscoelastic behavior (e.g. heat dissipation). The ratio of the loss to the storage modulus is called loss factor, damping or  $\tan(\delta)$ . It is a measure of how well a material dissipates energy under a cyclic load.<sup>[223]</sup> In a typical experiment, these key figures are recorded as a function of temperature, frequency or amplitude. An exemplary course of a temperature-dependent measurement of a viscoelastic polymer is outlined in Figure 10.2. At low temperatures, a polymer is in its glassy state, meaning that it shows almost exclusively elastic behavior and little viscoelastic behavior. Consequently, a high storage modulus  $E'$  and a low loss modulus  $E''$  resulting in a low  $\tan(\delta)$ . Near the glass temperature of the polymer ( $T_g$ ), the storage modulus decreases since stored energy is irreversibly used for chain movements and rearrangements.<sup>[206]</sup> Friction of polymer chains leads to energy loss and therefore to an increased loss modulus and  $\tan(\delta)$ . Both reach a maximum at the glass transition temperature, whereas the storage modulus shows a large drop. Further rise of the temperature increases the chain agility to a point, where

friction is negligible resulting in a decrease of the loss modulus and  $\tan(\delta)$  to a nearly constant low value.<sup>[225]</sup>

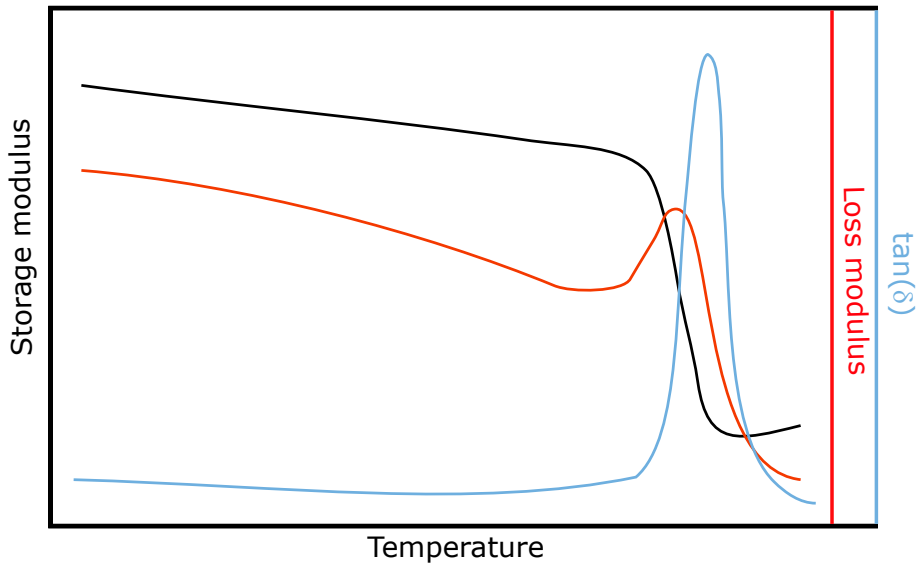


Figure 10.2: Exemplary diagram of a typical DMA curve of an amorphous polymer.<sup>[224]</sup>



# 11 Mechanical analysis of composites

This chapter deals with the preparation and examination of polymer composites based on a poly(methyl acrylate) matrix and surface-modified wood particles as additive. The overall aim was to create a composite, which maintains the ductility of the polymer matrix but additionally possesses a higher strength and toughness. The poly(methyl acrylate) matrix was synthesized by RAFT polymerization (see Section 6.2) with 2-cyano-2-propyl trithiocarbonate as chain transfer agent and azobisisobutyronitrile (AIBN) as radical starter. Several batches of the polymer were prepared under identical conditions and mixed afterwards to guarantee the same features of all prepared composites. The average molecular weight of PMA was  $3.6 \cdot 10^4 \text{ g mol}^{-1}$ . It had a dispersity of 1.09 and a glass transition temperature of approximately  $19 \text{ }^\circ\text{C}$  (determined via DSC).

## 11.1 Preparation of the composites

The wood reinforced polymer specimens were prepared via solvent casting. Therefore, a polymer is dissolved in an organic solvent. If desired, filler materials are added to this solution and the mixture is casted in a three-dimensional mold afterwards.<sup>[226]</sup> Evaporation of the solvent results in a composite material consisting of particles in a polymer matrix. In this context, the polymer solution must be very viscous to ensure that added particles do not agglomerate at the bottom of the mold. Additionally, evaporation should be slow and above the glass transition temperature of the polymer because otherwise, bubbles are trapped inside the specimen, greatly distorting the mechanical properties since these cavities act as potential breaking points. A slow evaporation is guaranteed by the choice of a high-boiling solvent, at least  $20 \text{ }^\circ\text{C}$  above the evaporation temperature. In this work, the composites were cured at  $100 \text{ }^\circ\text{C}$  in a vacuum oven for several days by slowly reducing pressure. Propylene glycol methyl ether acetate (PGMEA) was chosen as solvent, because it combines good dissolving

## 11.1 Preparation of the composites

---

properties with a sufficiently high boiling point of 145 – 146 °C.<sup>[227]</sup> Figure 11.1 shows an image of the cured DMA and tensile testing samples in their respective PTFE molds.

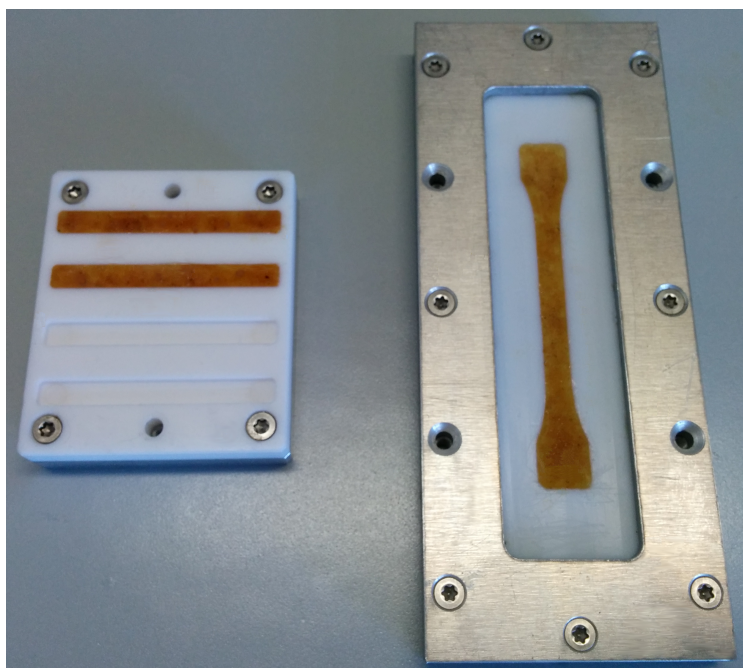


Figure 11.1: Filled DMA (left) and tensile testing specimen (right) in their respective PTFE molds.

An optical microscope was used to better assess the quality of the cured specimen (*e.g.* the distribution of the wood particles, voids). Figure 11.2 shows the images of tensile testing specimens without added wood particles, 5 wt% of added unfunctionalized particles as well as 5 wt% and 10 wt% of added grafted wood particles with a polymerization time of 2 h. As expected, the matrix polymer (a) exhibited a flawless appearance with no enclosed bubbles except for grooves originating from the PTFE mold. The wood polymer composites (b) feature a homogenous distribution of the wood particles inside the PMA matrix and no obvious inclusion of air. However, some defects including agglomerated wood or other impurities were rarely seen (indicated by the red and blue circle). Nevertheless, under right conditions solvent casting was found to be a

suitable method for the synthesis of these composites. At least three identical specimens were measured to prevent that individual impurities from influencing the mechanical properties. Scanning electron microscopy (SEM) micrographs of a fractured sample containing 5 wt% of functionalized wood particles with a polymerization time of 2 h show grafted particles embedded into the PMA matrix (see Figure 11.3). The particles are well distributed and no signs of larger aggregates in the composite were visible.

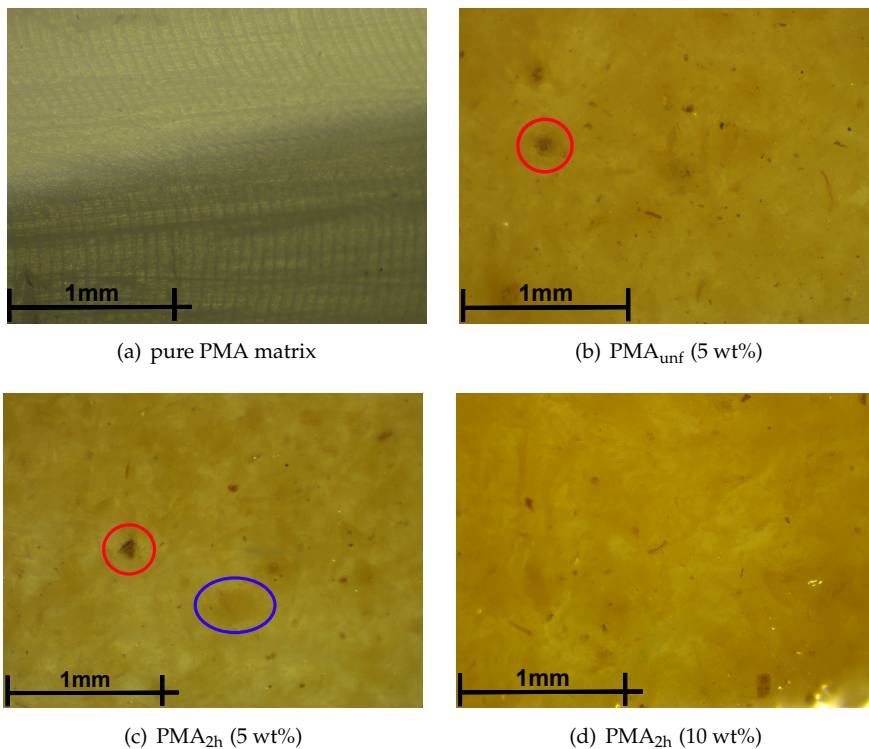


Figure 11.2: Microscope images of tensile testing specimen at 40x magnification. a) pure PMA, b) a composite containing 5 wt% of unfunctionalized wood particles, c) a composite containing 5 wt% of functionalized wood particles with a polymerization time of 2 h and d) a composite containing 10 wt% of functionalized wood particles with a polymerization time of 2 h. Red and blue circles show defects of the composites. The red and blue circles represent impurities found inside the specimen.

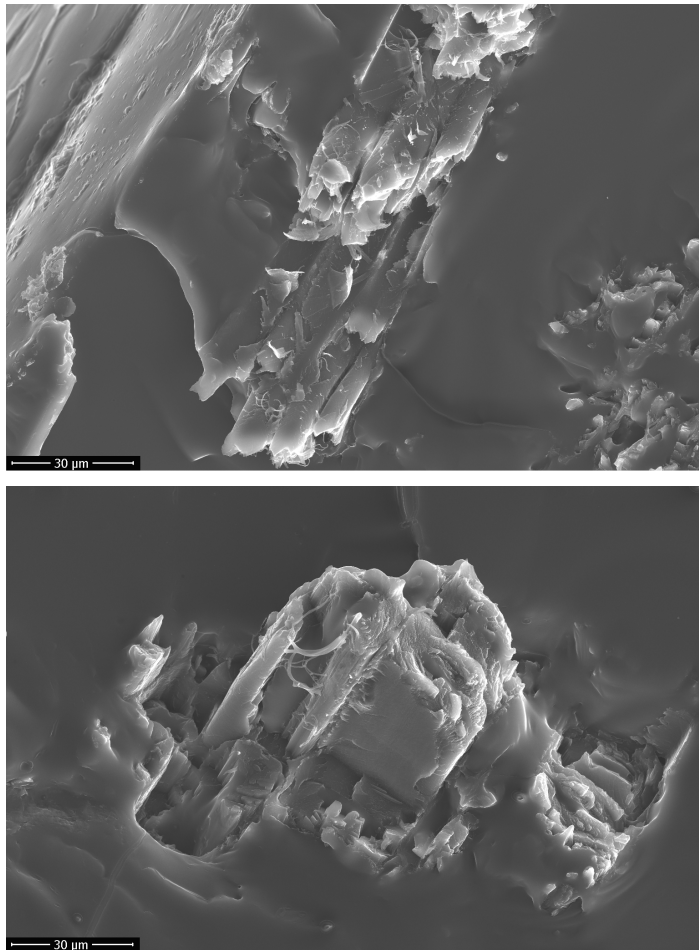


Figure 11.3: SEM images of a composite containing 5 wt% of functionalized wood particles with a polymerization time of 2 h.

## 11.2 Tensile testing measurements

Tensile testing is a well-established technique to investigate mechanical properties of any material. In this part, the tensile testing results of the pure matrix polymer PMA and the corresponding wood polymer composites are presented. Starting with the pure matrix polymer, the effect of unfunctionalized wood particles incorporated into the polymer matrix on the mechanical properties of the composite is shown. Afterwards, the influence of the polymer-grafted wood particles on the mechanical properties is evaluated.

Firstly, wood particles with varying amount of grafted polymer obtained through varying polymerization times ranging from 1 h to 9.5 h were incorporated into the matrix in a constant mass fraction of 5 wt%. Secondly, the effect of 2 h grafted wood particles with different mass fractions of 3 wt% to 10 wt% incorporated into the matrix was elucidated. It is important to note that the mechanical properties of thermoplastics such as PMA are significantly dependent on the temperature. Since the glass transition temperature of poly(methyl acrylate) ( $T_g = 19\text{ }^\circ\text{C}$ ) is very close to room temperature, a great influence on the mechanical properties is expected.<sup>[228,229]</sup> Therefore, all tensile testing experiments were conducted at  $(24.9 \pm 0.3)\text{ }^\circ\text{C}$  using a temperature controlled chamber. Four specimens of the pure polymer and three specimens of each composite material were examined to determine the YOUNG'S modulus  $E$ , yield point  $\sigma_y$  and tensile toughness  $U_T$ . Hereinafter, one representative stress-strain curve of each series of measurements is shown. All further measurements and the mechanical characteristics in tabular form including errors are presented in the appendix. Considering the test results, the specimen showed no true strain softening. The reduction in stress resulted from the reduction in the actual cross section.

### Composites consisting of wood with varying amount of grafted polymer

In this section, the tensile testing results of the pure PMA matrix and the composites including unmodified wood flour and wood flour with varying amount of grafted polymer are presented. The stress-strain curves and the progression of the corresponding mechanical characteristics are shown in Figure 11.4. The PMA homopolymer (black curve) exhibited a typical stress-strain curve of a thermoplastic above its glass transition temperature. At first, PMA showed a small elastic region with an  $E$  modulus of 8 MPa, where HOOKE'S law applies. The yield point  $\sigma_y$  was reached at 0.27 MPa, followed by a region, where the

## 11.2 Tensile testing measurements

sample started to flow and were drawn until a maximum elongation of 1100 %, indicating a lack of internal cohesion.<sup>[230]</sup> The tensile toughness of pure PMA, which can be expressed by the area under the curve, was 126 MPa. The addition of 5 % unfunctionalized wood flour ( $\text{Composite}_{\text{unf}}$ ) resulted in a similar  $E$  modulus, in a slightly increased yield strength of 0.30 MPa, but most importantly in a halving of toughness to 50 MPa. The observed increase in yield strength and dramatic drop in toughness is described by two reasons: first incorporated stiff particles may disrupt the ability of unbranched polymer chains to flow past each other and second unfunctionalized wood particles possess a highly hydrophilic surface, resulting in a poor interfacial adhesion with the hydrophobic polymer matrix and therefore an insufficient stress transfer between both phases.<sup>[10,16]</sup> In this case, the particles act as potential breaking points weakening the composite.

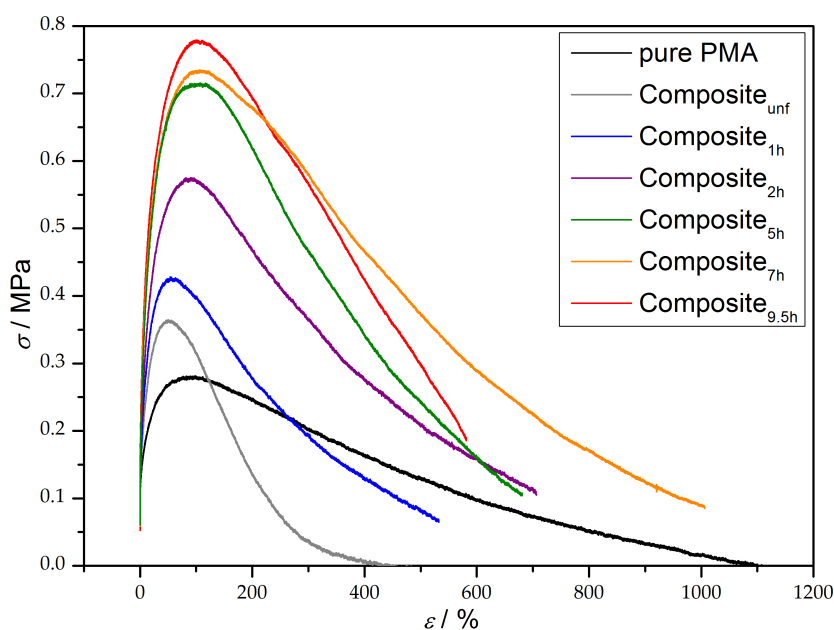


Figure 11.4: Representative stress-strain curves of pure PMA and wood reinforced thermoplastics. 5 wt% of wood flour with varying amount of grafted polymer was incorporated into the matrix.<sup>[231]</sup>

In contrast, all measured composites made of PMA-grafted wood flour incorporated into the PMA matrix exhibited overall enhanced mechanical properties as a result of an increased compatibility of both phases. In general, the longer the polymerization time and hence the higher the amount of grafted polymer on the wood flour, the higher the reinforcing effect on the resulting composite. The results are illustrated in Figure 11.5. For reasons of clarity, error bars are not shown here. Instead, the results including errors are presented in tabular form in the appendix. The YOUNG'S modulus  $E$  (black squares) increased almost linearly with progressing polymerization time, whereas the yield strength  $\sigma_y$  (red circles) initially started to increase linearly but presumably reached a saturation around 0.8 MPa. The area under the curve  $U_T$  (blue triangles) increased rapidly to a maximum at a polymerization time of between 5 h and 7 h and decreased afterwards.

However, the reinforcing character of the grafted wood particles cannot purely be explained by a better interfacial adhesion mediated by longer polymer chains on the particle surface leading to chain entanglements with the polymer matrix. In addition, one has to keep in mind that the presence of an additive, regardless of its nature or interaction with the polymer matrix, can have a big influence on the properties of the composite, such as formation of defects due to agglomeration, influence on the curing process or on polymeric chain orientations of the matrix. Moreover, the intrinsic composition of the grafted particles, describing the ratio of wood to grafted polymer, plays an important role on reinforcing character. Longer polymerization times of the grafting process result in a lower wood to polymer ratio. Therefore, addition of the same weight percentages of grafted particles with different polymerization times results in different amounts of added wood. This is particularly well illustrated by the grafted particles with a polymerization time of 9.5 h consisting of approximately 83 % polymer (see TGA experiments, Table 7.4). Nevertheless, addition of a constant weight fraction of grafted particles regardless of the polymerization time is a more natural approach compared to addition of a constant mass fraction of wood. Considering the results from the series of measurements, grafted particles incorporated into the PMA matrix with a polymerization time of 5 h to 7 h led to a more ductile and stronger composite with a two and a half times higher YOUNG'S modulus, a two times higher yield point and a two times higher tensile toughness.

## 11.2 Tensile testing measurements

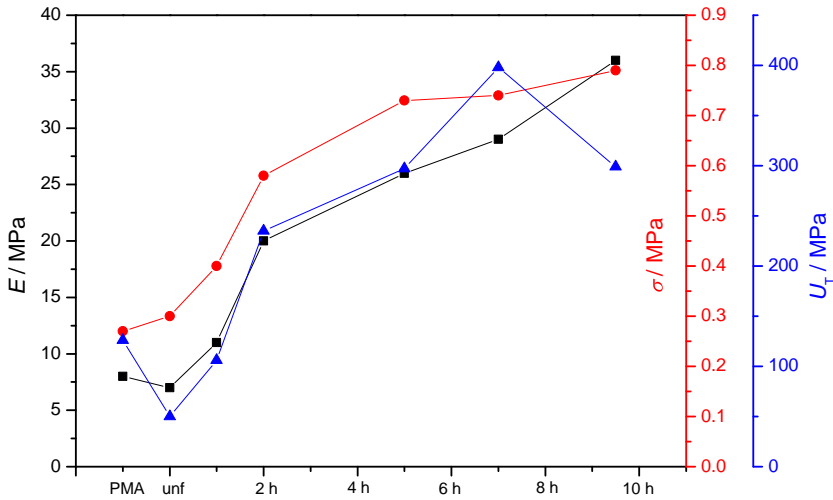


Figure 11.5: Graphical presentation of the mechanical characteristics ( $E$ ,  $\sigma_y$ ,  $U_T$ ) of pure PMA and wood reinforced thermoplastics. 5 wt% of wood flour with varying amount of grafted polymer was incorporated into the matrix.

### Composites consisting of grafted wood in varying weight percentages

Grafted wood particles with an identical amount of grafted polymer were added in different mass percentages into the PMA matrix and the effect on the mechanical properties of the composites were elucidated. In this experimental series, grafted wood particles with a polymerization time of 2 h were added in 3 wt%, 5 wt%, 7 wt% and 10 wt% into the PMA matrix. Based on the used preparation method (solvent casting) addition of 10 wt% grafted particles was the maximum amount, which could have been added to obtain a homogeneous distribution of the particles into the matrix. The stress-strain curves of the tensile testing measurements of the composites are depicted in Figure 11.6. Generally, the higher the amount of added grafted wood particles, the higher the YOUNG'S modulus  $E$  and yield strength  $\sigma_y$ , whereas the toughness  $U_T$  of the composite passed through a maximum. As depicted in Figure 11.7, starting from the pure PMA matrix, the YOUNG'S modulus of 8 MPa (black squares) and yield strength of approximately 0.3 MPa (red circles) were not significantly affected after addition of 3 wt% grafted particles, whereas the tensile toughness (blue triangles) slightly dropped from 129 MPa to 97 MPa.

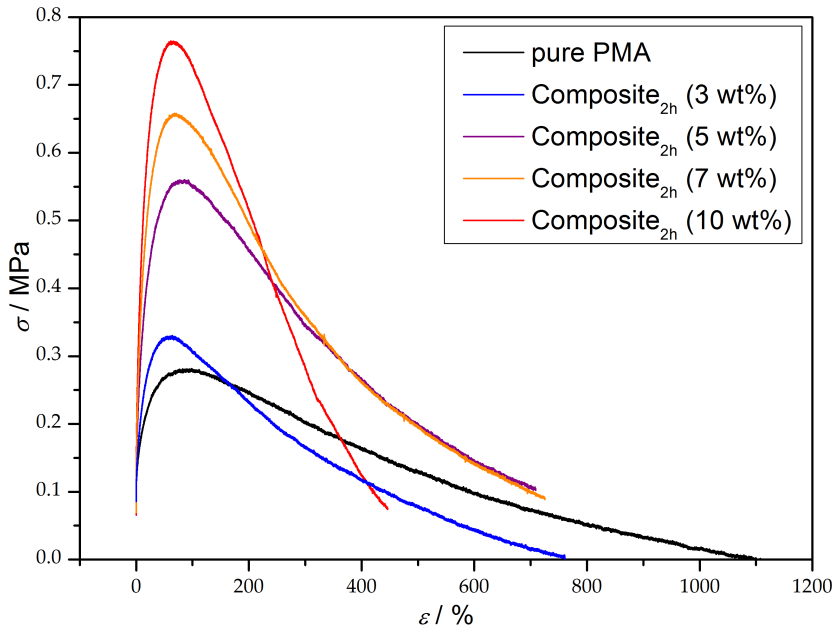


Figure 11.6: Representative stress-strain curves of pure PMA and wood reinforced thermoplastics with a constant amount of grafted polymer and varying weight percentages.<sup>[231]</sup>

This can be explained by the low amount of added filler that disrupts the package of the polymeric chains and acts as potential breaking point. With higher added amount, all three characteristics increased rapidly. The YOUNG'S modulus reached a saturation of 22 MPa between 5 wt% and 7 wt%, the yield point increased almost linearly to 0.74 MPa and the maximum tensile toughness was found at 235 MPa by 5 wt% of added grafted particles. Considering these results, addition of 5 wt% to 7 wt% of grafted wood particles (with polymerization time of 2 h) seemed to be the optimum ratio. The composite is stronger and more ductile compared to the pure polymer matrix indicated by a two and a half times higher YOUNG'S modulus, a two times higher yield point and a roughly two times higher tensile toughness.

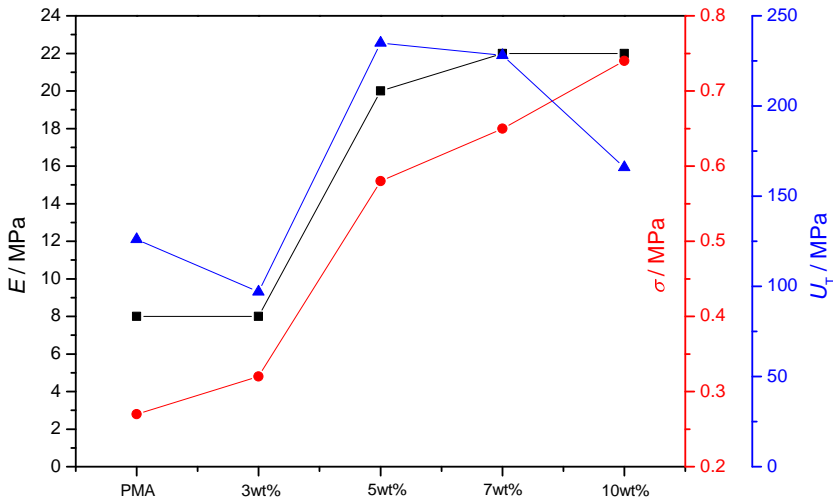


Figure 11.7: Graphical presentation of the mechanical characteristics ( $E$ ,  $\sigma_\gamma$ ,  $U_T$ ) of pure PMA and wood reinforced thermoplastics with a constant amount of grafted polymer and varying weight percentages.

## 11.3 Dynamic mechanical measurements

DMA give information about the modification introduced by the addition of a filler.<sup>[232]</sup> In this section, the results of dynamic mechanical analysis of the pure matrix polymer and the resulting composites with unfunctionalized wood particles and grafted wood particles are discussed. The measurements were conducted in dependance of temperature at a constant frequency of 1 Hz. The storage modulus  $E'$ , loss modulus  $E''$  and loss factor  $\tan(\delta)$  were calculated. The results of three measurements per composite species were averaged and given as mean values with the respective standard deviation as error.

At first, the pure PMA matrix was examined to understand the behavior prior to incorporation of wood particles. The results demonstrated by the storage modulus, loss modulus and  $\tan(\delta)$  are shown in Figure 11.8. Upon heating from  $-30^\circ\text{C}$ ,  $E'$  and  $E''$  barely changed until the glass transition temperature was reached. In this region,  $E'$  exhibited a large decrease of three orders of magnitudes, whereas  $E''$  and  $\tan(\delta)$  reached maxima. The polymer transitioned from the glassy to the rubbery state. In the glassy state, only small parts of the polymer chain move, whereas in the rubbery state cooperative motions of

large parts of the main polymer chain start.<sup>[233]</sup> At temperatures well above the glass transition temperature, the polymer starts to soften. This resulted in a loss of signal quality of  $E''$  and therefore  $\tan(\delta)$  due to the fixation loosening of the sample in the used instrumental set-up (single cantilever mode).

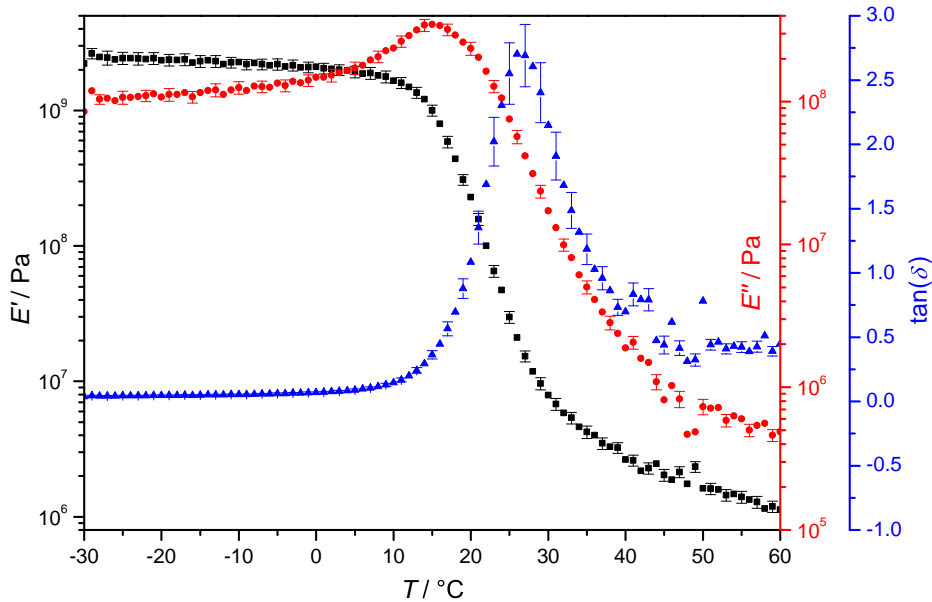


Figure 11.8: Dynamic mechanical analysis of the matrix polymer PMA. For reasons of clarity, error bars are shown every two data points.

## Composites consisting of wood with varying amount of grafted polymer

This section deals with the question of how the incorporation of a constant weight percentages of unmodified and grafted wood particles with different polymerization times influences the dynamic mechanical behavior of the matrix polymer. For this purpose, the storage modulus  $E'$ , loss modulus  $E''$  and  $\tan(\delta)$  in the glassy state at  $-10^\circ\text{C}$  were compared to identify certain trends. In the glassy state, the modulus is primarily determined by nature of the added particles, the strength of the intermolecular forces and the package of the polymeric chains.<sup>[234]</sup> Figure 11.9 shows the changes in mechanical behavior as a function of the nature and amount of the incorporated particles. For further information, the data in tabular form

including errors and the graphs from which the data were taken are displayed in the appendix. Starting from the pure PMA matrix, addition of unfunctionalized wood particles resulted in a reduction of the three observed characteristics. The added particles led to a dilution of the polymeric arrangement.<sup>[234]</sup> The storage modulus decreased due to the addition of hydrophilic particles in the hydrophobic matrix leading to a disruption of the polymeric chain arrangements and complicates energy transfer. Additionally, the added particles reduce the chain mobility of the matrix polymer manifesting itself in a lower loss modulus.<sup>[235,236]</sup> The loss factor decreased since the effect on the loss modulus is observed to be greater than the effect on the storage modulus.

The interpretation of the results of composites containing grafted particles is more complicated. On the one hand, the ratio of polymer to wood within one particle increases with progressing polymerization time, as already briefly discussed in Section 11.2. This means that addition of the same weight percentages of grafted particles with different polymerization times results in different amounts of added wood. On the other hand, longer polymerization times lead to longer polymeric chains on the surface and hence more entanglements with the polymer matrix. In general, addition of particles decreases the inelastic response ( $E''$ ) due to aggravated viscous flow and increases the elastic response ( $E'$ ) by forming stiff agglomerates or due to their inherent stiff character.<sup>[232,237]</sup> Chain entanglements show exclusively elastic behavior, resulting in an increase of the storage modulus and a decrease of the loss modulus and hence decline of  $\tan(\delta)$ .<sup>[238]</sup>

These two opposing effects most likely determine the influence of the filler on the mechanical properties displayed by the resulting composites. Figure 11.9 shows that starting from PMA<sub>1h</sub>, the storage modulus decreased with increasing polymerization time to a minimum for PMA<sub>7h</sub> and started to increase afterwards. The overall drop of  $E'$  is explained by the reduction of the number of added particles, which seems to be the predominant cause until a polymerization time of 7 h. In this region, the effect of entanglements presumably starts to play the major role with the result that ( $E'$ ), ( $E''$ ) and  $\tan(\delta)$  approached the values obtained for pure PMA. The loss modulus increased with progressing polymerization time resulting in more energy dissipation during one cycle, which can be explained by the fact that more entanglements lead to less chain mobility and higher internal friction.<sup>[235,236]</sup> The loss factor provided the same course as the loss modulus: higher polymerization time resulted in higher  $\tan(\delta)$  and therefore in a higher nonelastic behavior as less particles are added. A high  $\tan(\delta)$  means that more energy is absorbed in viscous motions resulting in a tougher material.<sup>[235]</sup>

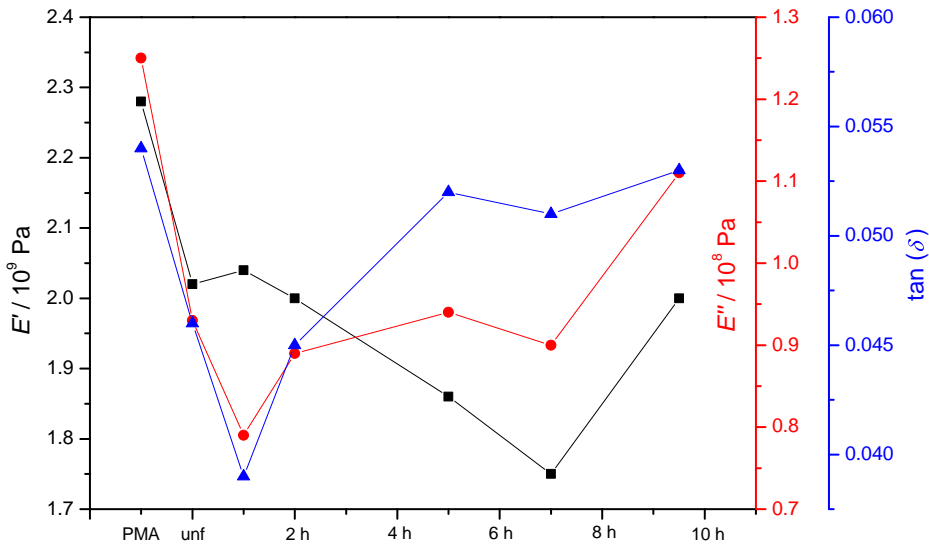


Figure 11.9: Dynamic mechanical behavior of the composites as a function of the incorporated particles with different polymerization times in the glassy state at  $-10\text{ }^\circ\text{C}$ .

### Composites consisting of grafted wood in varying weight percentages

In this section, the influence of the weight percentages of added grafted particles on the mechanical properties of the composites is discussed. The storage modulus  $E'$ , loss modulus  $E''$  and  $\tan(\delta)$  of composites including particles with a polymerization time of 2 h at  $-10\text{ }^\circ\text{C}$  are plotted against the amount of added particles. For reasons of clarity, errors are given in tabular form in the appendix. In general, addition of higher amounts of filler into the matrix should result in increased storage and loss moduli since viscous flow is reduced and more stress is transferred to the filler.<sup>[239,240]</sup> Figure 11.10 shows that the storage and loss moduli are U-shaped. Starting from pure PMA, both moduli decreased to a minimum at around addition of 5 wt% grafted particles. Afterwards, the storage modulus rapidly increased to a higher value than pure PMA, whereas the loss modulus moderately raised to a slightly smaller value compared to pure PMA. A possible explanation for the U-shape is the formation of particle islands instead of a good dispersion at low filler contents, that do not enhance

### 11.3 Dynamic mechanical measurements

mechanical properties in the glassy state.<sup>[241]</sup> At this point added particles are imperfections and disrupt the polymer arrangement. Upon increasing of the filler content, a more homogenous composite with greatly increased storage modulus is formed. This effect is attributed to the formation of a so-called glassy layer that is formed around the grafted particles by strong entanglements with the polymer matrix. In this layer, chain mobility is strongly aggravated, manifesting itself as an increase of the storage modulus.<sup>[225]</sup> Addition of more particles led to a higher ratio of the glassy layer and hence a higher storage modulus.<sup>[213,241]</sup> However,  $\tan(\delta)$  decreased upon increasing amounts of grafted particles due to the restricted movement of the polymer.<sup>[234]</sup> In principle, the lower  $\tan(\delta)$ , the lower the energy dissipation and the more energy is restored after the loading cycle.<sup>[232]</sup> It can be concluded that it is possible to adjust the amount of reversibly stored energy through variation of the amount of added grafted particles.<sup>[225]</sup>

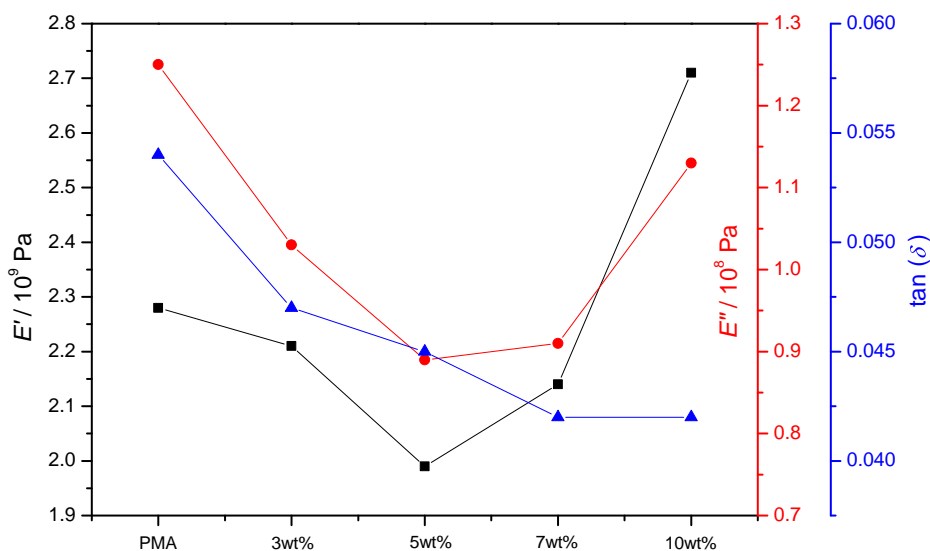


Figure 11.10: Dynamic mechanical behavior of the composites as a function of the mass percentages of incorporated particles with different polymerization times of 2 h at  $-10^\circ\text{C}$ .

## Determination of the glass transition temperatures and damping behavior

Table 11.1 shows the determined glass transition temperatures ( $T_g$ ) of the composites by using the maximum of the  $\tan(\delta)$ . The additionally determined  $T_g$  using the maximum of the loss modulus and the inflection point of the storage modulus are depicted in the appendix. In general, the measurements showed no significant change of the composites' glass transition temperature with varying amount of grafted polymer. However, the  $T_g$  of the composites consisting of particles with a polymerization time of 1 h exhibited the highest shift. Figure 11.9 already showed that this composite had the lowest loss modulus and  $\tan(\delta)$  indicating a pronounced interruption of chain mobility, that results in a strong shift. The glass transition temperature of the composites consisting of grafted wood in varying weight percentages are slightly shifted towards higher temperatures. The more particles are added, the higher is the glass transition temperatures, resulting in a reduction of chain mobility.<sup>[239,242]</sup>

Nevertheless, the glass transition temperature of nearly all measured composites scatter closely around the glass transition temperature of PMA within their respective error interval. These findings indicate that the mechanically enhanced composites can be used in the same temperature range, resulting in an extended scope of application.

Table 11.1: Determined glass transition temperature via the maximum of  $\tan(\delta)$ .

sample	$T_{g,\tan(\delta)} / ^\circ\text{C}$
PMA	$27.2 \pm 1.2$
PMA <sub>unf</sub>	$27.4 \pm 1.2$
PMA <sub>1h</sub>	$28.4 \pm 0.4$
PMA <sub>2h</sub>	$27.7 \pm 0.3$
PMA <sub>5h</sub>	$25.3 \pm 2.9$
PMA <sub>7h</sub>	$27.5 \pm 1.7$
PMA <sub>9,5h</sub>	$27.6 \pm 1.7$
PMA	$27.2 \pm 1.2$
PMA <sub>2h</sub> (3 wt%)	$28.2 \pm 1.2$
PMA <sub>2h</sub> (5 wt%)	$27.7 \pm 0.3$
PMA <sub>2h</sub> (7 wt%)	$28.1 \pm 1.3$
PMA <sub>2h</sub> (10 wt%)	$28.6 \pm 0.3$

### 11.3 Dynamic mechanical measurements

---

Additionally, the intensity from the  $\tan(\delta)$  peak can be interpreted as a measure for the effect of reinforcement. A reduced loss factor at the glass transition temperature indicates a good energy transfer between both phases, less energy dissipation and hence an enhanced reinforcing effect.<sup>[242,243]</sup> This behavior is confirmed by comparing the  $\tan(\delta)$  of the composites with increasing amount of added particles (as can be seen in Figure 11.11). However, the same trend is not found in the analysis of the composites consisting of wood with varying amount of grafted polymer, possibly due to the two opposing effects discussed above in Section 11.3.

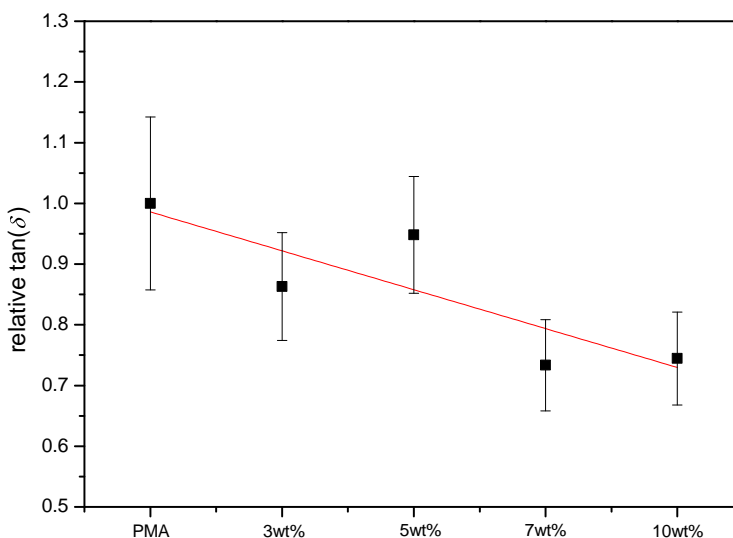


Figure 11.11: Relative  $\tan(\delta)$  of composites including grafted wood in varying weight percentages at the glass transition temperature.

## 12 Conclusions of Chapter IV

In summary, wood-flour-reinforced thermoplastics with poly(methyl acrylate) as polymer matrix were prepared by solvent casting and investigated by means of tensile testing and dynamic mechanical analysis. Firstly, unmodified wood particles and functionalized wood particles with varying amount of grafted polymer were incorporated into the polymer matrix in a constant mass fraction of 5 wt%. Secondly, wood particles with a constant polymerization time of 2 h were incorporated into the polymer matrix in different mass fractions of 3 wt% to 10 wt%. Tensile testing results of the first series of measurements showed that the addition of unfunctionalized wood flour resulted in a marginally stronger but less ductile composite compared to the pure matrix. In contrast, composites made of grafted wood flour incorporated into the matrix exhibited overall enhanced mechanical properties. In general, the longer the polymerization time, the higher the reinforcing effect on the resulting composite. The second series of measurements showed that a higher amount of added wood particles led to a higher YOUNG's modulus and yield strength, whereas the tensile toughness of the composite passed through a maximum. Therefore, addition of 7 wt% of grafted wood particles seemed to be the optimum ratio resulting in a stronger and more ductile composite compared to the pure polymer matrix. Considering the tensile testing results presented here, a composite possessing a two and a half times higher YOUNG's modulus, a two times higher yield point and a two times higher tensile toughness could be produced. Dynamic mechanical analysis (DMA) revealed decreased viscous behavior of the composite when wood with a low amount of grafted polymer was incorporated and increased viscous behavior with longer polymerization times. The higher the amount of added grafted wood, the higher the elastic behavior of the composite. It was observed that the glass transition temperature of the composites was barely affected by the incorporation of the wood particles.



## **Chapter V**

# **Experimental part**



# 13 Instrumentation

## 13.1 Chromatography

### 13.1.1 Column chromatography

Column chromatography was performed using silica gel 60 (70 – 230 mesh, 60 – 200  $\mu\text{m}$ , 60  $\text{\AA}$ , SIGMA ALDRICH).

### 13.1.2 Thin-layer Chromatography (TLC)

Precoated silica plates of the type “Kieselgel F254” MERCK were used for thin-layer chromatography. Staining was accomplished with basic potassium permanganate.

### 13.1.3 Size-exclusion chromatography (SEC)

Molar-mass distributions were determined with an AGILENT 1260 infinity system consisting of an autosampler (AGILENT 1260 ALS G1329B), an isocratic HPLC pump (AGILENT 1260 Infinity ISO), a PSS-SDV (POLYMER STANDARD SERVICES, styrene-divinylbenzene copolymer-network) precolumn, three PSS-SDV separation columns ( $8 \times 300$  mm, particle size 10  $\mu\text{m}$ , pore sizes of  $10^6$   $\text{\AA}$ ,  $10^5$   $\text{\AA}$ , and  $10^3$   $\text{\AA}$ ), an 80 Hz UV detector (AGILENT 1260 G1314B, set to a wavelength of 280 nm) and an RI detector (AGILENT 1260 G1362A). Tetrahydrofuran was used as the eluent maintained with a flow rate of  $1 \text{ mL min}^{-1}$  at  $35^\circ\text{C}$ . The setup was calibrated against narrowly distributed PMMA standards (PSS) with molar masses ranging from 0.8 – 1600  $\text{kg mol}^{-1}$  with toluene as internal standard. The molar masses of PMA and PVAc were obtained using the Mark–Houwink parameters (PMA:  $K = 1.95 \times 10^{-2} \text{ mL g}^{-1}$ ,  $a = 0.660$ ; PVAc:  $K = 1.56 \times 10^{-2} \text{ mL g}^{-1}$ ,  $a = 0.708$ ) according to the principle of universal calibration.<sup>[244–246]</sup> Prior to injection, all samples (approximately  $4 \text{ g L}^{-1}$ ) were filtered through a 25 mm VWR syringe filter containing a 0.45  $\mu\text{m}$  porous polytetrafluoroethylene membrane.

## 13.2 Spectroscopy

### 13.2.1 UV/vis spectroscopy (UV/vis)

The UV/vis absorption spectra were acquired with a CARY 300 scan, AGILANT spectrophotometer against 3 mM DTNB solution (as baseline), using a HELIMA quartz cuvette with a thickness of 10 mm. The spectra were recorded in steps of 1 nm, in the range between 352 nm and 600 nm, using a scan rate of 600 nm min<sup>-1</sup> and a spectral bandwidth of 2 nm.

#### Calibration curve for thiol contents

A linear calibration curve ( $R^2 > 0.998$ ) was obtained from measurements on five phosphate buffer solutions (pH 7 at 20 °C) containing 3.0 mM DTNB and different concentrations of reduced L-glutathione as thiol compound (method adopted from MALMSTRÖM and HANSSON).<sup>[201]</sup> For this purpose, five glutathione solutions (3.9, 7.8, 15.6, 31.3 and 62.5 μM) were freshly prepared and kept on ice before use. The respective glutathione solutions were mixed with an equal volume of a 6.0 mM DTNB solution and the absorbance at 412 nm was recorded after 5 min of mixing. The recorded UV/vis spectra are represented in Figure 13.1 and the obtained calibration curve is shown in Figure 13.2. The slope ( $m$ ) of the calibration curve corresponds to the absorption coefficient and was  $0.01237 \cdot 10^{-3} \text{ M}^{-1} \text{ cm}^{-1}$ . By rearranging Equation 13.2, the thiol concentration (and thus the concentration of the initiator) are directly related to the measured absorbance:

$$A = m \cdot c_{\text{thiol}} + b \quad (13.1)$$

$$c_{\text{thiol}} = \frac{A - b}{m} \quad (13.2)$$

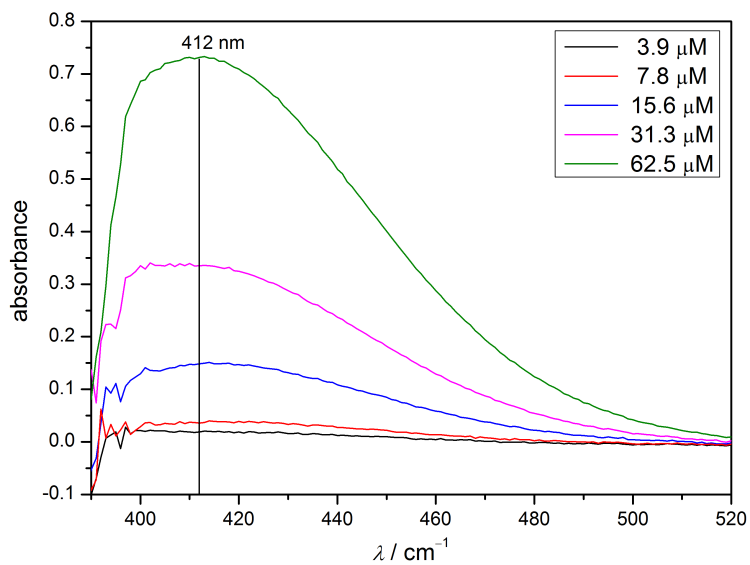


Figure 13.1: UV/vis absorption spectra of different concentration of glutathione.

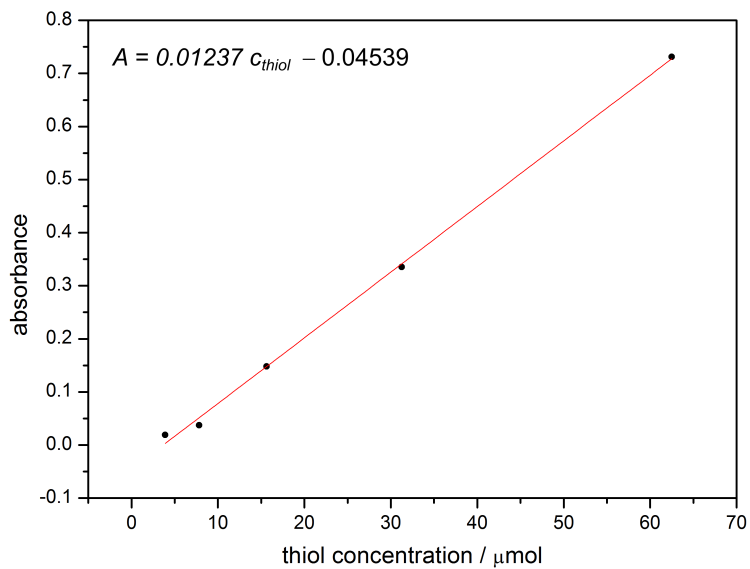


Figure 13.2: Calibration curve of different concentration of glutathione at 412 nm.

### Determination of the initiator content of modified wood

The cleaved disulfide-modified particles (see Section 14.6.2) were washed via Soxhlet extraction (THF, 24 h) and dried at 80 °C under reduced pressure. In a typical UV/vis experiment, 250 mg of the thiol containing particles were stirred in 100 mL of 3 mM DTNB solution (aqueous, pH 7) for 5 min at room temperature. After 30 min, the solution above the settled particles was taken via a syringe equipped with a 0.45  $\mu\text{m}$  PTFE filter. The absorbance of the solution was recorded using 3 mM DTNB solution as baseline. The recorded UV/vis spectra are represented in Figure 13.3

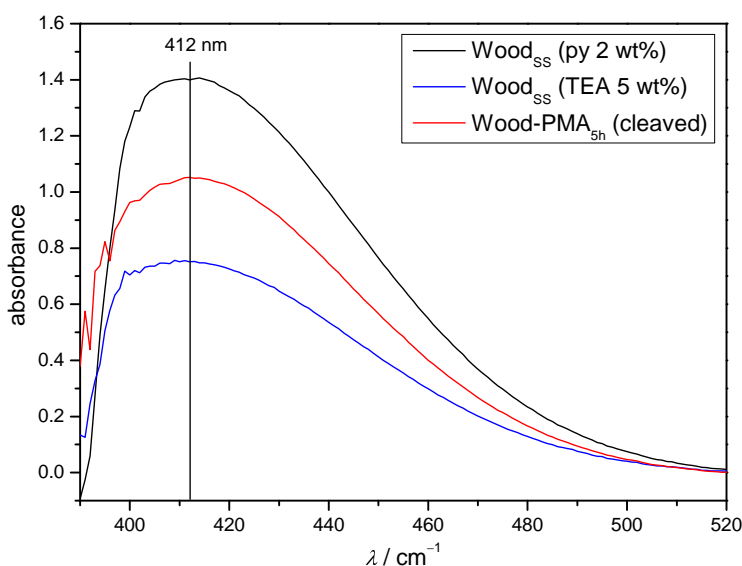


Figure 13.3: UV/vis absorption spectra of different DTT-treated wood particles.

### 13.2.2 Nuclear magnetic resonance (NMR) spectroscopy

$^1\text{H}$ -NMR and  $^{13}\text{C}$ -NMR spectra were recorded at room temperature with tetramethylsilane as external and the residual solvent protons as internal standard using a BRUKER AMX-300 or a VARIAN Unity 300. The concentration of the substances was approximately 20  $\text{mg mL}^{-1}$ . Chemical shifts are given in parts per million (ppm) on the tetramethylsilane scale.

### 13.2.3 Attenuated total reflection Fourier-transform infrared spectroscopy (ATR-FTIR)

ATR-FTIR spectra were recorded on a BRUKER IFS 88, equipped with a HARRICK MVP 2 Star™ ATR unit, a KBr beam splitter, a mercury cadmium telluride (MCT) detector, a globar and a tungsten halogen lamp or on a JASCO FT/IR-4100 equipped with Ge/KBr splitter. The spectra were recorded with 32 scans per sample, in a range from 750 – 4000  $\text{cm}^{-1}$  or 650 – 4000  $\text{cm}^{-1}$  and a resolution of 2  $\text{cm}^{-1}$  or 4  $\text{cm}^{-1}$ , respectively.

## 13.3 Microscopy

### 13.3.1 Scanning electron microscopy (SEM) and Energy-dispersive X-ray spectroscopy (EDX)

Scanning electron microscopy was recorded on a FEI Quanta FEG 250 equipped with an Everhart-Thornley Detector (ETD). The samples were coated with gold prior to investigation. The images were taken using an acceleration voltage of 30 kV in high vacuum with a magnification of 2000. Energy-dispersive X-ray (EDX) spectroscopy measurements were conducted 3 times per sample using the same acceleration voltage but recorded with a SUTW detector. Bromine content is given as weight percent (wt%). Errors are given as the error of the respective integral.

### 13.3.2 Fluorescence microscopy

Dried wood flour containing thiol groups was immersed in a solution of 32  $\mu\text{g mL}^{-1}$  fluorescence dye (ABBERIOR LIVE 510, NHS Ester) in PBS (phosphate-buffered saline, pH 7) and shaken overnight in the dark. Afterwards, the flour was washed 4 times with PBS, centrifuged and put on a microscope glass slide (THERMO FISHER). Fluorescence images were taken with a microscope LEICA DMi8 equipped with a 63x oil immersion objective. The excitation was performed with an argon krypton laser, which was set to a gain of 500 mV and an intensity of 2%. The excitation wavelength was set to 488 nm and the detection range set to 500 – 570 nm.

### 13.3.3 Optical microscopy

Pictures were taken with a LEICA S6 D microscope equipped with a camera (LEICA MC170 HD) at a maximum magnification of 40.

## 13.4 Mechanical analysis

### 13.4.1 Tensile testing

Tensile testing was performed on a ZWICK & ROELL Z2.5 instrument equipped with an air conditioner at a temperature of  $(24.9 \pm 0.3)^\circ\text{C}$ . All measurements were performed with a strain rate of  $0.25\text{ mm s}^{-1}$  and a contact pressure of 0.8 bar. The cross section of the dogbone shaped specimen was measured at three different places and averaged. Tensile data (YOUNG's modulus  $E$ , tensile toughness  $U_T$  and yield strength  $\sigma_y$ ) reported herein are averages taken from at least three specimens per polymer sample. The YOUNG's modulus ( $E$ ) was calculated in the linear region of 0.05% to 0.20% elongation. Errors are given as maximum error. The data were collected and analyzed with the computer programs testXpert II and ORIGINPRO 8.5G.

### 13.4.2 Dynamic mechanical analysis (DMA)

Dynamic mechanical analysis was performed on a PERKINELMER DMA8000 in *single cantilever* mode with a frequency of  $\nu = 1\text{ Hz}$ , a displacement of 0.01 mm, a heating rate of  $2^\circ\text{C min}^{-1}$  and a nitrogen flow of  $20\text{ mL min}^{-1}$ .

## 13.5 Thermal analysis

### 13.5.1 Thermogravimetric analysis (TGA)

Thermogravimetric analysis was conducted with a NETZSCH TG 209 F3 Tarsus instrument. The sample was placed in an aluminum oxide crucible and heated from  $25^\circ\text{C}$  to  $1000^\circ\text{C}$  with a heating rate of  $10^\circ\text{C min}^{-1}$  and under a nitrogen flow rate of  $20\text{ mL min}^{-1}$ . The data was collected and analyzed with the computer program NETZSCH Proteus Thermal Analysis 6.1.0. TGA experiments of bulk wood were performed with a  $100\text{ }\mu\text{m}$  thick cut of the surface.

### 13.5.2 Differential scanning calometry (DSC)

DSC measurements were conducted on a NETZSCH DSC 214 Polyma with automatically controlled liquid nitrogen cooling device in a temperature range from  $-50$  to  $150$  °C. Measurements were performed with a heating rate of  $10$  °C  $\text{min}^{-1}$  and a constant nitrogen flow of  $40$  mL  $\text{min}^{-1}$ . The experimental errors in the measurements were estimated to be about  $\pm 1$  °C.

## 13.6 Wetting analysis

### 13.6.1 Water contact angle (WCA)

Water contact angle measurements were performed using the static sessile drop technique on a DATAPHYSICS OCA 15EC with a measuring range of  $0 - 180$ °, equipped with a LED backlight and a VGA camera with  $752 \times 480$  pixel. Measurements were conducted at  $(21 \pm 0.2)$  °C and with droplets of  $5$   $\mu\text{L}$  demineralized water. Prior to WCA measurements, the wood flour was dried at  $60$  °C under reduced pressure and pressed into a pellet with a diameter of  $1$  cm.

### 13.6.2 Dynamic vapor sorption (DVS)

The sorption behavior was recorded on a DVS intrinsic device SURFACE MEASUREMENT SYSTEMS. The samples (approximately  $18$  mg) were measured as powder in a thermostatically controlled cabinet. The sorption processes were run at a constant temperature of  $20$  °C. The relative humidity (RH) was increased stepwise in the following sequence ( $0\%$ ,  $5\%$ ,  $15\%$ ,  $25\%$ ,  $35\%$ ,  $45\%$ ,  $55\%$ ,  $65\%$ ,  $75\%$ ,  $85\%$ ,  $95\%$ ) before decreasing to  $0\%$  RH in reverse order. A target RH was remained constant until the weight change per minute ( $dm/dt$ ) of the sample was less than  $0.002\%$   $\text{min}^{-1}$  over a period of  $10$  min. The target RH, actual RH, sample mass and testing time were recorded. The equilibrium moisture content (EMC) and reduced equilibrium moisture content ( $\text{EMC}_R$ ) were calculated according to Equation 13.3 and Equation 13.4.<sup>[247,248]</sup>

$$\text{EMC} (\%) = \frac{m_2 - m_1}{m_1} \cdot 100 \quad (13.3)$$

$$\text{EMC}_R(\%) = \text{EMC} \cdot \left(1 + \frac{\text{WPG}}{100}\right) \quad (13.4)$$

where  $m_2$  is the weight of the sample in equilibrium at a given RH,  $m_1$  is the oven-dry weight of the sample and WPG the weight percent gain of the sample owing to its chemical modification. The WPG of initiator-functionalized wood was calculated according to Equation 14.1 in Section 14.4.2, whereas the WPG of PMA-grafted wood was determined via TGA experiments (see Table 7.4 in Section 7.2).

## 13.7 Other Methods

### 13.7.1 Electrospray ionization mass spectrometry (ESI-MS)

Electrospray ionization (ESI) spectra were recorded with a BRUKER Daltonik ESI-ToF-MS (micrOTOF-) spectrometer in the analytic laboratory of the University's Institute for Organic Chemistry.

### 13.7.2 Elemental analysis (EA)

Elemental analysis of the carbon, hydrogen and sulfur content of the samples was performed using an ELEMENTAR "Vario El III" element analyzer in the analytic laboratory of the University's Institute for Inorganic Chemistry. A double determination was carried out and the average was taken. The error is assumed to be 0.3%.

## 14 Substances and synthesis

### 14.1 Commercially acquired substances

All chemicals were used as received unless otherwise noted. Ascorbic Acid (AsAc, reagent grade, SIGMA ALDRICH),  $\alpha$ -bromoisobutyryl bromide (BIBB, 98 %, SIGMA ALDRICH), Copper(II) bromide (99 %, SIGMA ALDRICH), 2-cyano-2-propyl dodecyl trithiocarbonate (98 %, SIGMA ALDRICH), 4-dimethylamino-pyridine (DMAP, 99 %, SIGMA ALDRICH), 5,5'-dithiobis(2-nitrobenzoic acid) (DTNB, Ellman's reagent, 99 %, SIGMA ALDRICH), dithiothreitol (DTT, Cleland's reagent,  $\geq 99$  %, SIGMA ALDRICH), ethanol (absolute, RIEDEL-DE HAEN), ethyl 2-bromobutyrate (EBIB, no purity specified, SIGMA ALDRICH), ethyl 2-mercaptopropionate ( $\geq 95$  %, SIGMA ALDRICH), L-glutathione ( $\geq 98$  %, SIGMA ALDRICH, reduced), 2-hydroxyethyl disulfide (techn. grade, SIGMA ALDRICH), oxalyl chloride (98 %, ALFA AESAR), *N,N,N',N'',N''*-pentamethyldiethylenetriamine (PMDETA, 99 %, SIGMA ALDRICH), pyridine (Py, SeccoSolv, MERCK), succinic anhydride ( $\geq 99$  %, SIGMA ALDRICH), 1,1'-Thiocarbonyldiimidazole (TCDI,  $\geq 95$  %, SIGMA ALDRICH), triethylamine (TEA,  $\geq 99$  %, SIGMA ALDRICH).

#### 14.1.1 Solvents

Acetone (ACS reagent, VWR CHEMICALS), anisole (99 %, ACROS ORGANICS), dichloromethan (DCM, HPLC Grade, FLUKA), dimethylformamide (DMF, ACS reagent, ROTH), propylene glycol methyl ether acetate (PGMEA,  $\geq 99$  %, Reagent-Plus, SIGMA ALDRICH), 2-propanol (IPA,  $\geq 99.5$  %, SIGMA ALDRICH), tetrahydrofuran (THF,  $\geq 99.5$  %, ROTH), toluene (tol, ACS reagent, ROTH), *o*-xylene (99 %, ACROS ORGANICS).

#### 14.1.2 Monomers and initiator

*tert*-Amyl peroxy acetate (TAPA, 97 %, AKZO), methyl acrylate (MA, 99 %, ACROS ORGANICS) and vinyl acetate (VAc,  $\geq 99$  %, FLUKA) were passed through a column containing aluminum oxide (basic, Brockmann I, 150 mesh, SIGMA

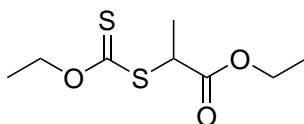
ALDRICH) or inhibitor remover (SIGMA ALDRICH) before use. All purified monomers were stored at 4 °C until use. Azobisisobutyronitrile (AIBN,  $\geq 98\%$ , FLUKA) was recrystallized twice from methanol and stored at 4 °C.

### 14.1.3 Miscellaneous

Pine sapwood was cut in cubes of  $10 \times 10 \times 5 \text{ mm}^3$  (tangential  $\times$ , radial  $\times$  longitudinal). Wood dust/flour (Arbocel<sup>®</sup>, natural raw cellulose, Grade C 100) was purchased from J. RETTENMAIER & SÖHNE GMBH & CO KG. The particle size was 70 – 150  $\mu\text{m}$  with spruce as dominant component. Soxhlet sleeves (MN 645, 22  $\times$  80 mm) were purchased from MACHEREY-NAGEL.

## 14.2 Synthesis of substances

### 14.2.1 2-Ethoxythiocarbonylsulfanyl-propionic acid ethyl ester<sup>[21]</sup> (1)



1,1'-Thiocarbonyldiimidazole (TCDI, 2.00 g, 11.2 mmol, 1.0 eq.) was dissolved in dry toluene (60 mL) under argon atmosphere. Ethanol (0.52 g, 0.66 mL, 1.0 eq.) was added dropwise and the solution was stirred for 6 h at 60 °C. After that, the solution was cooled to room temperature over night. 2-Mercaptopropionate (1.50 g, 1.46 mL, 11.2 mmol, 1.0 eq.) was added and the resulting suspension was stirred for additional 6 h at 60 °C. The solvent was removed under reduced pressure and the product was purified via column chromatography (*n*-hexane/ethyl acetate 9 : 1). The product **1** was obtained as a yellowish oil (2.07 g, 9.31 mmol, 83 %).

TLC:  $R_f = 0.5$  (*n*-hexane/ethyl acetate 9 : 1).

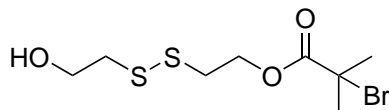
<sup>1</sup>H-NMR (300 MHz, CDCl<sub>3</sub>):  $\delta$  (ppm) = 1.28 (t,  $J = 7.1 \text{ Hz}$ , 3 H, CH<sub>3</sub>), 1.41 (t,  $J = 7.4 \text{ Hz}$ , 3 H, CH<sub>3</sub>), 1.57 (d,  $J = 7.7 \text{ Hz}$ , 3 H, CH<sub>3</sub>), 4.20 (q,  $J = 7.4 \text{ Hz}$ , 2 H,

OCH<sub>2</sub>CH<sub>3</sub>), 4.38 (q, *J* = 7.4 Hz, 1 H, SCHCH<sub>3</sub>), 4.64 (q, *J* = 7.1 Hz, 2 H, OCH<sub>2</sub>CH<sub>3</sub>).

<sup>13</sup>C-NMR (75 MHz, CDCl<sub>3</sub>): δ (ppm) = 13.8, 14.3, 17.1, 47.4, 61.9, 70.4, 171.5, 212.3.

HR-MS (ESI<sup>+</sup>, C<sub>8</sub>H<sub>14</sub>O<sub>3</sub>S<sub>2</sub>): *m/z* = 245.0277 [C<sub>8</sub>H<sub>14</sub>O<sub>3</sub>S<sub>2</sub> + Na]<sup>+</sup>.

#### 14.2.2 2-((2-hydroxyethyl)disulfanyl)ethyl 2-bromo-2-methylpropanoate<sup>[201]</sup> (2)



2-Hydroxyethyl disulfide (20.0 g, 15.9 mL, 130 mmol, 1.0 eq.) and triethylamine (19.6 g, 26.9 mL, 194 mmol, 1.5 eq.) were dissolved in THF (300 mL) and cooled to 0 °C. α-Bromoisobutyryl bromide (29.8 g, 16.0 mL, 130 mmol, 1.0 eq.) was added dropwise and the solution was stirred at room temperature for 3 h. The precipitate was filtered off and the solution was concentrated under reduced pressure, followed by addition of DCM (150 mL). The solution was washed with a saturated solution of NaHSO<sub>4</sub> (3 × 40 mL), Na<sub>2</sub>CO<sub>3</sub> (3 × 40 mL), and brine (40 mL) and dried using MgSO<sub>4</sub>. After filtration the solvent was removed *in vacuo* and the crude product was purified using column chromatography (gradient, *n*-hexane to *n*-hexane/ethyl acetate 3 : 2). The product 2 was obtained as yellowish oil (13.4 g, 44.2 mmol, 34 %).

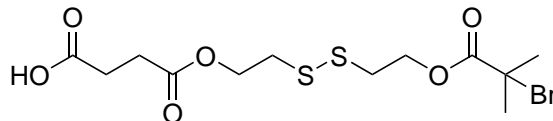
TLC: R<sub>f</sub> = 0.3 (*n*-hexane/ethyl acetate 3 : 2).

<sup>1</sup>H-NMR (300 MHz, CDCl<sub>3</sub>): δ (ppm) = 1.94 (s, 6 H, 2 × CH<sub>3</sub>), 2.00 (s, 1 H, OH), 2.89 (t, *J* = 5.8 Hz, 2 H, HOCH<sub>2</sub>CH<sub>2</sub>S), 2.97 (t, *J* = 6.7 Hz, 2 H, SCH<sub>2</sub>CH<sub>2</sub>O), 3.89 (t, *J* = 5.8 Hz, 2 H, HOCH<sub>2</sub>CH<sub>2</sub>S), 4.44 (t, *J* = 6.7 Hz, 2 H, SCH<sub>2</sub>CH<sub>2</sub>O).

<sup>13</sup>C-NMR (75 MHz, CDCl<sub>3</sub>): δ (ppm) = 30.7, 36.5, 41.6, 55.5, 60.2, 63.7, 171.5.

HR-MS (ESI<sup>+</sup>, C<sub>8</sub>H<sub>15</sub>BrO<sub>3</sub>S<sub>2</sub>): *m/z* = 324.9540 [C<sub>8</sub>H<sub>15</sub><sup>79</sup>BrO<sub>3</sub>S<sub>2</sub> + Na]<sup>+</sup>, 326.9520 [C<sub>8</sub>H<sub>15</sub><sup>81</sup>BrO<sub>3</sub>S<sub>2</sub> + Na]<sup>+</sup>.

### 14.2.3 4-(2-((2-(2-bromo-2-methylpropanoyloxy)ethyl)disulfanyl)ethoxy)-4-oxobutanoic acid<sup>[201]</sup> (3)



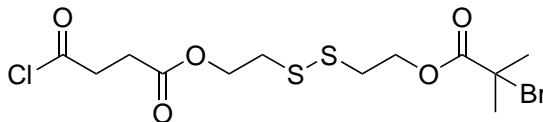
Succinic anhydride (4.75 g, 47.5 mmol, 1.2 eq.) was added to a flask containing alcohol **2** (12.0 g, 39.6 mmol, 1.0 eq.), DMAP (966 mg, 7.91 mmol, 0.2 eq.) and DCM (50 mL). The reaction was stirred over night at room temperature and the remaining anhydride was quenched by adding of H<sub>2</sub>O (15 mL). After addition of DCM (100 mL) the organic phase was washed using a solution of NaHSO<sub>4</sub> (3 × 30 mL) and brine (30 mL) and dried using MgSO<sub>4</sub>. After filtration and removal of the solvent the yellowish, oily product **3** was obtained (17.3 g, 42.9 mmol, 90 %) (solvent corrected).

<sup>1</sup>H-NMR (300 MHz, CDCl<sub>3</sub>): δ (ppm) = 1.93 (s, 6 H, 2 × CH<sub>3</sub>), 2.61–2.72 (m, 4 H, HO<sub>2</sub>CCH<sub>2</sub>CH<sub>2</sub>), 2.93 (t, *J* = 6.6 Hz, 2 H, CH<sub>2</sub>SSCH<sub>2</sub>), 2.96 (t, *J* = 6.6 Hz, 2 H, CH<sub>2</sub>SSCH<sub>2</sub>S), 4.36 (t, *J* = 6.6 Hz, 2 H, OCH<sub>2</sub>CH<sub>2</sub>S), 4.43 (t, *J* = 6.6 Hz, 2 H, OCH<sub>2</sub>CH<sub>2</sub>S).

<sup>13</sup>C-NMR (75 MHz, CDCl<sub>3</sub>): δ (ppm) = 28.9, 29.0, 30.8, 36.9, 37.3, 55.7, 62.7, 63.7, 171.6, 172.0, 178.0.

HR-MS (ESI<sup>+</sup>, C<sub>12</sub>H<sub>19</sub>BrO<sub>6</sub>S<sub>2</sub>): *m/z* = 424.9706 [C<sub>12</sub>H<sub>19</sub><sup>79</sup>BrO<sub>6</sub>S<sub>2</sub> + Na]<sup>+</sup>, 426.9684 [C<sub>12</sub>H<sub>19</sub><sup>81</sup>BrO<sub>6</sub>S<sub>2</sub> + Na]<sup>+</sup>.

### 14.2.4 2-((2-(2-bromo-2-methylpropanoyloxy)ethyl)disulfanyl)ethyl 4-chloro-4-oxobutanoate<sup>[201]</sup> (4)



Oxalyl chloride (9.42 g, 6.28 mL, 74.2 mmol, 2.0 eq.) and acid **3** (15.0 g, 37.2 mmol, 1.0 eq.) were dissolved in DCM (20 mL) and cooled down to 0 °C. A catalytic amount of DMF was added and the solution was stirred at room temperature

for 2.5 h. The remaining oxalyl chloride was azeotropically removed by use of chloroform (6 × 20 mL) and the product **4** was obtained as yellow to brown oil. Since the product slowly gets hydrolyzed over time, it was prepared freshly, purified by distillation and immediately immobilized on the wood surface.

**<sup>1</sup>H-NMR** (300 MHz, CDCl<sub>3</sub>: δ (ppm) = 1.94 (s, 6 H, 2 × CH<sub>3</sub>), 2.71 (t, 2 H), 2.93–3.01 (m, 4 H), 3.23 (t, 2 H), 4.34–4.47 (m, 4 H).

**<sup>13</sup>C-NMR** (75 MHz, CDCl<sub>3</sub>: δ (ppm) = 29.3, 30.7, 36.8, 41.7, 55.5, 62.8, 63.5, 170.7, 171.5, 173.0.

**HR-MS** (ESI<sup>+</sup>, C<sub>12</sub>H<sub>18</sub>BrClO<sub>5</sub>S<sub>2</sub>): *m/z* = 434.0309 [C<sub>13</sub>H<sub>21</sub><sup>79</sup>BrO<sub>6</sub>S<sub>2</sub> + NH<sub>4</sub>]<sup>+</sup>, 436.0286 [C<sub>13</sub>H<sub>21</sub><sup>81</sup>BrO<sub>6</sub>S<sub>2</sub> + NH<sub>4</sub>]<sup>+</sup>.

## 14.3 Pretreatment of wood

### 14.3.1 Soxhlet extraction

The wood cubes were extracted using a Soxhlet apparatus with DCM as solvent for 16 h, followed by a Soxhlet extraction with a solution of H<sub>2</sub>O, acetone and IPA (1 : 1 : 1, vol%) for 16 h to remove soluble components. Afterwards, the samples were dried at 60 °C under reduced pressure and kept in a desiccator until use.

The wood particles were extracted with a Soxhlet apparatus using DCM for 16 h followed by drying at 60 °C under reduced pressure, grounded with mortar and pestle and kept in a desiccator until use.

### 14.3.2 Alkaline treatment

The wood sample was immersed in a 2 M NaOH solution at room temperature and stirred for 2 h. The wood was filtered off, stirred in demineralized water for 2 h, dried at 105 °C under reduced pressure and kept in a desiccator until use.

## 14.4 Immobilization reactions

### 14.4.1 Immobilization of xanthate on wood surface

1,1'-Thiocarbonyldiimidazole (TCDI, 950 mg, 5.33 mmol, 1.0 eq.) was dissolved in either dry toluene or dimethylformamide (30 mL) under argon atmosphere. 2-Mercapto propionate (670 mg, 0.65 mL, 1.0 eq.) was added dropwise and the

solution was stirred for 6 h at 60 °C. After that, the wood cube (10 × 10 × 5 mm<sup>3</sup>) was immersed in the solution and the mixture was stirred for additional 16 h at 60 °C. The wood specimen was removed, washed with copious amounts of the solvent and tetrahydrofuran, dried at 105 °C and kept in a desiccator until further use.

### 14.4.2 Immobilization of BIBB on wood

The immobilization of the initiator was inspired by SCHWELLENBACH *et al.* and two different initiator densities were targeted (A, B).<sup>[185]</sup> It has been achieved by placing 1 g of dry wood dust in a solution of 100 mL DCM containing TEA or pyridine (A: 2 wt%, B: 5 wt%). The resulting suspension was cooled to 0 °C and BIBB (A: 2 wt%, B: 5 wt%) was added dropwise over 15 min and stirred additional 30 min at that temperature. Subsequently, the reaction mixture was stirred at room temperature until complete conversion (A: 2.5 h, B: 23 h). Afterwards the wood particles were filtered off and washed with copious amounts of tetrahydrofuran, acetone, IPA and DCM, dried at 60 °C under reduced pressure, weighed and kept in a desiccator until use. The weight percent gain (WPG) describes the percentage increase in weight of a sample after a modification step and was calculated as follow:

$$\text{WPG (\%)} = \frac{(w_2 - w_1)}{w_1} \cdot 100 \quad (14.1)$$

where  $w_2$  is the oven-dry weight of the modified wood sample and  $w_1$  is the oven-dry weight of the wood sample before modification.<sup>[177,248]</sup>

### 14.4.3 Immobilization of the disulfide initiator on wood

The immobilization was done by placing 100 mg dry wood particles in 7 mL dry DCM (93 wt%) containing dry pyridine (2 wt%). The suspension was cooled to 0 °C and stirred for 15 min. The disulfide containing acyl chloride **4** (freshly prepared, 5 wt%) was added dropwise to the wood particles over a period of 15 min and the resulting mixture was stirred for 24 h at room temperature. Ethanol (10 mL) was added slowly to quench unreacted acyl chloride and the solution was stirred for additional 15 min. The particles were filtered off, washed with copious amounts of tetrahydrofuran and DCM, dried at 60 °C under reduced pressure and kept in a desiccator until use.

## 14.5 Polymerizations

### 14.5.1 Synthesis of poly(methyl acrylate) as polymer matrix

Methyl acrylate (MA, 5.3 mL, 58.1 mmol, 480 eq.), 2-cyano-2-propyl trithiocarbonate (40.0 mg, 0.166 mg, 1 eq.) and AIBN (2.0 mg, 12.0  $\mu\text{mol}$ , 0.1 eq.) were dissolved in toluene (10.5 mL) and degassed for 10 min at 0 °C. The mixture was polymerized at 60 °C for 23 h, cooled down to room temperature, precipitated twice in methanol and dried at 80 °C under reduced pressure. Poly(methyl acrylate) (PMA) had a molecular weight of  $3.6 \cdot 10^4 \text{ g mol}^{-1}$ , a dispersity of 1.09 and a glass transition temperature of 19 °C (measured via DSC).

### 14.5.2 Grafting of vinyl acetate via MADIX Polymerization

A wood cube (approximately 230 mg) was introduced in a round-bottom flask and degassed via one vacuum-argon cycle. A solution of vinyl acetate (VAc, 15 mL, 14.0 g, 162 mmol, 300 eq.), toluene (15 mL), xanthate **1** (118 mg, 0.54 mmol, 1 eq.) and AIBN (10 mg, 0.06 mmol, 0.1 eq.) were cooled to 0 °C, degassed with argon for 30 min and afterwards added to the wood cube. The resulting mixture was gently stirred for 16 h at 60 °C. The reaction was stopped by cooling and exposure to air. A small amount of polymerization solution was drawn to measure the monomer conversion gravimetrically or via  $^1\text{H-NMR}$  and the molar mass of the free polymer was determined by SEC. The wood specimen was filtered off, washed with toluene and extracted via a Soxhlet extraction with DCM and dried at 80 °C under reduced pressure.

### 14.5.3 Grafting of methyl acrylate via MADIX Polymerization

A wood cube (approximately 230 mg) was introduced in a round-bottom flask and degassed via one vacuum-argon cycle. A solution of methyl acrylate (MA, 15 mL, 15.8 g, 183 mmol, 300 eq.), toluene (15 mL), xanthate **1** (136 mg, 0.61 mmol, 1 eq.) and AIBN (10 mg, 0.06 mmol, 0.1 eq.) were cooled to 0 °C, degassed with argon for 10 min and afterwards added to the wood. The mixture was gently stirred for 5.5 h at 60 °C. The reaction was stopped by exposure to air. A small amount of polymerization solution was drawn to measure the monomer conversion gravimetrically or via  $^1\text{H-NMR}$  and the molar mass of the free polymer was determined by SEC. The wood specimen was filtered off and extracted via a Soxhlet extraction with DCM and dried at 80 °C under reduced pressure.

### 14.5.4 Grafting from wood dust via ARGET ATRP

The procedure of the solid-supported ARGET ATRP was adopted from HANSSON *et al.*, but in the absence of sacrificial initiator.<sup>[164]</sup> The initiator-modified wood particles (see Section 14.4.2, 200 mg) were suspended in a solution of methyl acrylate (MA, 10 g, 116 mmol, 400 eq.), anisole (10 g), CuBr<sub>2</sub> (6.5 mg, 29 μmol, 0.1 eq.), *N,N,N',N'',N''*-pentamethyldiethylenetriamine (50 mg, 290 μmol, 1 eq.) before ascorbic acid (AsAc, 51 mg, 290 μmol, 1 eq.) was added. The flask was sealed and degassed with argon for 5 min. Afterwards, the reaction mixture was heated to 60 °C for the specific period (45 min to 9.5 h). When the polymerization time was reached, the particles were filtered off, washed with tetrahydrofuran and acetone, dried at 60 °C under reduced pressure and stored in a desiccator.

## 14.6 Detachment of surface-tethered polymer

### 14.6.1 Cleavage of polymer grafts via radicals

The polymer-coated wood specimen (approximately 270 mg) was dispersed in a solution of *tert*-amyl peroxy acetate (TAPA, 400 mg) in toluene (5 mL), that had been degassed with argon for 5 min prior to use. The mixture was then heated to 130 °C for 3.5 h. The wood specimen was filtered off and washed with toluene and tetrahydrofuran, dried at 60 °C and kept in a desiccator. The polymer solution was concentrated under reduced pressure and analyzed by SEC.

### 14.6.2 Cleavage of disulfide-initiator polymer grafts

The PMA-grafted disulfide-containing wood particles (100 mg) were placed in a solution containing DTT (160 mg) and TEA (0.3 mL) in THF (10 mL) and stirred for 7 d.<sup>[201]</sup> After that, the particles were separated by centrifugation and washed with tetrahydrofuran (3 × 15 mL). The polymer solution was concentrated under reduced pressure and analyzed by SEC. The particles were dried at 60 °C and kept in a desiccator.

## 14.7 Preparation of composite materials

Poly(methyl acrylate) (see Section 14.5.1, 4 g) was dissolved in propylene glycol methyl ether acetate (PGMEA, 8 mL) to obtain a highly viscous solution. Wood particles (0 to 10 wt%, preparation in Section 14.5.4) were added to this solution and the mixture was stirred until the particles were well dispersed (4 – 6 h). The specimen were prepared via solvent casting of the mixture by slowly drying in a PTFE mold for 3 d at 100 °C under reduced pressure. Tensile testing was conducted with dogshaped specimen, whereas dynamic mechanical analysis was performed using rod-shaped specimen (see Figure 14.1 and Figure 14.2).

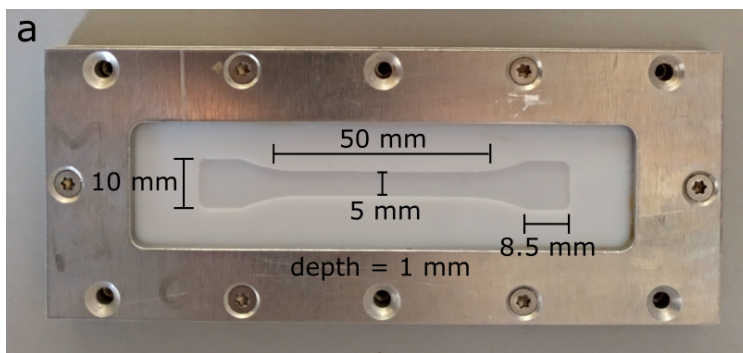


Figure 14.1: Image of a PTFE mold used for tensile testing, relevant dimensions are indicated.

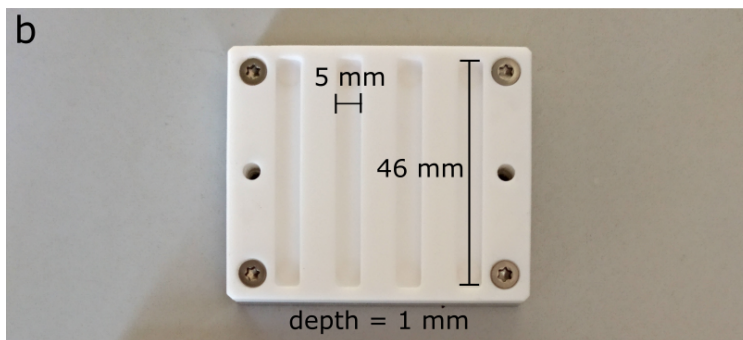


Figure 14.2: Image of a PTFE mold used for dynamic mechanical analysis, relevant dimensions are indicated.



# **Chapter VI**

## **References**



## References

- [1] Plastics – the Facts 2016, <http://www.plasticseurope.org>, accessed October 09th, **2017**.
- [2] M. Lechner, K. Gehrke, E. Nordmeier, *Makromolekulare Chemie*, 5. Edition, Springer-Verlag, Berlin Heidelberg, **2014**.
- [3] W. Kaiser, *Kunststoffchemie für Ingenieure - Von der Synthese bis zur Anwendung*, 4. Edition, Carl Hanser Verlag, München, **2015**.
- [4] D. A. Shipp, *Polymer Reviews* **2011**, 51, 99–103.
- [5] *Fundamentals of Controlled/Living Radical Polymerization*, (Eds.: B. Sumerlin, N. Tsarevsky), The Royal Society of Chemistry, Cambridge, **2013**.
- [6] A. Shenoy, *Thermoplastic melt rheology and processing*, 1. Edition, CRC Press, New York, **1997**.
- [7] C. P. MacDermott, A. Shenoy, *Selecting thermoplastics for engineering applications*, 2. Edition, CRC Press, New York, **1997**.
- [8] H.-J. Bargel, G. Schulze, H. Hilbrans, K.-H. Hübner, O. Krüger, *Werkstoffkunde*, 9. Edition, (Eds.: H.-J. Bargel, G. Schulze), Springer-Verlag, Heidelberg, **2013**.
- [9] Y. Li in *Advances in Composite Materials - Analysis of Natural and Man-Made Materials*, (Ed.: P. Tesinova), InTech, Rijeka, **2011**, Chapter 9, pp. 229–284.
- [10] P. K. Kim. Jin Kuk, *Recent Advances in the Processing of Wood–Plastic Composites*, Springer Berlin, Heidelberg, **2010**, pp. 1–13.
- [11] Y.-F. Li, Y.-X. Liu, X.-M. Wang, Q.-L. Wu, H.-P. Yu, J. Li, *Journal of Applied Polymer Science* **2011**, 119, 3207–3216.
- [12] A. Wagenführ, F. Scholz, R. Wagenführ, *Taschenbuch der Holztechnik*, 2. Edition, Carl Hanser Verlag GmbH & Co. KG, München, **2012**.
- [13] Y. Fu, G. Li, H. Yu, Y. Liu, *Applied Surface Science* **2012**, 258, 2529–2533.
- [14] H. Yu, Y. Fu, G. Li, Y. Liu, *Holzforschung* **2013**, 67, 455–461.
- [15] *Wood-polymer Composites*, 1. Edition, (Eds.: K. Oksma-Niska, M. Sain), CRC Press, Boca Raton, **2008**.
- [16] A. K. Bledzki, S. Reihmane, J. Gassan, *Polymer-Plastics Technology and Engineering* **1998**, 37, 451–468.
- [17] A. Wechsler, S. Hiziroglu, *Building and Environment* **2007**, 42, 2637–2644.

- 
- [18] A. A. Klyosov, *Wood–Plastic Composites*, John Wiley & Sons, New York, **2007**.
- [19] *Controlled and Living Polymerizations*, 1. Edition, (Eds.: K. Matyjaszewski, A. H. E. Müller), WILEY-VCH Verlag, Weinheim, **2009**.
- [20] P. Vana, C. Rossner in *Advances in Polymer Science*, Vol. 270, (Ed.: P. Vana), Springer International Publishing, Basel, **2016**.
- [21] D. H. Nguyen, M. R. Wood, Y. Zhao, *Macromolecules* **2008**, *41*, 7071–7078.
- [22] W. Jakubowski, K. Min, K. Matyjaszewski, *Macromolecules* **2006**, *39*, 39–45.
- [23] K. Babu, R. Dhamodharan, *Nanoscale Research Letters* **2008**, *3*, 109–117.
- [24] M. Z. Rong, M. Q. Zhang, Y. Liu, G. C. Yang, H. M. Zeng, *Composites Science and Technology* **2001**, *61*, 1437–1447.
- [25] E. Sjostrom, *Wood chemistry: fundamentals and applications*, 2. Edition, Academic Press, San Diego, **2013**.
- [26] D. Fengel, G. Wegener, *Wood: chemistry, ultrastructure, reactions*. Kessel, München, **2003**.
- [27] C. A. S. Hill in *Wood Modification: Chemical, Thermal and Other Processes*, (Ed.: C. V. Stevens), Wiley, New York, **2006**, Chapter 2, pp. 46–76.
- [28] D. Klemm, B. Heublein, H.-P. Fink, A. Bohn, *Angewandte Chemie International Edition* **2005**, *44*, 3358–3393.
- [29] C. Zhou, Q. Wu in *Nanocrystals - Synthesis, Characterization and Applications*, (Ed.: S. Neralla), IntechOpen, Rijeka, **2012**, Chapter 6, pp. 103–120.
- [30] S. J. Eichhorn, A. Dufresne, M. Aranguren, N. E. Marcovich, J. R. Capadona, S. J. Rowan, C. Weder, W. Thielemans, M. Roman, S. Renneckar, W. Gindl, S. Veigel, J. Keckes, H. Yano, K. Abe, M. Nogi, A. N. Nakagaito, A. Mangalam, J. Simonsen, A. S. Benight, A. Bismarck, L. A. Berglund, T. Peijs, *Journal of Materials Science* **2010**, *45*, 1–33.
- [31] L. J. Gibson, *Journal of the Royal Society Interface* **2012**, *9*, 2749–2766.
- [32] *Tensile Testing*, 2. Edition, (Ed.: J. Davis), ASM International, Materials Park, **2004**.
- [33] R. M. Rowell, R. Pettersen, J. S. Han, J. S. Rowell, M. A. Tshabalala in *Handbook Of Wood Chemistry And Wood Composites*, (Ed.: R. M. Rowell), CRC Press, New York, **2005**, Chapter 3, pp. 35–74.

- [34] V. K. Thakur, M. K. Thakur, P. Raghavan, M. R. Kessler, *ACS Sustainable Chem. Eng.* **2014**, *2*, 1072–1092.
- [35] T. Grüneberg, PhD thesis, Georg-August-University Göttingen, **2010**.
- [36] Forest Products Laboratory, *Wood Handbook: Wood as an Engineering Material*, (Ed.: R. J. Ross), CreateSpace Independent Publishing Platform, Madison, **2010**.
- [37] J. Fahlén, PhD thesis, Royal Institute of Technology (KTH), Stockholm, **2005**.
- [38] D. Fengel, *TAPPI* **1970**, *53*, 497–503.
- [39] J. Brandstrom, PhD thesis, Swedish University of Agricultural Science Uppsala, **2002**.
- [40] R. E. Booker, J. Sell, *European Journal of Wood and Wood Products* **1998**, *56*, 1–8.
- [41] M. Eder, N. Terziev, G. Daniel, I. Burgert, *Holzforschung* **2008**, *62*, 77–81.
- [42] J. Peydecastaing, PhD thesis, Université de Toulouse, **2008**.
- [43] D. Fengel, G. Wegener, *Wood - Chemistry, Ultrastructure, Reactions*, Walter de Gruyter, Berlin, **1989**.
- [44] G. Mantanis, R. Young, R. M. Rowell, *Wood Science and Technology* **1994**, *28*, 480–490.
- [45] W. McDonough, M. Braungart, *Cradle to Cradle: Remaking the Way We Make Things*, 1. Edition, North Point Press, New York, **2002**.
- [46] S. M. El-Haggag, M. A. Kamel in *Advances in Composite Materials - Analysis of Natural and Man-Made Materials*, (Ed.: P. Tesinova), Intech, Rijeka, **2011**, Chapter 13, pp. 325–344.
- [47] V. Kumar, L. Tyagi, S. Sinha, *Reviews in Chemical Engineering* **2011**, *27*, 253–264.
- [48] C. Clemons, *Forest Products Journal* **2002**, *52*, 10–18.
- [49] S. K. Yeh, R. K. Gupta, *Composites Part A: Applied Science and Manufacturing* **2008**, *39*, 1694–1699.
- [50] A. K. Bledzki, J. Gassan, *Prog. Polym. Sci.* **1999**, *24*, 221–274.
- [51] N. M. Stark, R. E. Rowlands, *Wood and fiber science* **2003**, *35*, 167–174.
- [52] A. Nourbakhsh, A. Ashori, *Bioresource Technology* **2010**, *101*, 2525–2528.

- 
- [53] L. Teuber, PhD thesis, Georg-August-University Göttingen, **2016**.
- [54] I. Zivkovic, C. Fragassa, A. Pavlovic, *International Journal for Quality Research* **2016**, *10*, 205–218.
- [55] G. W. Ehrenstein, *Faserverbundkunststoffe – Werkstoff, Verarbeitung, Eigenschaften*, 2. Edition, Carl Hanser Verlag GmbH & Co. KG, München, **2006**.
- [56] C. Guo, L. Zhou, J. Lv, *Polymers and Polymer Composites* **2013**, *21*, 449–456.
- [57] T. J. Keener, R. K. Stuart, T. K. Brown, *Composites Part A: Applied Science and Manufacturing* **2004**, *35*, 357–362.
- [58] Q. Li, L. M. Matuana, *Journal of Thermoplastic Composite Materials* **2003**, *16*, 551–564.
- [59] S. Borysiak, B. Doczekalska, *Fibres & Textiles in Eastern Europe* **2008**, *16*, 101–103.
- [60] S. Borysiak, *Journal of Thermal Analysis and Calorimetry* **2012**, *109*, 595–603.
- [61] *Handbook of Radical Polymerization*, 1. Edition, (Eds.: K. Matyjaszewski, T. P. Davis), John Wiley & Sons, Hoboken, **2002**.
- [62] B. Ebeling, PhD thesis, Georg-August-University Göttingen, **2015**.
- [63] W. A. Braunecker, K. Matyjaszewski, *Progress in Polymer Science* **2007**, *32*, 93–146.
- [64] O. W. WEBSTER, *Science* **1991**, *251*, 1–48.
- [65] M. Szwarc, M. Levy, R. Milkovich, *Journal of the American Chemical Society* **1956**, *78*, 2656–2657.
- [66] A. D. Jenkins, R. G. Jones, G. Moad, *Pure and Applied Chemistry* **2009**, *82*, 483–491.
- [67] G. Moad, E. Rizzardo, D. H. Solomon, *Macromolecules* **1982**, *15*, 909–914.
- [68] R. B. Grubbs, *Polymer Reviews* **2011**, *51*, 104–137.
- [69] J. Nicolas, Y. Guillaneuf, C. Lefay, D. Bertin, D. Gigmès, B. Charleux, *Progress in Polymer Science* **2013**, *38*, 63–235.
- [70] G. Moad, E. Rizzardo, *The History of Nitroxide-mediated Polymerization*, Polymer Chemistry Series, Cambridge, **2015**.
- [71] M. Kato, M. Kamigaito, M. Sawamoto, T. Higashimura, *Macromolecules* **1995**, *28*, 1721–1723.
- [72] N. Ayres, *Polymer Reviews* **2011**, *51*, 138–162.

- [73] J.-S. Wang, K. Matyjaszewski, *Macromolecules* **1995**, *28*, 7901–7910.
- [74] G. Moad, E. Rizzardo, S. H. Thang, *Australian Journal of Chemistry* **2005**, *58*, 379–410.
- [75] G. Moad, E. Rizzardo, S. H. Thang, *Australian Journal of Chemistry* **2006**, *59*, 669–692.
- [76] G. Moad, E. Rizzardo, S. H. Thang, *Australian Journal of Chemistry* **2009**, *62*, 1402–1472.
- [77] G. Moad, B. E. Rizzardo, S. H. Thang, *Australian Journal of Chemistry* **2012**, *65*, 985–1076.
- [78] L. Lavanant, D. Paripovic, N. Schu, C. Sugnaux, S. Tugulu, H.-A. Klok, *Chemical Reviews* **2009**, 5437–5527.
- [79] D. Hübner, PhD thesis, Georg-August-Universität Göttingen, **2016**.
- [80] M. Henze, D. Mädge, O. Prucker, J. Rühle, *Macromolecules* **2014**, *47*, 2929–2937.
- [81] J. O. Zoppe, N. C. Ataman, P. Mocny, J. Wang, J. Moraes, H. A. Klok, *Chemical Reviews* **2017**, *117*, 1105–1318.
- [82] J. Chiefari, Y. K. Chong, F. Ercole, J. Krstina, J. Jeffery, T. P. T. Le, R. T. A. Mayadunne, G. F. Meijs, C. L. Moad, G. Moad, E. Rizzardo, S. H. Thang, *Macromolecules* **1998**, *31*, 5559–5562.
- [83] D. Charmot, P. Corpart, H. Adam, S. Z. Zard, T. Biadatti, G. Bouhadir, *Macromol. Symp.* **2000**, *150*, 23–32.
- [84] M. Destarac, C. Brochon, J.-M. Catala, A. Wilczewska, S. Z. Zard, *Macromolecular Chemistry and Physics* **2002**, *203*, 2281–2289.
- [85] J. Chiefari, E. Rizzardo in *Handbook of Radical Polymerization*, (Eds.: K. Matyjaszewski, T. P. Davis), John Wiley & Sons, Inc., Hoboken, **2002**, Chapter 12, pp. 629–690.
- [86] Y. Zhao, S. Perrier in *Controlled Radical Polymerization at and from Solid Surfaces*, (Ed.: P. Vana), Springer International Publishing, Basel, **2016**, Chapter 3, pp. 77–106.
- [87] S. Perrier, P. Takolpuckdee, *Journal of Polymer Science Part A: Polymer Chemistry* **2005**, *43*, 5347–5393.
- [88] S. Perrier, *Macromolecules* **2017**, *50*, 7433–7447.

- 
- [89] C. L. McCormick, A. B. Lowe, *Accounts of Chemical Research* **2004**, *37*, 312–325.
- [90] D. H. Nguyen, PhD thesis, Georg-August-Universität Göttingen, **2007**.
- [91] M. H. Stenzel, L. Cummins, G. E. Roberts, T. P. Davis, P. Vana, C. Barner-Kowollik, *Macromolecular Chemistry and Physics* **2003**, *204*, 1160–1168.
- [92] D. H. Nguyen, P. Vana, *Polymers for Advanced Technologies* **2006**, *17*, 625–633.
- [93] S. Perrier, P. Takolpuckdee, C. A. Mars, *Macromolecules* **2005**, *38*, 2033–2036.
- [94] S. Perrier, P. Takolpuckdee, *Journal of Polymer Science Part A: Polymer Chemistry* **2005**, *43*, 5347–5393.
- [95] S. Gatti, A. Agostini, R. Ferrari, D. Moscatelli, *Polymers* **2017**, 389.
- [96] M. Baum, W. J. Brittain, *Macromolecules* **2002**, *35*, 610–615.
- [97] S. Perrier, P. Takolpuckdee, C. A. Mars, *Macromolecules* **2005**, *38*, 6770–6774.
- [98] B. Ebeling, F. Ehlers, P. Vana, *Nachrichten aus der Chemie* **2014**, *62*, 24–28.
- [99] D. Tastet, M. Save, F. Charrier, B. Charrier, J. B. Ledeuil, J. C. Dupin, L. Billon, *Polymer* **2011**, *52*, 606–616.
- [100] A. Boujemaoui, S. Mazières, E. Malmström, M. Destarac, A. Carlmark, *Polymer (United Kingdom)* **2016**, *99*, 240–249.
- [101] D. Roy, J. T. Guthrie, S. Perrier, *Soft Matter* **2007**, *4*, 145–155.
- [102] E. Zeinali, V. Haddadi-Asl, H. Roghani-Mamaqani, *RSC Advances* **2014**, *4*, 31428.
- [103] D. Roy, J. T. Guthrie, S. Perrier, *Macromolecules* **2005**, *38*, 10363–10372.
- [104] J. Yuan, X. Huang, P. Li, L. Li, J. Shen, *Polymer Chemistry* **2013**, *4*, 5074.
- [105] J. Chen, J. Yi, P. Sun, Z.-T. Liu, Z.-W. Liu, *Cellulose* **2009**, *16*, 1133–1145.
- [106] X. Liu, J. Chen, P. Sun, Z. W. Liu, Z. T. Liu, *Reactive and Functional Polymers* **2010**, *70*, 972–979.
- [107] S. Demirci, A. Celebioglu, T. Uyar, *Carbohydrate Polymers* **2014**, *113*, 200–207.
- [108] A. Hufendiek, V. Trouillet, M. A. Meier, C. Barner-Kowollik, *Biomacromolecules* **2014**, *15*, 2563–2572.

- [109] A. S. Goldmann, T. Tischer, L. Barner, M. Bruns, C. Barner-Kowollik, *Biomacromolecules* **2011**, *12*, 1137–1145.
- [110] M. H. Stenzel, T. P. Davis, A. G. Fane, *Journal of Materials Chemistry* **2003**, *13*, 2090–2097.
- [111] M. Hernández-Guerrero, T. P. Davis, C. Barner-Kowollik, M. H. Stenzel, *European Polymer Journal* **2005**, *41*, 2264–2277.
- [112] R. Fleet, J. B. McLeary, V. Grumel, W. G. Weber, H. Matahwa, R. D. Sanderson, *European Polymer Journal* **2008**, *44*, 2899–2911.
- [113] P. Takolpuckdee, C. A. Mars, S. Perrier, *Organic Letters* **2005**, *7*, 3449–3452.
- [114] Y. Zhao, S. Perrier, *Macromolecules* **2006**, *39*, 8603–8608.
- [115] M. R. Wood, D. J. Duncalf, S. P. Rannard, S. Perrier, *Organic Letters* **2006**, *8*, 553–556.
- [116] S. Harrisson, X. Liu, J.-N. Ollagnier, O. Coutelier, J.-D. Marty, M. Destarac, *Polymers* **2014**, *6*, 1437–1488.
- [117] E. Chiellini, A. Corti, S. D'Antone, R. Solaro, *Progress in Polymer Science* **2003**, *28*, 963–1014.
- [118] G. Müller, PhD thesis, Georg-August University of Göttingen, **2008**.
- [119] L. Little, G. Poling, J. Leja, *Canadian Journal of Chemistry* **1961**, *39*, 745–754.
- [120] M. Shankaranarayana, C. Patel, *Canadian Journal of Chemistry* **1961**, *39*, 1633–1637.
- [121] C. Da Cunha, A. Deffieux, M. Fontanille, *Journal of Applied Polymer Science* **1992**, *44*, 1205–1212.
- [122] K. B. R. Devi, R. Madivanane, *Engineering Science and Technology: An International Journal* **2012**, *2*, 795–799.
- [123] J. K. Haken, R. L. Werner, *British Polymer Journal* **2007**, *3*, 263–265.
- [124] L. Gašparovič, Z. Koreňová, L. Jelemenský, *Chemical Papers* **2010**, *64*, 174–181.
- [125] T. M. Legge, A. T. Slark, S. Perrier, *Journal of Polymer Science Part A: Polymer Chemistry* **2006**, *44*, 6980–6987.
- [126] B. Rimez, H. Rahier, G. Van Assche, T. Artoos, M. Biesemans, B. Van Mele, *Polymer Degradation and Stability* **2008**, *93*, 800–810.
- [127] M. Buback, H. Frauendorf, F. Günzler, P. Vana, *Journal of Polymer Science Part A: Polymer Chemistry* **2007**, *45*, 2453–2467.

- 
- [128] X. Hao, C. Nilsson, M. Jesberger, M. H. Stenzel, E. Malmström, T. P. Davis, E. Östmark, C. Barner-Kowollik, *Journal of Polymer Science Part A: Polymer Chemistry* **2004**, *42*, 5877–5890.
- [129] M. H. Stenzel, T. P. Davis, *Journal of Polymer Science Part A: Polymer Chemistry* **2002**, *40*, 4498–4512.
- [130] A. Khabibullin, E. Mastan, K. Matyjaszewski, S. Zhu in *Controlled Radical Polymerization at and from Solid Surfaces*, (Ed.: P. Vana), Springer International Publishing, Basel, **2016**, pp. 29–76.
- [131] K. Matyjaszewski, J. Xia, *Chemical Reviews* **2001**, *101*, 2921–2990.
- [132] E. Malmström, A. Carlmark, *Polymer Chemistry* **2012**, *3*, 1702–1713.
- [133] J. Xia, S. G. Gaynor, K. Matyjaszewski, *Macromolecules* **1998**, *31*, 5958–5959.
- [134] P. F. Cañamero, J. L. D. L. Fuente, E. L. Madruga, M. Fernández-García, *Macromolecular Chemistry and Physics* **2004**, *205*, 2221–2228.
- [135] C. Routray, B. Tosh, *Cellulose* **2012**, *19*, 2115–2139.
- [136] C. Boyer, N. A. Corrigan, K. Jung, D. Nguyen, T.-K. Nguyen, N. N. M. Adnan, S. Oliver, S. Shanmugam, J. Yeow, *Chemical Reviews* **2015**, *116*, 1803–1949.
- [137] W. Tang, K. Matyjaszewski, *Macromolecules* **2007**, *40*, 1858–1863.
- [138] H. Tang, N. Arulsamy, M. Radosz, Y. Shen, N. V. Tsarevsky, W. A. Braunecker, W. Tang, K. Matyjaszewski, *Journal of the American Chemical Society* **2006**, *128*, 16277–16285.
- [139] N. Bortolamei, A. A. Isse, V. B. Di Marco, A. Gennaro, K. Matyjaszewski, *Macromolecules* **2010**, *43*, 9257–9267.
- [140] N. V. Tsarevsky, K. Matyjaszewski, *Chemical Reviews* **2007**, *107*, 2270–2299.
- [141] H. Fischer, *Journal of Polymer Science Part A: Polymer Chemistry* **1999**, *37*, 1885–1901.
- [142] H. Schroeder, PhD thesis, Georg-August-Universität Göttingen, **2015**.
- [143] K. Matyjaszewski, *Journal of Macromolecular Science - Pure and Applied Chemistry* **1997**, *34*, 1785–1801.
- [144] K. Matyjaszewski, H. Gao, K. Min, *Macromolecules* **2007**, *40*, 1789–1791.
- [145] K. Matyjaszewski, W. Jakubowski, K. Min, W. Tang, J. Huang, W. A. Braunecker, N. V. Tsarevsky, *Proceedings of the National Academy of Sciences* **2006**, *103*, 15309–15314.

- [146] P. Krys, Y. Wang, K. Matyjaszewski, S. Harrisson, *Macromolecules* **2016**, *49*, 2977–2984.
- [147] J. Mosnáček, M. Ilčíková, *Macromolecules* **2012**, *45*, 5859–5865.
- [148] P. Chmielarz, M. Fantin, S. Park, A. A. Isse, A. Gennaro, A. J. D. Magenau, A. Sobkowiak, K. Matyjaszewski, *Progress in Polymer Science* **2017**, *69*, 47–78.
- [149] W. Jakubowski, K. Matyjaszewski, *Angewandte Chemie - International Edition* **2006**, *45*, 4482–4486.
- [150] K. Matyjaszewski, W. Jakubowski, J. Spanswick, Polymerization process with catalyst reactivation (Patent), **2007**.
- [151] Y. Kwak, K. Matyjaszewski, *Polymer International* **2009**, *58*, 242–247.
- [152] K. Schröder, D. Konkolewicz, R. Poli, K. Matyjaszewski, *Organometallics* **2012**, *31*, 7994–7999.
- [153] T. G. Ribelli, S. M. Wahidur Rahaman, J. C. Daran, P. Krys, K. Matyjaszewski, R. Poli, *Macromolecules* **2016**, *49*, 7749–7757.
- [154] K. Matyjaszewski, B. E. Woodworth, *Macromolecules* **1998**, *31*, 4718–4723.
- [155] H. Dong, W. Tang, K. Matyjaszewski, *Macromolecules* **2007**, *40*, 2974–2977.
- [156] J. Pietrasik, H. Dong, K. Matyjaszewski, *Macromolecules* **2006**, *39*, 6384–6390.
- [157] Q. Wei, X. Wang, F. Zhou, *Polymer Chemistry* **2012**, *3*, 2129–2137.
- [158] T. Xing, W. Hu, S. Li, G. Chen, *Applied Surface Science* **2012**, *258*, 3208–3213.
- [159] J. Lindqvist, E. Malmström, *Journal of Applied Polymer Science* **2006**, *100*, 4155–4162.
- [160] S. M. Morsi, A. Pakzad, A. Amin, R. S. Yassar, P. A. Heiden, *Journal of Colloid and Interface Science* **2011**, *360*, 377–385.
- [161] H. Chung, A. Al-Khouja, N. R. Washburn in *Green Polymer Chemistry: Biocatalysis and Materials II*, (Eds.: H. Cheng, R. H. Gross, P. B. Smith), American Chemical Society, Washington DC, **2013**, Chapter 25, pp. 373–391.
- [162] X. Liu, H. Yin, Z. Zhang, B. Diao, J. Li, *Colloids and Surfaces B: Biointerfaces* **2015**, *125*, 230–237.
- [163] J. Yang, J. Li, *Carbohydrate Polymers* **2018**, *181*, 264–274.

- 
- [164] S. Hansson, E. Östmark, A. Carlmark, E. Malmström, *ACS Applied Materials and Interfaces* **2009**, *1*, 2651–2659.
- [165] H. Kang, R. Liu, Y. Huang, *Polymer (United Kingdom)* **2015**, *70*, A1–A16.
- [166] A. Carlmark, E. E. Malmström, *Biomacromolecules* **2003**, *4*, 1740–1745.
- [167] A. Carlmark, E. Larsson, E. Malmström, *European Polymer Journal* **2012**, *48*, 1646–1659.
- [168] T. Meng, X. Gao, J. Zhang, J. Yuan, Y. Zhang, J. He, *Polymer* **2009**, *50*, 447–454.
- [169] D. Nyström, J. Lindqvist, E. Östmark, P. Antoni, A. Carlmark, A. Hult, E. Malmström, *ACS Applied Materials and Interfaces* **2009**, *1*, 816–823.
- [170] V. Castelvetro, M. Geppi, S. Giaiacopi, G. Mollica, *Biomacromolecules* **2007**, *8*, 498–508.
- [171] C. H. Worthley, K. T. Constantopoulos, M. Ginic-Markovic, R. J. Pillar, J. G. Matisons, S. Clarke, *Journal of Membrane Science* **2011**, *385–386*, 30–39.
- [172] M. Xiao, S. Li, W. Chanklin, A. Zheng, H. Xiao, *Carbohydrate Polymers* **2011**, *83*, 512–519.
- [173] D. Plackett, K. Jankova, H. Egsgaard, S. Hvilsted, *Biomacromolecules* **2005**, *6*, 2474–2484.
- [174] X. M. Zhang, J. F. Ji, Y. J. Tang, Y. Zhao in *Advances in Chemical Engineering: ICCMME 2011*, Trans Tech Publications, **2012**, pp. 1458–1461.
- [175] G. Zampano, M. Bertoldo, S. Bronco, *Carbohydrate Polymers* **2009**, *75*, 22–31.
- [176] F. Yu, W. Yang, J. Song, Q. Wu, L. Chen, *Wood Science and Technology* **2014**, *48*, 289–299.
- [177] E. Cabane, T. Keplinger, T. Künniger, V. Merk, I. Burgert, *Nature Publishing Group* **2016**, 1–10.
- [178] R. Chen, W. Feng, S. Zhu, G. Botton, B. Ong, Y. Wu, *Journal of Polymer Science Part A: Polymer Chemistry* **2006**, *44*, 1252–1262.
- [179] Y. Tsujii, K. Ohno, S. Yamamoto, A. Goto, T. Fukuda, *Advances in Polymer Science* **2006**, 1–45.
- [180] L. Bombalski, K. Min, H. Dong, C. Tang, K. Matyjaszewski, *Macromolecules* **2007**, *40*, 7429–7432.

- [181] J. Pyun, S. Jia, T. Kowalewski, G. D. Patterson, K. Matyjaszewski, *Macromolecules* **2003**, *36*, 5094–5104.
- [182] G. Louis Chakkalakal, M. Alexandre, C. Abetz, A. Boschetti-De-Fierro, V. Abetz, *Macromolecular Chemistry and Physics* **2012**, *213*, 513–528.
- [183] K. Ohno, T. Akashi, Y. Huang, Y. Tsujii, *Macromolecules* **2010**, *43*, 8805–8812.
- [184] K. Matyjaszewski, P. J. Miller, N. Shukla, B. Immaraporn, A. Gelman, B. B. Luokala, T. M. Siclovan, G. Kickelbick, T. Vallant, H. Hoffmann, T. Pakula, *Macromolecules* **1999**, *32*, 8716–8724.
- [185] J. Schwellenbach, F. Taft, L. Villain, J. Strube, *Journal of Chromatography A* **2016**, *1447*, 92–106.
- [186] G. I. Mantanis, R. A. Young, R. M. Rowell, *Holzforschung* **1994**, *48*, 480–490.
- [187] C. A. S. Hill in *Wood Modification: Chemical, Thermal and Other Processes*, (Ed.: C. V. Stevens), Wiley, New York, **2006**, Chapter 3, pp. 45–76.
- [188] Z. Aji, *Revue Roumaine de Chimie* **2008**, *53*, 1065–1068.
- [189] H. Garbalińska, M. Bochenek, W. Malorny, J. von Werder, *Cement and Concrete Research* **2017**, *91*, 97–105.
- [190] E. E. Thybring, M. Kymäläinen, L. Rautkari, *Wood Science and Technology* **2017**, 1–33.
- [191] C. Skaar, *Wood-Water Relations*, 1. Edition, Springer-Verlag Berlin Heidelberg, **1988**.
- [192] S. Brunauer, *Princeton University Press* **1943**, *1*, 528.
- [193] L. Malmquist, *Holzforschung* **1995**, *49*, 555–564.
- [194] R. Runkel, M. Lüthgens, *Holz als Roh-und Werkstoff* **1956**, 424–441.
- [195] Q. Zhou, L. Greffe, M. J. Baumann, *Macromolecules* **2005**, *38*, 3547–3549.
- [196] M. Barsbay, O. Güven, M. H. Stenzel, T. P. Davis, C. Barner-Kowollik, L. Barner, *Macromolecules* **2007**, *40*, 7140–7147.
- [197] S. B. Lee, R. R. Koepsel, S. W. Morley, K. Matyjaszewski, Y. Sun, A. J. Russell, *Biomacromolecules* **2004**, *5*, 877–882.
- [198] J. O. Zoppe, Y. Habibi, O. J. Rojas, R. A. Venditti, L.-s. Johansson, K. Efimenko, O. Monika, M. Osterberg, J. Laine, *Biomacromolecules* **2010**, *11*, 2683–91.

- 
- [199] J. Kamada, K. Koynov, C. Corten, A. Juhari, J. A. Yoon, M. W. Urban, A. C. Balazs, K. Matyjaszewski, *Macromolecules* **2010**, *43*, 4133–4139.
- [200] N. V. Tsarevsky, K. Matyjaszewski, *Macromolecules* **2002**, *35*, 9009–9014.
- [201] S. Hansson, P. Antoni, H. Bergenudd, E. Malmström, *Polymer Chemistry* **2011**, *2*, 556.
- [202] G. L. Ellman, *Archives of Biochemistry and Biophysics* **1959**, *82*, 70–77.
- [203] H. Collier, *Analytical Biochemistry* **1973**, *56*, 310–311.
- [204] P. W. Riddles, R. L. Blakeley, B. Zerner, *Methods in Enzymology* **1983**, *91*, 49–60.
- [205] M. D. Lechner, E. H. Nordmeier, K. Gehrke, *Synthese von Makromolekülen, Polyreaktionen*, 4. Edition, Birkhäuser Verlag, Basel, **2010**.
- [206] B. Tieke, *Makromolekulare Chemie*, 3. Edition, Wiley-VCH, Weinheim, Weinheim, **2014**.
- [207] W. Hellerich, G. Harsch, E. Baur, *Werkstoff-Führer Kunststoffe*, 10. Edition, Carl Hanser Verlag, München, **2010**.
- [208] S. A. Baeurle, A. Hotta, A. A. Gusev, *Polymer* **2006**, *47*, 6243–6253.
- [209] G. Holden in *Applied Plastics Engineering Handbook*, (Ed.: M. Kutz), Plastics Design Library, William Andrew Publishing, Oxford, **2011**, Chapter 6, pp. 77–91.
- [210] <http://polymerdatabase.com/polymer-classes/Polyacrylate-type.html>, Properties of Polyacrylates, accessed 2018-07-09.
- [211] *POLYMERS - A PROPERTY DATABASE*, 2. Edition, (Eds.: B. Ellis, R. Smith), CRC, Boca Raton, **2009**.
- [212] A. Akdogan, A. S. Vanli, *Journal of Thermoplastic Composite Materials* **2013**, *26*, 1237–1248.
- [213] J. Jordan, K. I. Jacob, R. Tannenbaum, M. A. Sharaf, I. Jasiuk, *Materials Science and Engineering A* **2005**, *393*, 1–11.
- [214] S. Sinha, *Reviews in Chemical Engineering* **2011**, *27*, 253–264.
- [215] H. Zou, S. Wu, J. Shen, *Chemical Reviews* **2008**, *108*, 3893–3957.
- [216] A. Hashemi, N. Jouault, G. A. Williams, D. Zhao, K. J. Cheng, J. W. Kysar, Z. Guan, S. K. Kumar, *Nano Letters* **2015**, *15*, 5465–5471.
- [217] H. Czichos, T. Saito, S. Leslie, *Springer Handbook of Materials Measurement Methods*, Springer Berlin Heidelberg, **2006**.

- [218] K. P. Menard, *Dynamic Mechanical Analysis: A Practical Introduction*, 1. Edition, CRC Press LLC, Boca Raton, **1999**.
- [219] L.-K. Bi, L. J. Fetters, *Macromolecules* **1976**, 9, 732–742.
- [220] F. R. Schwarzl, *Polymermechanik - Struktur und mechanisches Verhalten von Polymeren*, 1. Edition, Springer-Verlag, Berlin, **1990**.
- [221] W. D. Callister, D. G. Rethwisch, *Materialwissenschaften und Werkstofftechnik*, 1. Edition, WILEY-VCH Verlag, Weinheim, **2012**.
- [222] M. Hendrich, PhD thesis, Georg-August-Universität Göttingen, **2016**.
- [223] C. Wrana in *Polymerphysik*, Springer Berlin, Heidelberg, **2014**, Chapter 3, pp. 27–277.
- [224] G. W. Ehrenstein, G. Riedel, P. Trawiel, *Praxis der thermischen Analyse von Kunststoffen*, 2. Edition, Carl Hanser Verlag, München, **2003**.
- [225] J. E. Steinhoff, Master thesis, Georg-August-Universität Göttingen, **2016**.
- [226] B. K. Kuila, A. K. Nandi, *Macromolecules* **2004**, 37, 8577–8584.
- [227] <https://www.sigmaaldrich.com/catalog/product/sial/484431>, accessed 2018-07-09.
- [228] J. R. Martin, J. F. Johnson, A. R. Cooper, *Journal of Macromolecular Science Part C* **1972**, 8, 57–199.
- [229] H. E. Meijer, L. E. Govaert, *Progress in Polymer Science* **2005**, 30, 915–938.
- [230] M. Hendrich, L. Lewerdomski, P. Vana, *Journal of Polymer Science Part A: Polymer Chemistry* **2015**, 1–11.
- [231] M. Kaßel, J. Gerke, A. Ley, P. Vana, *Polymers* **2018**, 10, 354.
- [232] S. Goyanes, P. G. König, J. Marconi, *Journal of Applied Polymer Science* **2003**, 88, 883–892.
- [233] J. Heijboer, *Annals Of The New York Academy Of Sciences* **1976**, 279, 104–116.
- [234] L. A. Pothan, Z. Oommen, S. Thomas, *Composites Science and Technology* **2003**, 63, 283–293.
- [235] P. S. Nagendra, V. V. S. Prasad, K. Ramji, *Materials Today: Proceedings* **2017**, 4, 9081–9086.
- [236] N. Saba, M. Jawaid, O. Y. Alothman, M. T. Paridah, *Construction and Building Materials* **2016**, 106, 149–159.
- [237] M. Hiljanen-Vainio, M. Heino, J. V. Seppälä, *Polymer* **1998**, 39, 865–872.

- 
- [238] C. Wrana, *Polymerphysik*, 1. Edition, Springer-Verlag, Heidelberg, 2014.
- [239] S. Shinoj, R. Visvanathan, S. Panigrahi, N. Varadharaju, *Biosystems Engineering* **2011**, 109, 99–107.
- [240] A. K. Rana, B. C. Mitra, A. N. Banerjee, *Journal of Applied Polymer Science* **1999**, 71, 531–539.
- [241] S. Cheng, V. Bocharova, A. Belianinov, S. Xiong, A. Kisliuk, S. Somnath, A. P. Holt, O. S. Ovchinnikova, S. Jesse, H. Martin, T. Etampawala, M. Dadmun, A. P. Sokolov, *Nano Letters* **2016**, 16, 3630–3637.
- [242] M. I. Reddy, V. S. Reddy, *International Journal of Engineering Research & Technology* **2014**, 3, 410–415.
- [243] N. Bleach, S. Nazhat, K. Tanner, M. Kellomäki, P. Törmälä, *Biomaterials* **2002**, 23, 1579–1585.
- [244] Z. Grubisic, P. Rempp, H. Benoit, *Journal of Polymer Science Part B: Polymer Letters* **1967**, 5, 753–759.
- [245] M. Buback, C. H. Kurz, C. Schmaltz, *Macromolecular Chemistry and Physics* **1998**, 199, 1721–1727.
- [246] C. M. L. Atkinson, R. Dietz, *European Polymer Journal* **1979**, 15, 21–26.
- [247] S. Himmel, C. Mai, *Holzforschung* **2015**, 69, 633–643.
- [248] C. M. Popescu, C. A. Hill, S. Curling, G. Ormondroyd, Y. Xie, *Journal of Materials Science* **2014**, 49, 2362–2371.

**Chapter VII**

**Appendices**



# Tables and figures

## Equilibrium moisture content (EMC)

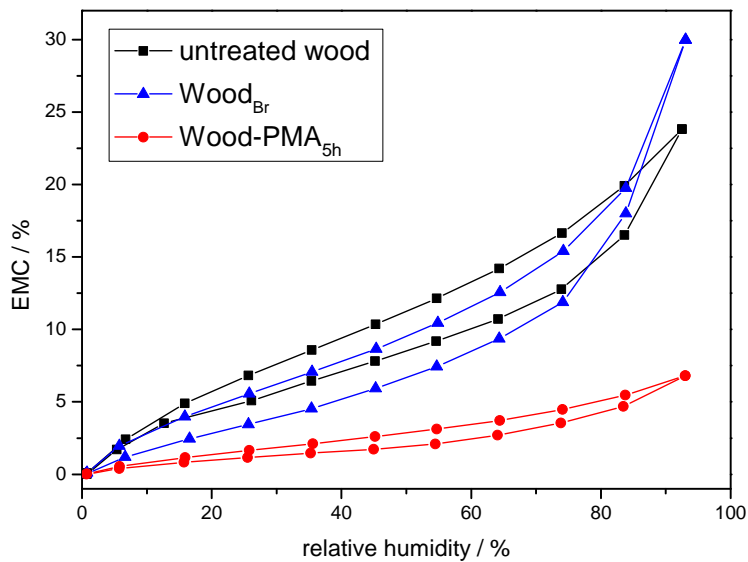


Figure A.1: Water sorption isotherm of untreated wood, initiator-functionalized wood (WPG of 8%) and PMA-grafted wood (WPG of 46%) with a polymerization time of 5 h depending on the relative humidity.

## Tensile testing measurements

### Mechanical characteristics of tensile tests

Table A.1 and Table A.2 show the mechanical characteristics shown in Figure 11.5 and Figure 11.7, respectively (see Section 11.2). Given results are mean values of all respective measurements with the respective maximum error. The following pages show the tensile test results of all series of measurements.

Table A.1: Mechanical characteristics of pure PMA and wood reinforced thermoplastics. 5 wt% of wood flour with varying amount of grafted polymer was incorporated into the matrix.<sup>[231]</sup>

sample	$E$ / MPa	$\sigma_y$ / MPa	$U_T$ / MPa
pure PMA	$8 \pm 3$	$0.27 \pm 0.06$	$126 \pm 31$
PMA <sub>unf</sub>	$7 \pm 2$	$0.30 \pm 0.11$	$50 \pm 14$
PMA <sub>1h</sub>	$11 \pm 1$	$0.40 \pm 0.03$	$106 \pm 18$
PMA <sub>2h</sub>	$20 \pm 2$	$0.58 \pm 0.02$	$235 \pm 16$
PMA <sub>5h</sub>	$26 \pm 1$	$0.73 \pm 0.02$	$297 \pm 5$
PMA <sub>7h</sub>	$29 \pm 2$	$0.73 \pm 0.01$	$389 \pm 13$
PMA <sub>9.5h</sub>	$36 \pm 2$	$0.79 \pm 0.02$	$299 \pm 68$

Table A.2: Mechanical characteristics of pure PMA and wood reinforced thermoplastics with a constant amount of grafted polymer and varying weight percentages.

sample	$E$ / MPa	$\sigma_y$ / MPa	$U_T$ / MPa
pure PMA	$8 \pm 3$	$0.27 \pm 0.06$	$126 \pm 31$
PMA <sub>2h</sub> (3 wt%)	$8 \pm 1$	$0.32 \pm 0.01$	$98 \pm 11$
PMA <sub>2h</sub> (5 wt%)	$20 \pm 2$	$0.58 \pm 0.02$	$235 \pm 16$
PMA <sub>2h</sub> (7 wt%)	$22 \pm 3$	$0.65 \pm 0.01$	$228 \pm 34$
PMA <sub>2h</sub> (10 wt%)	$22 \pm 8$	$0.74 \pm 0.14$	$166 \pm 49$

## Tensile testing results of pure PMA

Table A.3: Mechanical characteristics of the PMA matrix.

sample	$E$ / MPa	$\sigma_y$ / MPa	$U_T$ / MPa
1	11	0.33	157
2	8	0.28	140
3	6	0.25	106
4	7	0.24	101
$\emptyset$	$8 \pm 3$	$0.27 \pm 0.06$	$126 \pm 31$

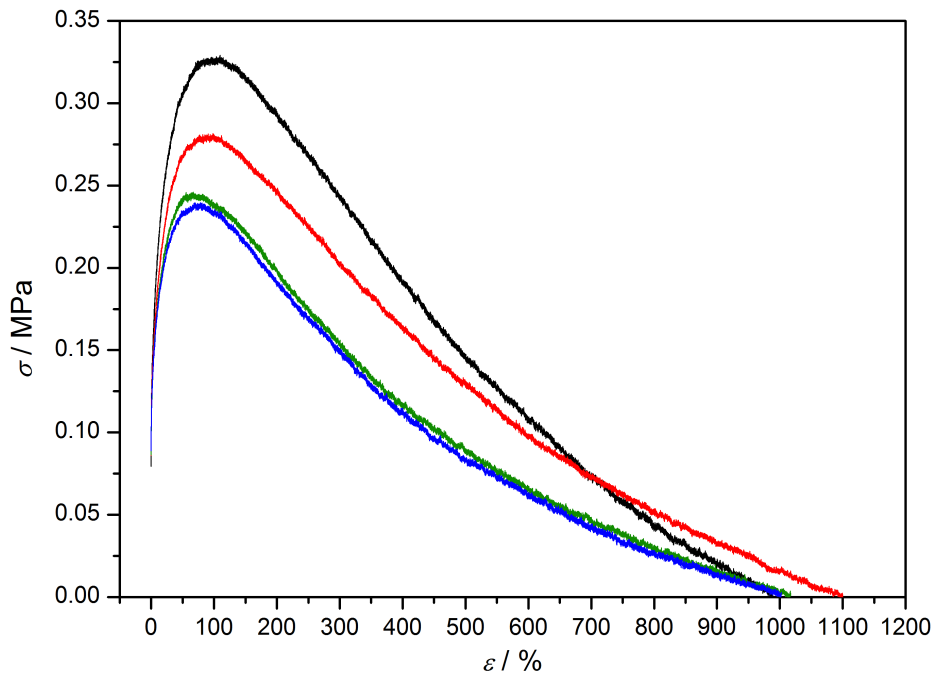


Figure A.2: Stress-strain curves of the PMA matrix.

## Tensile test results of PMA<sub>unf</sub>

Table A.4: Mechanical characteristics of a wood reinforced thermoplastics consisting of 5 wt% untreated wood flour (PMA<sub>unf</sub>).

sample	$E$ / MPa	$\sigma_y$ / MPa	$U_T$ / MPa
1	7	0.35	47
2	9	0.36	64
3	5	0.19	38
$\emptyset$	$7 \pm 2$	$0.30 \pm 0.11$	$50 \pm 14$

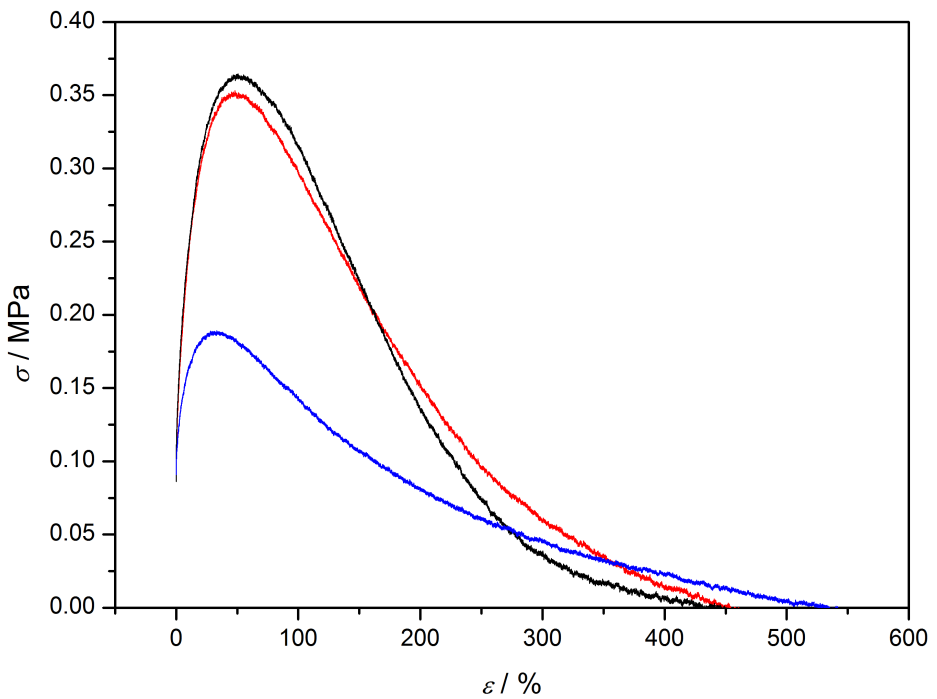


Figure A.3: Stress-strain curves of wood reinforced thermoplastics consisting of 5 wt% untreated wood flour (PMA<sub>unf</sub>).

## Tensile test results of PMA<sub>1h</sub>

Table A.5: Mechanical characteristics of a wood reinforced thermoplastics consisting of 5 wt% grafted wood flour with a polymerization time of 1 h (PMA<sub>1h</sub>).

sample	$E$ / MPa	$\sigma_y$ / MPa	$U_T$ / MPa
1	10	0.37	92
2	11	0.43	124
3	11	0.40	103
$\emptyset$	$11 \pm 1$	$0.40 \pm 0.03$	$106 \pm 18$

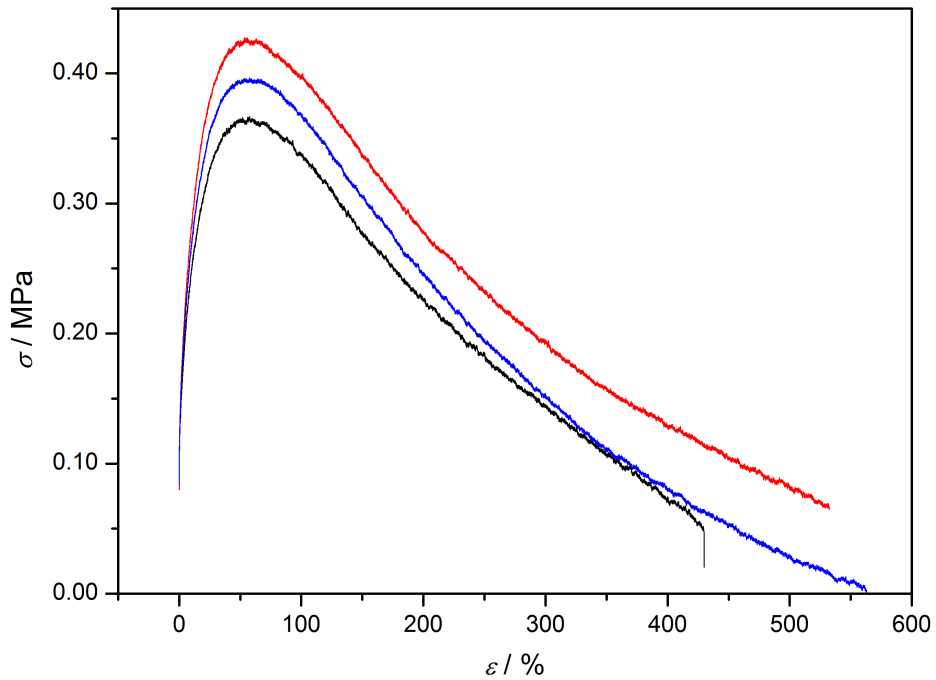


Figure A.4: Stress-strain curves of wood reinforced thermoplastics consisting of 5 wt% grafted wood flour with a polymerization time of 1 h (PMA<sub>1h</sub>).

## Tensile test results of PMA<sub>2h</sub>

Table A.6: Mechanical characteristics of a wood reinforced thermoplastics consisting of 5 wt% grafted wood flour with a polymerization time of 2 h (PMA<sub>2h</sub>).

sample	$E$ / MPa	$\sigma_y$ / MPa	$U_T$ / MPa
1	18	0.56	223
2	22	0.57	251
3	20	0.60	231
$\emptyset$	$20 \pm 2$	$0.58 \pm 0.02$	$235 \pm 16$

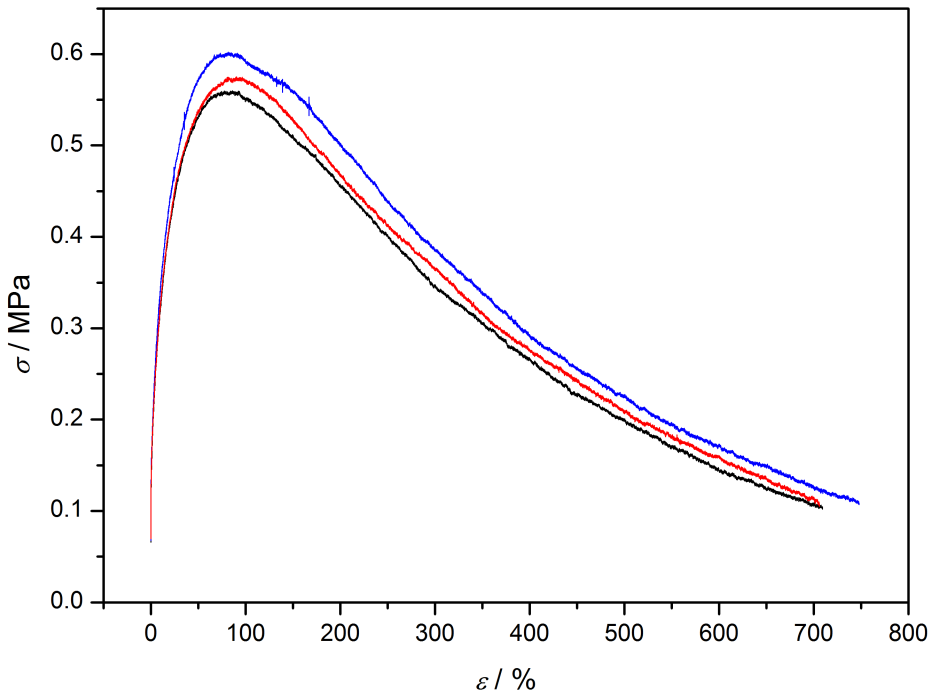


Figure A.5: Stress-strain curves of wood reinforced thermoplastics consisting of 5 wt% grafted wood flour with a polymerization time of 2 h (PMA<sub>2h</sub>).

## Tensile test results of PMA<sub>5h</sub>

Table A.7: Mechanical characteristics of a wood reinforced thermoplastics consisting of 5 wt% grafted wood flour with a polymerization time of 5 h (PMA<sub>5h</sub>).

sample	$E$ / MPa	$\sigma_y$ / MPa	$U_T$ / MPa
1	25	0.72	282
2	26	0.75	293
3	25	0.72	287
$\emptyset$	$26 \pm 1$	$0.73 \pm 0.02$	$297 \pm 5$

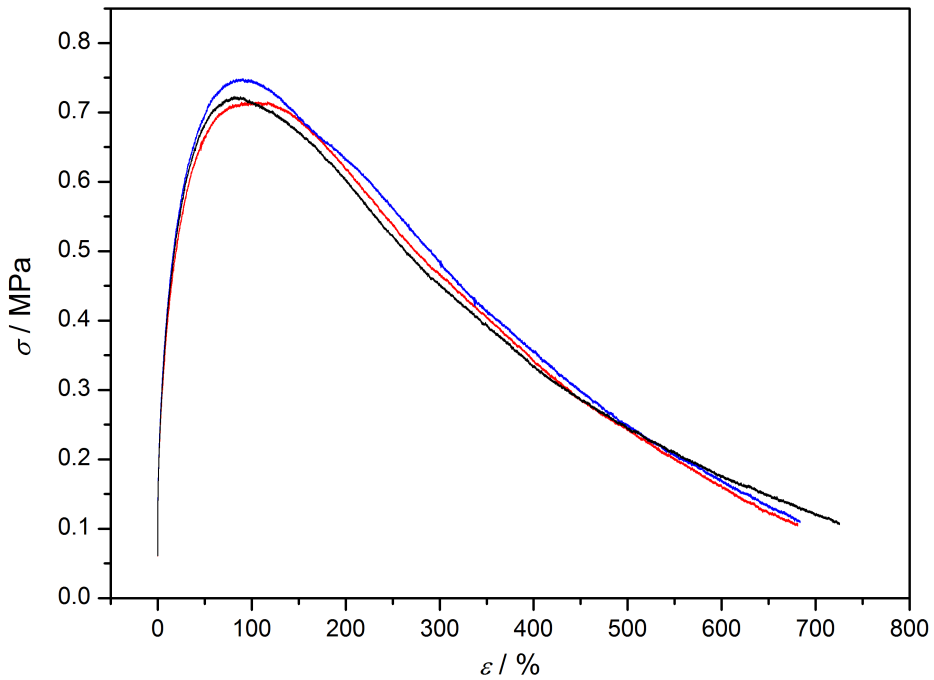


Figure A.6: Stress-strain curves of wood reinforced thermoplastics consisting of 5 wt% grafted wood flour with a polymerization time of 5 h (PMA<sub>5h</sub>).

## Tensile test results of PMA<sub>7h</sub>

Table A.8: Mechanical characteristics of a wood reinforced thermoplastics consisting of 5 wt% grafted wood flour with a polymerization time of 7 h (PMA<sub>7h</sub>).

sample	$E$ / MPa	$\sigma_y$ / MPa	$U_T$ / MPa
1	29	0.74	398
2	31	0.73	394
3	27	0.72	374
$\emptyset$	$29 \pm 2$	$0.73 \pm 0.01$	$389 \pm 13$

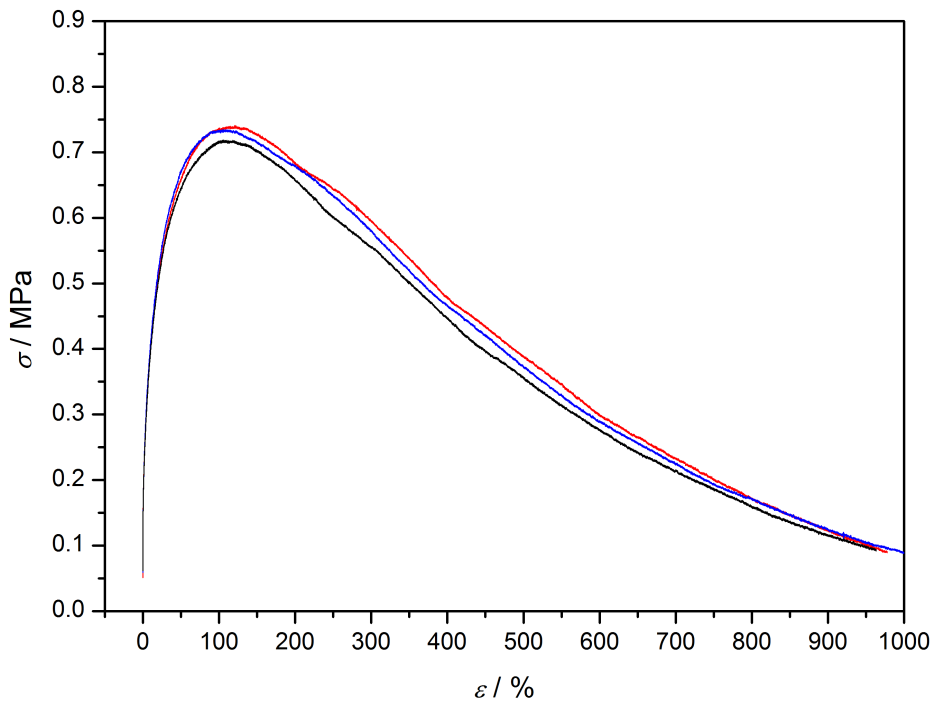


Figure A.7: Stress-strain curves of wood reinforced thermoplastics consisting of 5 wt% grafted wood flour with a polymerization time of 7 h (PMA<sub>7h</sub>).

### Tensile test results of PMA<sub>9.5h</sub>

Table A.9: Mechanical characteristics of a wood reinforced thermoplastics consisting of 5 wt% grafted wood flour with a polymerization time of 9.5 h (PMA<sub>9.5h</sub>).

sample	$E$ / MPa	$\sigma_y$ / MPa	$U_T$ / MPa
1	38	0.79	227
2	34	0.78	308
3	36	0.81	362
$\emptyset$	$36 \pm 2$	$0.79 \pm 0.02$	$299 \pm 68$

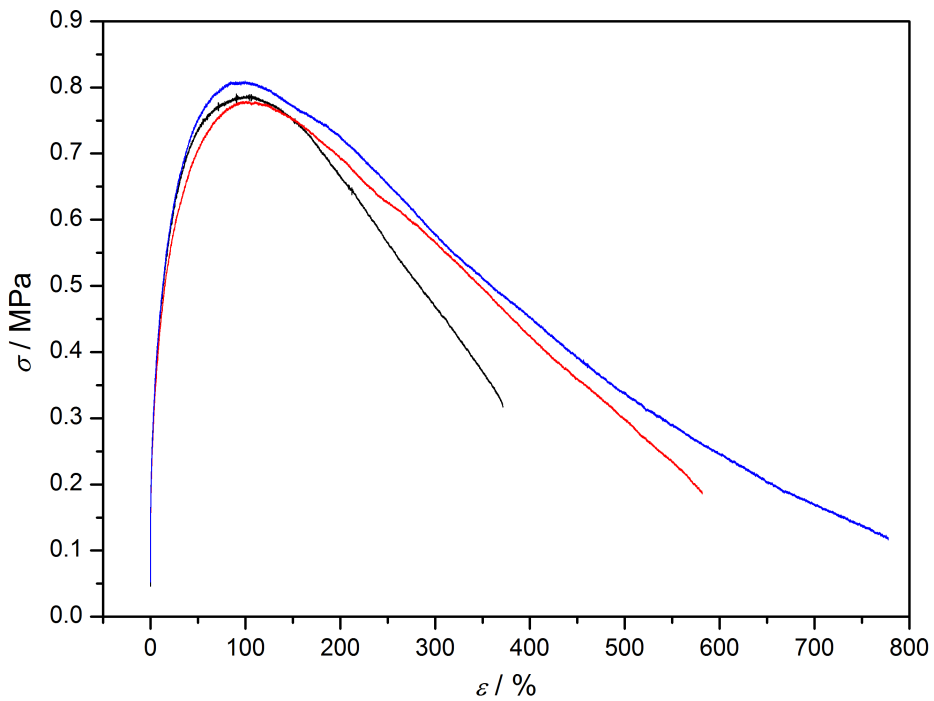


Figure A.8: Stress-strain curves of wood reinforced thermoplastics consisting of 5 wt% grafted wood flour with a polymerization time of 9.5 h (PMA<sub>9.5h</sub>).

### Tensile test results of PMA<sub>2h</sub> (3 wt%)

Table A.10: Mechanical characteristics of a wood reinforced thermoplastics consisting of 3 wt% grafted wood flour with a polymerization time of 2 h.

sample	$E$ / MPa	$\sigma_y$ / MPa	$U_T$ / MPa
1	9	0.32	87
2	8	0.32	98
3	8	0.33	109
$\emptyset$	$8 \pm 1$	$0.32 \pm 0.01$	$98 \pm 11$

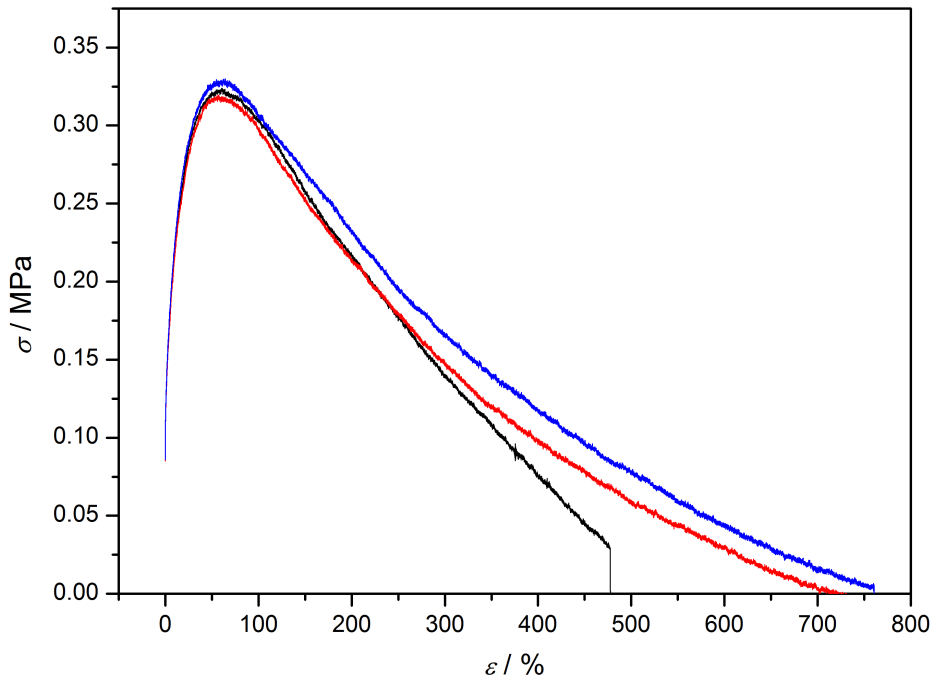


Figure A.9: Stress-strain curves of wood reinforced thermoplastics consisting of 3 wt% grafted wood flour with a polymerization time of 2 h.

## Tensile test results of PMA<sub>2h</sub> (7 wt%)

Table A.11: Mechanical characteristics of a wood reinforced thermoplastics consisting of 7 wt% grafted wood flour with a polymerization time of 2 h.

sample	$E$ / MPa	$\sigma_y$ / MPa	$U_T$ / MPa
1	24	0.65	194
2	23	0.66	242
3	19	0.64	249
$\emptyset$	$22 \pm 3$	$0.65 \pm 0.01$	$228 \pm 34$

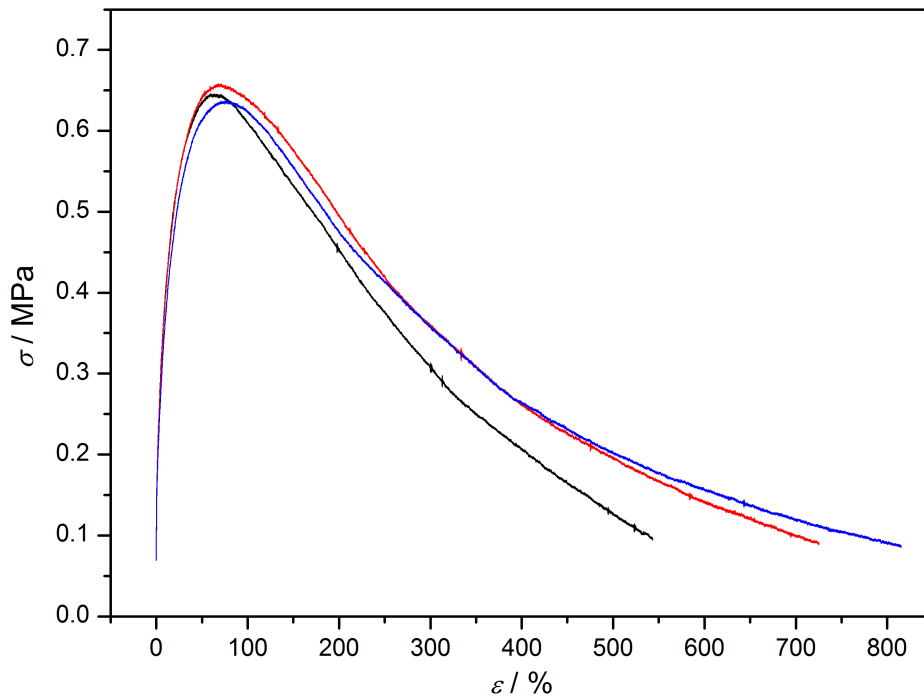


Figure A.10: Stress-strain curves of wood reinforced thermoplastics consisting of 7 wt% grafted wood flour with a polymerization time of 2 h.

### Tensile test results of PMA<sub>2h</sub> (10 wt%)

Table A.12: Mechanical characteristics of a wood reinforced thermoplastics consisting of 10 wt% grafted wood flour with a polymerization time of 2 h.

sample	$E$ / MPa	$\sigma_y$ / MPa	$U_T$ / MPa
1	25	0.76	193
2	14	0.60	117
3	27	0.86	188
$\emptyset$	$22 \pm 8$	$0.74 \pm 0.14$	$166 \pm 49$

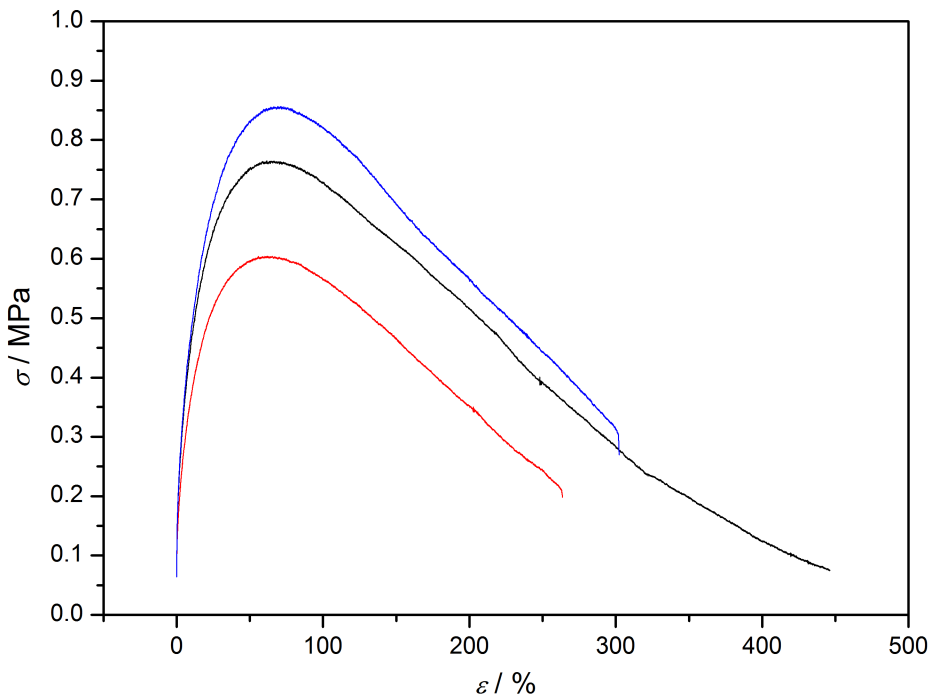


Figure A.11: Stress-strain curves of wood reinforced thermoplastics consisting of 10 wt% grafted wood flour with a polymerization time of 2 h.

## Dynamic mechanical analysis

Table A.13 and Table A.14 show the mechanical characteristics shown in Figure 11.9 and Figure 11.10, respectively (see Section 11.3). Given results are mean values of all respective measurements with the respective standard deviation. The following pages show the averaged results of the dynamic mechanical analysis of all series of measurements.

Table A.13: Dynamic mechanical properties of the composites in dependance of the incorporated particles with different polymerization times at  $-10^{\circ}\text{C}$  are shown.

sample	$E' / 10^9 \text{ Pa}$	$E'' / 10^8 \text{ Pa}$	$\tan(\delta)$
pure PMA	$2.28 \pm 0.22$	$1.25 \pm 0.13$	$0.054 \pm 0.005$
PMA <sub>unf</sub>	$2.02 \pm 0.18$	$0.93 \pm 0.08$	$0.046 \pm 0.004$
PMA <sub>1h</sub>	$2.04 \pm 0.20$	$0.79 \pm 0.08$	$0.039 \pm 0.004$
PMA <sub>2h</sub>	$2.00 \pm 0.21$	$0.89 \pm 0.10$	$0.045 \pm 0.005$
PMA <sub>5h</sub>	$1.86 \pm 0.19$	$0.94 \pm 0.10$	$0.052 \pm 0.005$
PMA <sub>7h</sub>	$1.75 \pm 0.17$	$0.90 \pm 0.09$	$0.051 \pm 0.005$
PMA <sub>9.5h</sub>	$2.01 \pm 0.26$	$1.10 \pm 0.11$	$0.053 \pm 0.005$

Table A.14: Dynamic mechanical properties of the composites in dependance of added mass persantages of incorporated particles with polymerization times of 2 h at  $-10^{\circ}\text{C}$  are shown.

ample	$E' / 10^9 \text{ Pa}$	$E'' / 10^8 \text{ Pa}$	$\tan(\delta)$
pure PMA	$2.28 \pm 0.22$	$1.25 \pm 0.13$	$0.054 \pm 0.005$
PMA <sub>2h</sub> (3 wt%)	$2.21 \pm 0.22$	$1.03 \pm 0.10$	$0.047 \pm 0.005$
PMA <sub>2h</sub> (5 wt%)	$2.00 \pm 0.21$	$0.89 \pm 0.10$	$0.045 \pm 0.005$
PMA <sub>2h</sub> (7 wt%)	$2.14 \pm 0.20$	$0.91 \pm 0.09$	$0.042 \pm 0.004$
PMA <sub>2h</sub> (10 wt%)	$2.71 \pm 0.26$	$1.13 \pm 0.11$	$0.042 \pm 0.004$

Table A.15: Determined glass transition temperature via DMA.

sample	$T_{g,E'} / ^\circ\text{C}$	$T_{g,E''} / ^\circ\text{C}$	$T_{g,\tan(\delta)} / ^\circ\text{C}$
PMA	$15.3 \pm 1.0$	$15.0 \pm 0.6$	$27.2 \pm 1.2$
PMA <sub>unf</sub>	$16.5 \pm 1.4$	$16.5 \pm 1.2$	$27.4 \pm 1.2$
PMA <sub>1h</sub>	$19.2 \pm 0.6$	$19.3 \pm 0.8$	$28.4 \pm 0.4$
PMA <sub>2h</sub>	$16.5 \pm 0.7$	$16.5 \pm 0.7$	$27.7 \pm 0.3$
PMA <sub>5h</sub>	$14.1 \pm 3.5$	$14.6 \pm 3.5$	$25.3 \pm 2.9$
PMA <sub>7h</sub>	$17.3 \pm 2.9$	$17.8 \pm 1.5$	$27.5 \pm 1.7$
PMA <sub>9.5h</sub>	$17.7 \pm 1.5$	$17.8 \pm 1.8$	$27.6 \pm 1.7$
PMA	$15.3 \pm 1.0$	$15.0 \pm 0.6$	$27.2 \pm 1.2$
PMA <sub>2h</sub> (3 wt%)	$18.6 \pm 1.2$	$18.7 \pm 0.9$	$28.2 \pm 1.2$
PMA <sub>2h</sub> (5 wt%)	$16.5 \pm 0.7$	$16.5 \pm 0.7$	$27.7 \pm 0.3$
PMA <sub>2h</sub> (7 wt%)	$18.1 \pm 1.9$	$18.0 \pm 1.7$	$28.1 \pm 1.3$
PMA <sub>2h</sub> (10 wt%)	$18.0 \pm 1.7$	$17.8 \pm 1.1$	$28.6 \pm 0.3$

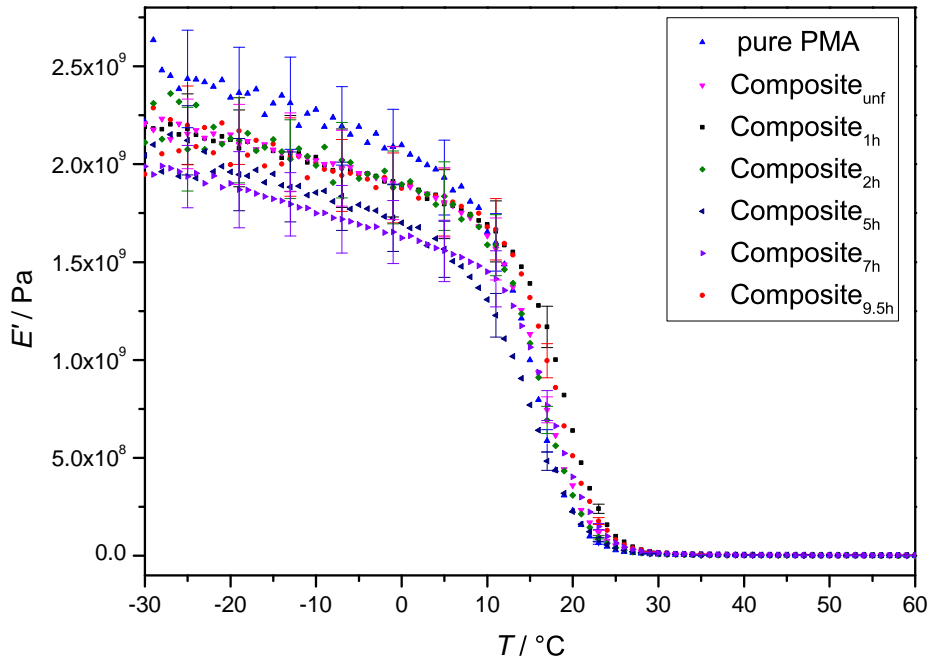


Figure A.12: Storage modulus of pure PMA and wood reinforced thermoplastics in dependence of temperature. 5 wt% of wood flour with varying amount of grafted polymer was incorporated into the matrix.

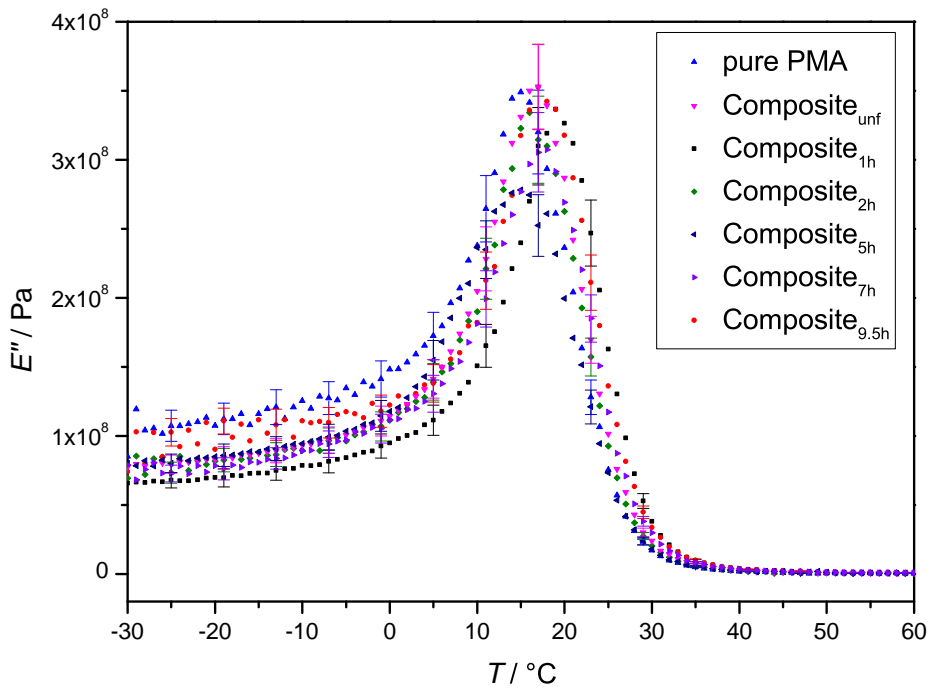


Figure A.13: Loss modulus of pure PMA and wood reinforced thermoplastics in dependence of temperature. 5 wt% of wood flour with varying amount of grafted polymer was incorporated into the matrix.

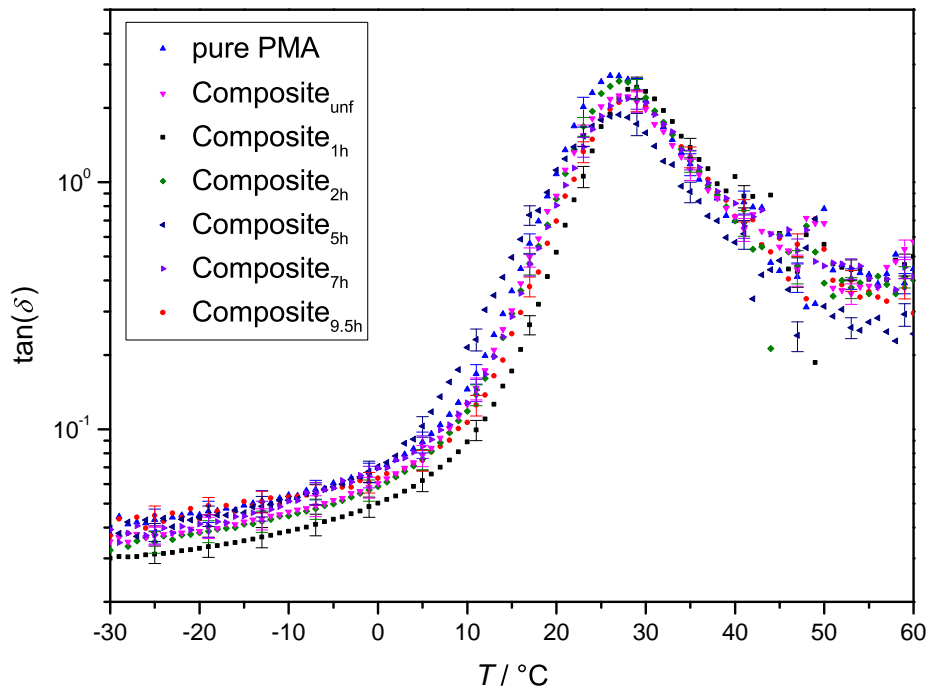


Figure A.14: Damping of pure PMA and wood reinforced thermoplastics in dependence of temperature. 5 wt% of wood flour with varying amount of grafted polymer was incorporated into the matrix.

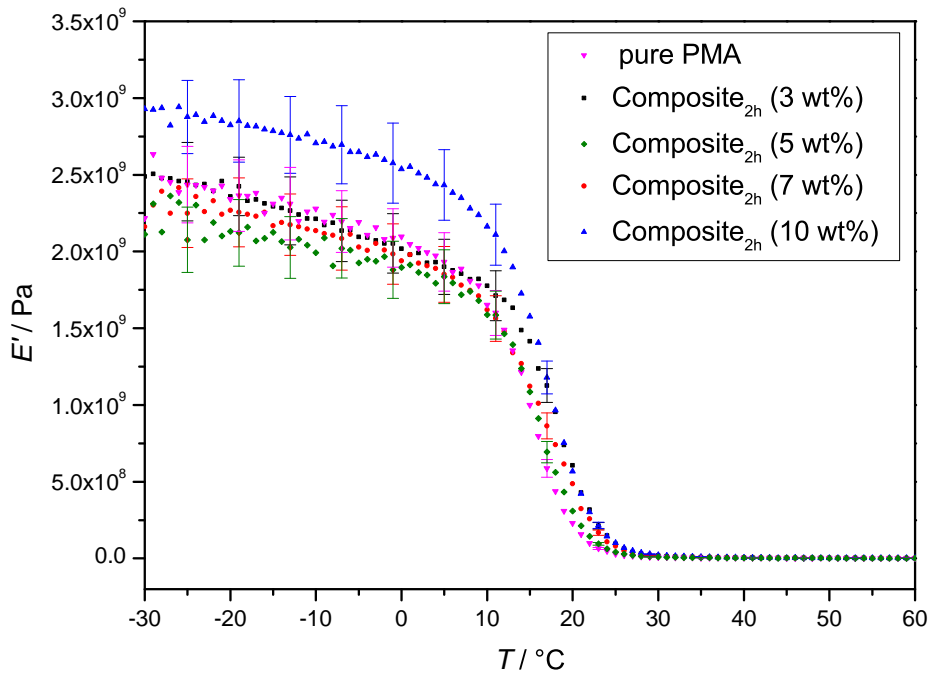


Figure A.15: Storage modulus of pure PMA and wood reinforced thermoplastics with a constant amount of grafted polymer and varying weight percentages in dependence of temperature.

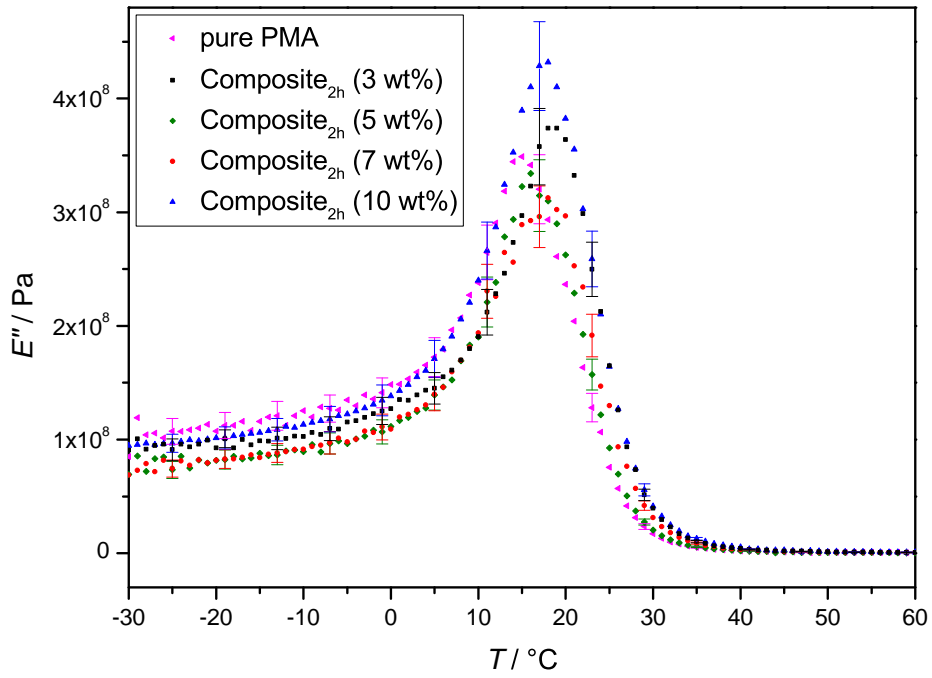


Figure A.16: Loss modulus of pure PMA and wood reinforced thermoplastics with a constant amount of grafted polymer and varying weight percentages in dependence of temperature.

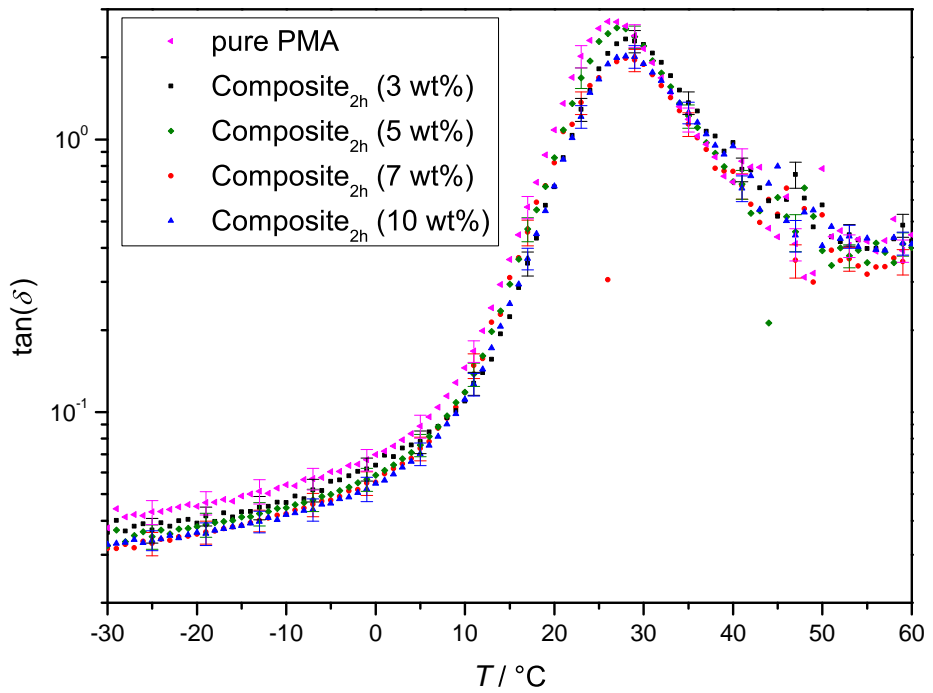


Figure A.17: Damping of pure PMA and wood reinforced thermoplastics with a constant amount of grafted polymer and varying weight percentages in dependence of temperature.

# Abbreviations

## Abbreviations and acronyms

AIBN	azobisisobutyronitrile
ARGET	activators regenerated by electron transfer
ATR	attenuated total reflection
ATRP	atom transfer radical polymerization
AsAc	ascorbic acid
BA	<i>n</i> -butyl acrylate
BIBB	$\alpha$ -bromoisobutyryl bromide
brine	high-concentration solution of salt (usually NaCl)
CA	contact angle
CTA	chain transfer agent
d	doublet
$\mathcal{D}$	dispersity
DCM	dichloromethane
DMA	dynamic mechanical analysis
DMAP	4-dimethylaminopyridine
DMF	<i>N,N</i> -dimethylformamide
DMSO	dimethyl sulfoxide
DP	degree of polymerization
DSC	differential scanning calorimetry
dTG	derived thermogram
DTNB	5,5'-dithiobis(2-nitrobenzoic acid)
DTT	dithiothreitol (Cleland's reagent)
DVS	dynamic vapor sorption
EA	elemental analysis
EBIB	ethyl 2-bromobutyrate
EDX	energy-dispersive X-ray
<i>e.g.</i>	for example ( <i>exempli gratia</i> )
EMC	equilibrium moisture content
EMC <sub>R</sub>	reduced equilibrium moisture content

## Abbreviations

---

eq.	equivalent
ESI	electrospray ionization
<i>et al.</i>	and others (et alii)
FTIR	fourier transform infrared
GPC	gel-permeation chromatography
GMA	glycidyl methacrylate
HR-MS	high-resolution mass spectrometry
<i>in vacuo</i>	under reduced pressure
IPA	2-propanol
IR	infrared
IUPAC	international union of pure and applied chemistry
m	multiplet
MA	methyl acrylate
MADIX	macromolecular design via the interchange of xanthates
MAPE	maleated polyethylene
MAPP	maleated polypropylene
MS	mass spectrometry
MW	molecular weight
MWD	molecular weight distribution
NMP	nitroxide mediated radical polymerization
NMR	nuclear magnetic resonance
PBS	phosphate buffered saline
<i>per se</i>	by itself
PE	polyethylene
PGMEA	propylene glycol methyl ether acetate
PMA	poly(methyl acrylate)
PMMA	poly(methyl methacrylate)
PMDETA	<i>N,N,N',N'',N''</i> -pentamethyldiethylenetriamine
PP	polypropylene
PS	polystyrene
PTFE	polytetrafluoroethylene
PVAc	poly(vinyl acetate)
PVC	polyvinyl chloride
Py	pyridine
q	quartet
RAFT	reversible addition-fragmentation chain transfer
RI	refractive index

---

RDRP	reversible-deactivation radical polymerization
RH	relative humidity
RM	residual mass
rt	room temperature
s	singlet
SEC	size-exclusion chromatography
SEM	scanning electron microscopy
SI	surface-initiated
t	triplet
TAPA	<i>tert</i> -Amyl peroxyacetate
TCDI	1,1'-thiocarbonyl diimidazole
TCEP	tris(2-carboxyethyl)phosphine
TEA	triethylamine
TG	thermogram
TGA	thermogravimetric analysis
THF	tetrahydrofuran
TLC	thin-layer chromatography
TNB	5-thio-2-nitrobenzoic acid
tol	toluene
UV	ultraviolet (radiation)
VAc	vinyl acetate
vis	visible
WCA	water contact angle
WL	weight loss
WPC(s)	wood-plastic composite(s)
WPG	weight percent gain

### Formula symbols and variables

$A$	absorbance
$A_0$	area
$a$	Mark–Houwink parameter
$c$	concentration
$\delta$	chemical shift
$\mathcal{D}$	dispersity
$E$	YOUNG's modulus

## Abbreviations

---

$E'$	storage modulus
$E''$	loss modulus
$\epsilon$	elongation
$F$	force
$J$	coupling constant
$K$	Mark-Houwink parameter
$k$	rate constant
$l$	length
$\lambda$	wavelength
$m$	mass
$M$	molar mass, number of molecules
$M_n$	number-weighted molar mass
$\bar{M}_n$	number-weighted mean of molar mass
$\sigma$	strain
$\sigma_y$	yield point
$t$	reaction time
$T$	temperature
$T_g$	glass transition temperature
$\tan(\delta)$	damping
$U_T$	tensile toughness
$w$	mass fraction

## Unit symbols

%	percent ( $10^{-2}$ )
Å	angstrom
C	carbon equivalents in $^{13}\text{C}$ -NMR
d	day
eq.	equivalent
eV	electron volt
°C	degree Celsius
g	gram
h	hour
H	proton equivalents in $^1\text{H}$ -NMR
Hz	hertz
l	liter

m	meter
M	molarity
min	minute
mol	mole
ppm	parts per million ( $10^{-6}$ )
wt/%	weight percent
vol/%	volume percent

### **Unit prefixes**

G	giga ( $10^9$ )
M	mega ( $10^6$ )
k	kilo ( $10^3$ )
m	milli ( $10^{-3}$ )
$\mu$	micro ( $10^{-6}$ )
n	nano ( $10^{-9}$ )



# Acknowledgements

Und nun ein paar Worte in eigener Sprache...

Zunächst danke ich Herrn Prof. Philipp Vana für die interessante und herausfordernde Aufgabenstellung, sein offenes Ohr bei jeglicher Art von Problemen, seine stets motivierenden Worte und dafür, dass ich meine Promotion in seiner Arbeitsgruppe durchführen durfte. Bei Herrn Jun.-Prof. Kai Zhang möchte ich mich für die Übernahme des Korreferats bedanken. Außerdem möchte ich mich bei meinem gesamten Prüfungskomitee bedanken.

Besonderer Dank gilt auch meiner Bachelorstudentin Julia Gerke, welche durch ihre aufmerksame Arbeit erheblich zum Erfolg dieser Arbeit beigetragen hat. Bei Dominik Ruhr und Philipp Schröder bedanke ich mich für die engagierte Arbeit und Unterstützung bei den Experimenten im Rahmen ihrer Forschungsaufenthalte. Simon Eichhorn, Jannik Wagner und Wentao Peng danke ich für das aufmerksame Korrekturlesen dieser Arbeit. Bei Torsten Fornefeld, Niklas Frerichs und Judith Steinhoff möchte ich mich nicht nur für die Hilfe bei der Korrektur dieser Arbeit, viele Diskussionen und Anregungen herzlich bedanken, sondern auch für die Unterstützung meiner Bachelorstudentin bei dringenden Fragen in meiner Abwesenheit.

Darüber hinaus möchte ich mich bei Dr. Hans-Peter Vögele, Sandra Lotze und Heike Rohmann für die Hilfe bei praktischen Problemen sowie Stefanie Kindler, Tim Koddenberg, Dr. Markus Hold und Dr. Gerhard Büttner für den Beistand bei administrativen Aufgaben bedanken. Außerdem möchte ich mich ganz herzlich bei allen aktuellen und ehemaligen Mitarbeitern der Arbeitskreise Buback und Vana, besonders meinen Bürokollegen, für die freundliche und unterhaltsame Arbeitsatmosphäre sowie für die vielen schönen Momente bedanken.

Mona Maaß und Adrian Ley danke ich sehr für die REM- bzw. Fluoreszenz-Messungen. Ein besonderer Dank gilt auch Lukas Emmerich für das Messen der dynamischen Wasserdampfsorption. Weiterhin möchte ich der gesamten

## Acknowledgements

---

Abteilung "Holzbiologie und Holzprodukte" der Georg-August-Universität Göttingen, insbesondere Dr. Marco Fleckenstein, Kim Christian Krause und Prof. Dr. Carsten Mai, für die freundliche Beantwortung jeglicher Fragen zum Thema Holz meinen Dank aussprechen. Natürlich gebührt ein besonderer Dank dem Land Niedersachsen und der Georg-August-Universität Göttingen für die finanzielle Unterstützung im Rahmen des Promotionsstudiengangs "Materialforschung Holz" (MaFo Holz).

Vielen Dank an alle Freunde, Sportkollegen und Wegbegleiter in und außerhalb von Göttingen für die wertvollen Ablenkungen vom Arbeitsalltag. Ein ganz besonderer Dank gilt meinen Kommilitonen Dr. Martin Werner, Dr. Alexander Brinkmeier und Dr. Markus Schön, welche mich durch mein gesamtes Studium begleitet haben. Besonders bei Dr. Jan Schwellenbach will ich mich für die sehr enge Freundschaft, die vielen Diskussionen und seine beständige Besorgnis über meine körperliche Fitness bedanken.

Schließlich möchte ich mich von ganzen Herzen bei meiner Familie bedanken, welche mich in den Jahren des Studiums uneingeschränkt unterstützt hat. Ausdrücklich hervorheben möchte ich natürlich meine verständnisvolle Frau, welche mir nicht nur in kritischen Phasen viel Kraft gegeben hat, sondern mir auch eine wundervolle Tochter geschenkt hat. Ich freue mich sehr auf unseren gemeinsamen zukünftigen Weg.

Danke!